THE PROPERTIES OF POST-STARBURST GALAXIES FROM SPECTRAL FITTING

Laith Talib Hadi Taj Aldeen

A Thesis Submitted for the Degree of PhD
at the
University of St Andrews

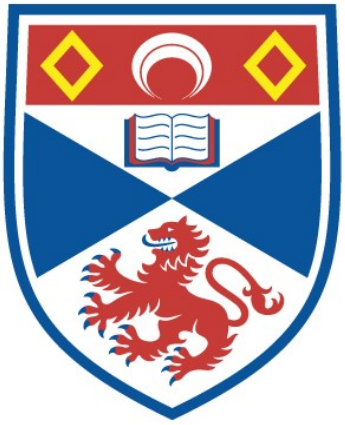

2018

The Properties of Post-Starburst Galaxies from Spectral Fitting

Laith Talib Hadi Taj Aldeen

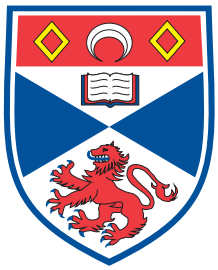

University
of
St Andrews

This thesis is submitted in partial fulfilment for the degree of

Doctor of Philosophy (PhD)
at the University of St Andrews

October 2018

Declaration

I, Laith Taj Aldeen, hereby certify that this thesis, which is approximately 32,000 words in length, has been written by me, and that it is the record of work carried out by me, or principally by myself in collaboration with others as acknowledged, and that it has not been submitted in any previous application for a higher degree.

I was admitted as a research student in September 2014 and as a candidate for the degree of PhD in September 2014; the higher study for which this is a record was carried out in the University of St Andrews between 2014 and 2018.

I, Laith Taj Aldeen, received assistance in the writing of this thesis in respect of grammar and spelling, which was provided by Carl Roberts, Isaac Nowell and Vivienne Wild .
Date Signature of candidate

I hereby certify that the candidate has fulfilled the conditions of the Resolution and Regulations appropriate for the degree of PhD in the University of St Andrews and that the candidate is qualified to submit this thesis in application for that degree.

Date Signature of supervisor

Copyright Agreement

In submitting this thesis to the University of St Andrews I understand that I am giving permission for it to be made available for use in accordance with the regulations of the University Library for the time being in force, subject to any copyright vested in the work not being affected thereby. I also understand that the title and the abstract will be published, and that a copy of the work may be made and supplied to any bona fide library or research worker, that my thesis will be electronically accessible for personal or research use unless exempt by award of an embargo as requested below, and that the library has the right to migrate my thesis into new electronic forms as required to ensure continued access to the thesis. I have obtained any third-party copyright permissions that may be required in order to allow such access and migration, or have requested the appropriate embargo below.

The following is an agreed request by candidate and supervisor regarding the publication of this thesis:
No embargo on print copy.
No embargo on electronic copy.

Date Signature of candidate

Date Signature of supervisor

Collaboration Statement

The work presented in this thesis was produced by me during my time as a Ph.D. student at the University of St Andrews between September 2014 and July 2018.

The primary code used during this work was STARLIGHT, a tool to fit a linear combination of synthetic stellar population models to spectroscopic and photometric data via a maximum likelihood method. The original version for fitting spectroscopic data alone can be downloaded at http://www.starlight.starlight.ufsc.br . The new STARLIGHT code to fit both spectroscopic and photometric data was provided by collaborators Natalia Vale Asari and Ariel Werle from the Universidade Federal de Santa Catarina, Brazil.

The work in chapter three was included in a peer reviewed and published paper: Pawlik, Taj Aldeen et al., 2018, Monthly Notices of the Royal Astronomical Society, 447, pp.1708-1743.

The UDS and UDSz data used in chapter four was obtained prior to public data release from Omar Almaini from the University of Nottingham. Collaborators David T. Maltby (University of Nottingham) and Aaron Wilkinson (University of Ghent) provided additional spectra of post-starburst galaxies and updated supercolour analysis of the dataset, in collarboration with my supervisor Vivienne Wild.

The Bagpipes code used in Chapter four was provided prior to public release by Adam Carnall (University of Edinburgh), and run on the UDSz spectra by my supervisor Vivienne Wild. I analysed the output from this code.

My supervisor, Vivienne Wild provided scientific advice on the work in all chapters. I have written all the text in this thesis, and all figures have been made by me from data produced during my own work, save eight figures in the chapters which are stated in their captions to be reproductions along with the citations to their sources.

Abstract

A bimodality has been seen in the morphology, colour and star-forming properties of galaxies. Throughout cosmic time, the number of galaxies that are quenched to join the red-sequence has increased, unlike the number of star forming galaxies. Post-starburst galaxies (PSB) are suspected to be a transition phase between these two stages.

We tried to answer the questions of the mechanism for this transformation. The goal of our work is to see whether or not all PSB in the nearby universe are being quenched to join the red-sequence and by which mechanism. We try to show if there is any difference between the low and high redshift PSB with regard to there accumulated stellar mass in the last 1 and 1.5 Gyr, the star formation history and the amount of dust within the galaxies. In this work we fit the observed galaxies with the new STARLIGHT code that can fit spectra with or without photometric data with a library of synthetic models.

First we investigate 189 PSB candidates in the low redshift Sloan Digital Sky Survey (SDSS) and 1877 comparison samples of star forming and passive galaxies. Depending on the mass, low or high, we found more than one pathway and mechanism that may transform the blue cloud to become red sequence type galaxies. Secondly we use Ultra Deep Survey (UDS) and the spectroscopic follow-up of the UKIDSS Ultra-Deep Survey (UDSz) data for the PSB galaxies at $0.9 \leq z \leq 1.2$. From the fitting of 323 galaxies, we determine more constrained physical properties of UDSz high redshift galaxies, such as the star formation history, mass fraction that formed at the time of the burst and the dust contents of the galaxies. We speculate that a higher gas content in these galaxies could have lead to the higher burst.

Acknowledgements

I would firstly like to thank my supervisor Vivienne Wild for always being their even before I arrived. She is a beacon of knowledge that guided me through the endless darkness of the Universe.

I offer my gratitude to both the Ministry of Higher Education and Scientific Research (MOHESR) and the University of Babylon in my beloved country Iraq for their financial support.

I would like to thank the English Language Teaching (ELT) staff members that showed me a new aspect not only in English but in life.

I would love to thank everyone that worked in room 321 between 2014 - 2018 for being great friends. William Lucas, I mention you here for not being a resident in room 321 at that time, nevertheless you were always there for me, thank you.

I thank all the staff members in the Astronomy group of the School of Physics and Astronomy, for putting me in the right pathway of Astronomy.

Finally I would like to dedicate this thesis to my family, thank you.

Contents

List of Figures

List of Tables

1 Introduction

1.1 Introduction

One means of studying galaxies is through the spectral energy distribution (SED) of galaxies. SED is the emitted radiation from a galaxy over all possible wavelength. Each type of galaxy has a unique SED which is rich with physical information about the galaxy. The SED can give an accurate profile of the galaxy properties. The SED ranges from gamma-ray to radio. The SED shows whether the galaxy is star forming via the emission lines caused by ionised gas, or whether the star formation has shut down, seen from the lack of emission lines. Such a galaxy may be considered a passive galaxy. The main contributions to a galaxy's SED are from the stars, gas and dust. Stars in a galaxy with various temperatures and luminosity are the main source, which builds up the continuum of the spectrum. The emitted energy from all or some of the stars O, B, A, F, G, K and M type make the continuum spectrum. Star-forming galaxies have higher intensity in the UV region of the spectrum than in quiescent galaxies due to having massive O and B type stars. These high temperatures stars, $>$ 10000 K, have the

required energy to ionise the nearby gas and the ionisation effect is seen in the emission lines of the spectrum. It is only the O and B stars have the required surface temperature to ionize a hydrogen atom from the ground state$\sim 13.6eV$. These are recombination lines, e.g. Lyman lines, Balmer lines, [OIII] and [OII].

The amount of gas varies in a galaxy depending on the galaxy type and its redshift. Star-forming and quiescent galaxies at low redshift are estimated to have 10% and 1% respectively of their mass as gas, whereas star-forming galaxies at high redshifts are estimated to have 50%. Gas in a galaxy is found in different states: neutral, ionised and molecular. Neutral hydrogen is detectable from the 21-cm line see paragraph 1.1.5. Molecular Hydrogen is undetectable at low temperatures therefore, carbon monoxide (CO) is used to trace H_2, taking advantage of the ratio of CO molecules to Hydrogen molecules of 10^{-4} (Schneider, 2015). CO emission lines can be observed in the millimetre wavelength range. Young & Knezek (1989) found that molecular to neutral gas ratio for late-type galaxies ranges between 4.0-0.2, depending on the galaxy's morphological type. The change in the the gas ratio can result from the efficiency of molecule cloud distribution and formation (Tacconi & Young, 1986). Star formation ratio is correlated with the galaxy's molecular cloud reservoir. Star formation is higher in spiral galaxies with a high gas ratio, than in lower galaxies'.

The intensity of the emission lines and the continuum of the spectrum in the UV and the optical is affected by the dust content of a galaxy. Dust surrounding newborn stars absorbs some of the high energy emitted from the hot stars and re-emits it at infrared wavelengths. The effect of the dust absorption is seen at the mid-IR, from dust molecules emission lines from Polycyclic aromatic hydrocarbons in the dust, and far-IR thermal emission of the SED clearly shown in figure(1.1).

Dust also scatters photons thereby contributing in dispersion of the light coming from the observed Galaxy. It causes the attenuation of SED of a stellar population, which makes the galaxy look redder then it actually is. Metal absorption lines in the spectrum are caused by the abundance of metals in the ISM. These absorption lines serve as a probe for metallicities in a galaxy.

The SED of a galaxy can also reveal an Active Galactic Nuclei (AGN) in the centre of the galaxy. An AGN is a concentrated area in the centre of some massive galaxies, which can by more luminous than the host galaxy. The effect of this highly luminous region affect the SED of the galaxy. Galaxies with AGN or more active galaxies than typical galaxies, can be identified

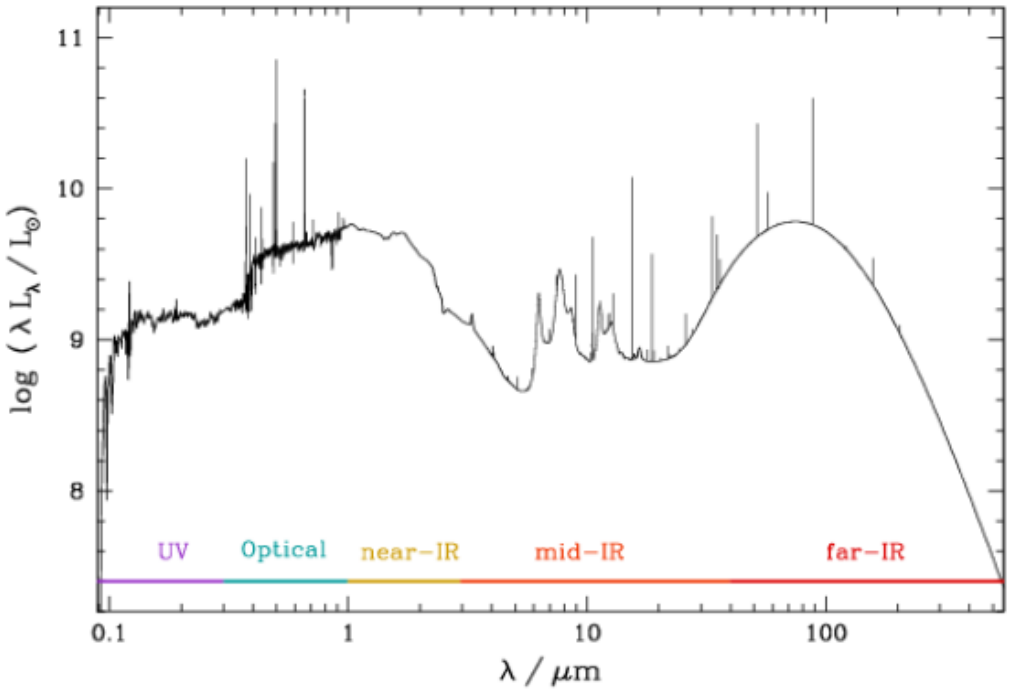

Figure 1.1: A simulated spectral energy distribution of a star forming galaxy figure taken from da Cunha et al. (2008).

in some cases very easily from their broad emission lines or by using the Baldwin et al. (1981) (BPT) diagram, see figure (3.2). The BPT diagram gives a graph of the measured emission lines ([O III] 5007 Å/ H_β; [N II] 6583 Å/ H_α and [S II] 6716 Å ,6731 Å / H_α) flux ratios. In the diagram, AGN have higher emission lines ratios than the star-forming galaxies.

The SED of a galaxy can usefully be divided into four main areas: high energy, visible, infra-red and radio.

1.1.1 High Energy Region

This region of the spectrum is defined by having high energy, going up to several MeV with a wavelength less than 1 Å, gamma-ray, up to the wavelength of 912 Å, which is the short wavelength end limit of the ultraviolet spectrum. Although it is beyond the ability of a ground-based telescope to observe this area directly, it has been a powerful tool in observing Supernova (SN), neutron stars, the interaction of black holes and massive stars with a mass exceeding 10 $M_\odot$. This region of the spectrum can also provide an inside look into the gas clouds in the line of sight of the galaxy (Rauch, 2000), the high energy wavelength will be absorbed by the clouds along the line-of sight to the observer, offering a glimpse at the intergalactic medium

(IGM).

1.1.2 Ultraviolet (UV) region

The UV spectrum in a star-forming galaxy is dominated by the energy coming from O and B type stars. These types of stars have a lifetime around 20 Myr, mass > 8 $M_\odot$, and effective temperatures between 10000 to 40000 K. They have enough energy to excite surrounding gas to produce Lyman-alpha emission line at 1216 Å (Wood et al., 2005). This emission line is a product of the transition electron from level n = 2 to the ground state n = 1, releasing a photon with the energy of 13.6 eV. This emission line is widely used to monitor and study AGN at high redshift (Bajtlik et al., 1988).

1.1.3 Optical Spectrum

This region is dominated be G and K type stars. These stars have mass $\sim$1 $M_\odot$, and effective temperatures less $\sim$6000 K. This region shows a grope of emission lines, see table (1.1). These emission lines are used to study various properties of galaxies such as metallicity, star forming rate (SFR), dust attenuation and gas dispersion, e.g., L(H_α) line of 7.9×10^{-42} erg /s, implies an SFR of 1 $M_\odot$/ year (Schneider, 2015).

Table 1.1: Some examples of common emission lines in the optical range of a spectrum, the wavelengths are measured in vacuum.

Chemical symbol	Wavelength Å
[OII]	3727.1, 3729.9
H_δ	4102.9
H_γ	4341.7
H_β	4862.7
[OIII]	4364.4, 4960.3, 5008.2
[NII]	5756.2, 6549.8, 6585.2
H_α	6564.6
[SII]	6718.3, 6732.7

On the other hand absorption lines, see table (1.2), are used for metallicity abundances.

Table 1.2: Some examples of common absorption lines in the optical range of the spectrum, the wavelengths are measured in vacuum.

Chemical symbol	Wavelength Å
CaII (k+h)	3934.8,3969.5
G-band	4305.6
Fe	4383.5 in air
MgI	5176.7
NaI D	5889.9,5895.9
Balmer seres	same as in emission

In quenched galaxies, the 4000 Å break is a distinguishing feature in the optical spectrum. The 4000 Å break separates between hot massive stars and somewhat colder and less massive old population stars therefore a strong break indicates a lack of young stars, and therefore a quenched galaxy. It is used as an index for the population age of a galaxy. This index measured from the ratio of the mean flux density 4050 - 4250 Å and 3750 - 3950 Å (Bruzual A., 1983), whereas Balogh et al. (1999) used narrower wavelength range 4000 - 4100 Å and 3850 - 3950 Å.

1.1.4 IR Region

The infrared area is divided into near (0.7-2.5 μm), mid (2.5-40 μm) and far (40-300 μm), infrared. Most of the near-IR is observed from the ground-based observatories, whereas the mid and far IR require space telescopes. Cooler stars, 5000 to 3000 K, contribute most to the continuum of the spectrum in the near-IR, whereas mid-IR and far-IR are primarily re-emitted light from heated dust grains, scaling from planetesimals to microscopic size and temperatures from 500 to 10 K. The far-IR provides information on the dust content of a galaxy, and is considered a reliable source for calculating the SFR.

1.1.5 Radio Wave Region

Many of the radio wavelengths are detected from the Earth surface. This region can be subdivided into submillimetre, millimetre, centimetre, decimetre, FM, short, medium and long waves(Osterbrock & Ferland, 2006). Some important research in this area includes radio galaxies, quasars, and the HI 21 cm emission line. The HI 21 cm emission line is produced when the parallel relative spin between the electron and the proton in the hydrogen atom flips to antiparallel. This natural phenomenon with the ubiquitous and high abundance of neutral

Hydrogen in the galaxy is used in tracing the distribution of the gas throughout the galaxy and its radial velocity. The HI line is used to measure the rotation curve and is used to calculate the dynamical mass of galaxies.

1.2 Galaxies Evolution

1.2.1 The Early Universe

At the beginning of the 20th century, there were two main theories of the cosmology of the Universe. The first is the steady-state model. It stated that the Universe always has and will always exist, and the sum of the matter within the Universe is constant. This model was disproved by the discovery of the expansion of the Universe. The discovery of redshift in the 1912 was achieved by Slipher. By linking the relationship between redshift and the distance of a galaxy Hubble, E., Humason (1931), revealed the Universe expansion. By using Einstein field equations, General Relativity (GR), combined with Friedmann - Lemaître - Robertson - Walker metric, scientists can explain the expansion of the Universe. From the present day contents and expansion of the Universe, we can deduce the presence of dark matter and dark energy and how they relate to the big bang (BB). In this model, the Universe started out as a singularity and expanded from that point 13.7 billion years ago. Through inflation, an era of extremely accelerated expansion during the Universe's earliest stages, which came after the BB, density fluctuation in the early Universe became the foundation for building up galaxies in the Universe.

1.2.2 Galaxy Formation

It was the work of Peebles (1970), that established the idea of the hierarchical galaxy formation: the large over-dense regions in the present were formed by the accretion of many smaller clumps of matter. This explains the formation of dark matter halos. This concept became later known as the merger trees hypothesis. A merger tree describes the formation of a dark matter halo through accretion and repeated mergers (Lacey & Cole, 1994). Dark matter haloes are believed to have formed galaxies within the that (Mo et al., 2010). The fuel of the galaxy is gas, which accumulated in the dense areas of the galaxy to form molecular clouds. Giant molecular clouds (GMCs) are within scales of about 10^4 - 10^6 $M_\odot$, density 500 to 1000 cm^3 and size larger than 100 pc. The random motion in the galaxy will split the cloud into smaller

clouds, plates, threads and denser clumps, which are the birthplace of stars within galaxies (Dobbs, 2013). The diversity of stars mass within a galaxy can by described by the initial mass function (IMF) (Salpeter, 1955), which is the distribution of the initial masses of a population of stars as they are joining the main sequence. Galaxies that form stars at a rapid rate using up almost all their gas to form stars in a short time scale compared with the galaxy lifetime are known as starburst galaxies (Johnson et al., 2001). Starburst galaxies have intense star formation rate in the central region of the galaxy (R <= 1 kpc) (Smith, 1996; Lester, 1995). Star formation in a starburst galaxy is roughly estimated to be 2.5 - 25 $M_{\odot}$ / yr within a radius of 0.05 - 0.5 Kpc, higher than what has been observed in the Milky Way 0.25 $M_{\odot}$ / yr (Güsten, 1989), or in the typical star-forming galaxy.

1.2.3 Galaxy Classification

The expanding Universe features many objects within it that vary in shape, mass and size a galaxy is such an object. Galaxies are large celestial bodies with hundreds to thousands of billions of stars, gas and dust. Sandage (1975) suggested that in order to study any celestial body, scientists have to classify that body. Hubble (1926) presented the first galaxies classification in astronomy know as the Hubble tuning fork figure (1.2). In that classification galaxies are divided into four main types depending on their morphology Elliptical, Spiral, Lenticular and Irregular.

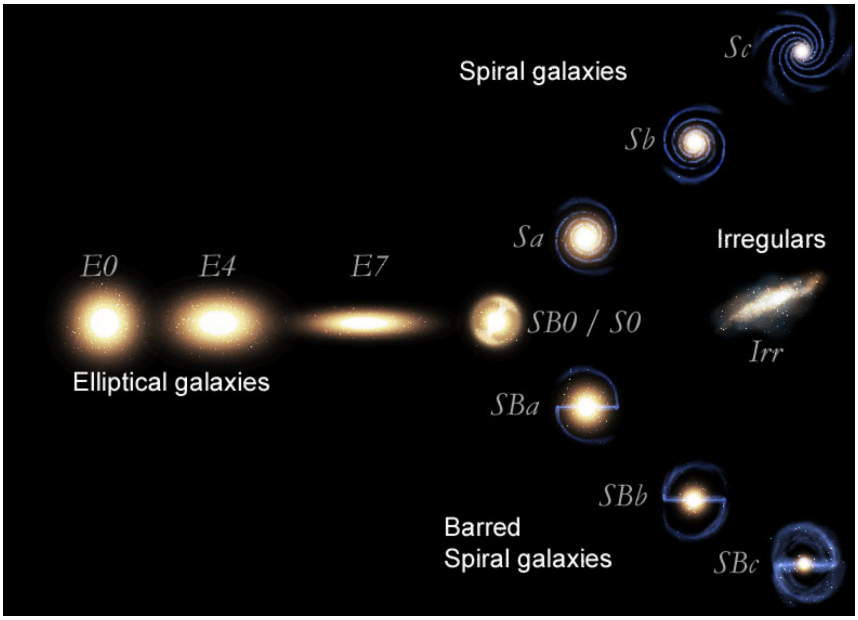

Figure 1.2: Hubble tuning fork his classification for galaxies, figure established by: Fahad Suleria, at (Astronomical illustrations and space art) www.novacelestia.com.

Elliptical galaxies are divided into subtypes (E0, E1, E2, En), where n = (1- (b/a))× 10, (a) is the semi major axis and (b) the semi minor axis for the observed galaxies. The number (n) is rounded to the nearest integer. A galaxy type E0 is almost seen as a circular, on the other hand a galaxy type E5 will be seen almost as elongated in the (a) axis with length twice more in than (b) (Sparke & Gallagher, 2007). Van den Bergh (2009) pointed out that galaxies type E0 to E4 are brighter than type E5 to E7. He recommended that E7 are type S0 galaxies, suggesting that elliptical galaxies may not have (n) higher then 6. The main population in elliptical galaxies is old evolved stars with almost no gas. Stars in this type of galaxies have random motions, making up the almost spheroidal shape of the galaxy.

Spiral galaxies are a well known type of galaxies in the local universe. Their general figures are having flat disc with a bulge in the center of the galaxy and spiral arms that may or may not have bars. Spiral galaxies have a dominated rotation support motion. The subtype divedied are normal spiral galaxies from early spiral (Sa) to late (Sc) and spiral with bars are classified from early (SBa) to late (SBc) spiral bar galaxies. The size of the bulge relative to its disc is decreasing from early to late type. Also an increase in young stars numbers is accompanied with moving from early to late spiral type. The contents of a spiral galaxies interstellar medium (ISM), gas and dust, increases as the type changing from (Sa) and (SBa) to Sc and (SBc) (Da Cunha et al., 2008).

An intermediary type of galaxies between the spiral and elliptical is the lenticular galaxies. This type of galaxies show a very distinguished bulge and disc from the bulge and disc of a spiral galaxy. In these galaxies star formation or gas content is relatively less than in a spiral galaxy. Lenticular galaxies lack the large-scale spiral arms. They are considered as a transform phase between spiral and elliptical galaxies. Irregular types of galaxies show no distinctive shape as the elliptical or spiral galaxies have. These type of galaxies do not fall into Hubble tuning fork.

1.2.4 Evolution

Spiral galaxies have a younger population of stars due to the ongoing star-forming, with a blue colour because of the relatively high number of O and B type of stars, and they have a strong disc component. On the other hand, quiescent galaxies have an older population, which is redder and lacks gas, with a dominating bulge. This bimodality is seen throughout the nearby and far Universe and documented very well (Kauffmann et al., 2003b; Blanton & Moustakas, 2009). The colour-mass diagram shows three regions: the blue cloud occupied by

spiral galaxies, the red sequence dominated by passive elliptical galaxies, and a less populated region known as the green valley that has an in between type of galaxies figure (1.3), in this region galaxies are in the process of shutting off their star formation (Tinsley, 1978; Strateva et al., 2001; Baldry et al., 2004).

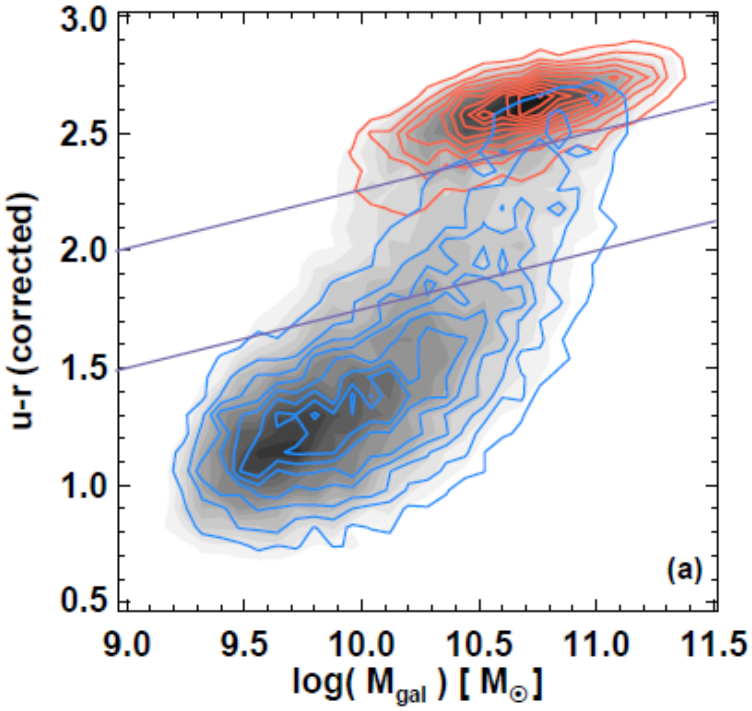

Figure 1.3: The colour mass diagram, showing the red sequence, early type galaxies that have old stellar population with high stellar mass density (red). The blue cloud shows the star forming galaxies (blue) and green valley boundary (purple) galaxies in this region are considered in a transition phase from the blue to the red type galaxies. Figure taken from (Alatalo et al., 2014).

Observations show that the blue cloud's mass has remained roughly the same since $z = 1$, whereas the red sequence has almost doubled its mass through the same time period (Bell et al., 2004). Studies have shown that a violent event like gas-rich mergers (Kannappan et al., 2009; McIntosh et al., 2014) may rapidly quench galaxies to the red sequence, but other slower mechanism may also cause quenching star formation in galaxies.

Some of the proposed evolution mechanisms include mergers, ram pressure stripping, strangulation, harassment and feedback from AGN.

1.2.4.1 Mergers

To determine the effect of gas-rich mergers on galaxy morphology and star formation rate, researchers have developed simulations to model merger events. In these simulations, a key factor is the mass ratio of the merger. In a galaxy merger, the value of the mass ratio between two galaxies either indicates a major or minor merger.

A minor merger happens when, for example, a small satellite merges with a more massive central galaxy. In a minor merger the satellite staler mass may be driven to the centre of the massive galaxy, increasing the bulge size. Also, a small starburst may result from the inflow of the gas from the satellite to the disc of the massive galaxy. Star formation tends to continue for more extended periods of time after the final minor merger. Hernquist & Mihos (1995), showed that minor mergers that involve a significantly smaller companion would not cause the more massive galaxy to change in its morphology.

A major merger happens if the masses of the progenitors are almost equal. A major merger between gas-rich galaxies generates a significant amount of starburst consuming a large fraction of the original gas in both galaxies. In this type of merger, it will destroy the discs of both galaxies to form a bulge where eventually all the stellar mass are driven to (Cox et al., 2006). Croton et al. (2006) used the mass ratio of 0.3 to separate between the minor and major merger.

Another factor that may affect the gas-rich mergers simulations is the gas density and distribution in the galaxies. Mergers lead to a strong tidal force that causes turbulences to the gas over a large area in the galaxy. The effected gas will crash into denser regions. These regions will further collapse to form a star. Therefore gas-rich mergers may trigger a starburst throughout the galaxy.

In a merger it is estimated that the time from the gravitational force to take control to the ignition of starburst is between 10 to 30 Myr (Renaud et al., 2014). Hence a merger is considered to be a fast mechanism that may consume nearly all of the gas in the colliding galaxies. The merger may form a new galaxy with a morphology different from the original two merging galaxies.

1.2.4.2 Ram pressure stripping

It was in (1972) that Gunn and Gott suggested that ram pressure stripping may be happening in galaxies in clusters after noting the absence of normal spirals in rich clusters. Galaxies falling

into the dense cluster environment will be stripped of their gas, causing the galaxy to shut off the star formation (Chung et al., 2009). From simulations, Hester (2006), showed that ram pressure stripping of the gas-rich galaxy depends mainly on the ratio of the galaxy mass to the mass of the host cluster. Spiral galaxies are strongly stripped in dense clusters and mildly stripped in groups, whereas the dwarf galaxies are strongly stripped in both high or low dense environments. Yoon et al. (2017), from observing 35 galaxies in the Virgo cluster that are undergoing ram-pressure stripping, found that galaxies are strongly stripped in the centre of the cluster or in the outskirts with low orbital velocities around the cluster. They showed that the outskirt galaxies are not falling into the cluster for the first time and considered backsplash galaxies.

1.2.4.3 Strangulation

Galaxy strangulation is the process of stopping the inflow of gas from the intracluster medium (ICM) in a cluster. Halting the gas inflow will eventually stop star-formation in the galaxy. The heating of the gas in the ICM is suspected to be caused by the turbulence that is driven from the outflow of matter pouring from the central super-massive black hole (BH) in the cluster (Zhuravleva et al., 2014). The strangulation mechanism will eventually quench the galaxy but on a longer time scale, > 4 Gyrs, than any other known mechanism. Peng et al. (2015) found from an analysis of SDSS spectra sample of galaxies that strangulation is the main mechanism for quenching star formation in a galaxy. The paper showed that star forming in a galaxy of steller mass $< 10^{11}$ $M_{\odot}$ would be quenched in a typical timescale of 4 Gyrs. Maier et al. (2016), showed that strangulation might be the mechanism that can explain the high metallicities abundance of accreted galaxies to the MAC0416 cluster.

1.2.4.4 Harassment

Harassment happens in a cluster when a galaxy experiences high-speed fly-bys, e.g. relative velocity of 1500 km/s. Harassment is the cumulative effect of repeated encounters between galaxies in the cluster. The fly-bys can happen once every 1 Gyr, and it can occur many times in a time of 4-5 Gyrs. Harassment can reform the internal properties of a galaxy within a cluster, changing the gas distribution and mass within the galaxy. It also can affect the distribution of stars within the galaxy, primarily changing the shape of the galaxy. A galaxy can evolve from spiral star-forming galaxy to quenched ellipticals through many close encounters. Each

encounter will cause the harassed galaxy to lose angular momentum to the galaxy halo, gradually changing the galaxy morphology. Additionally, encounters also cause turbulence within the galaxy gas. The tidal forces of the turbulent gas leads to a series of multiple starbursts, whereas the heated gas from the newborn stars will later on stop star formation (Moore et al., 1996).

1.2.4.5 Feedback from AGN

AGN is a strong source of thermal radiation energy found in massive galaxies. The source of AGN energy is a result of the gas accreting into the centre of the host galaxy. The AGN host is super-massive BH. AGN feedback is suspected to have a role in the evolution of the host galaxy. The claimed link between AGN and star formation raises the question of how the centralised activity can affect the host galaxy evolution. Lagos et al. (2008) found that for the AGN feedback to have any effect on the host galaxy, the AGN must expel the reheated gas away from the galaxy halo. Hopkins & Elvis (2010), claimed that it is difficult for the winds from the accretion disc, or from another kind of feedback near the accretion disk, to influence directly the star formation regions which are several kpc away. But they also argued that the AGN feedback driving out the hot gas into the interstellar medium, which may heat push the nearby cold gas, ejecting it from the galaxy and thereby stopping star formation.
Some AGN show jets, strong and fast gas outflows in two opposite directions from the host galaxy. Although the AGN jet drives out the gas from the centre area of the host galaxy, Gaibler et al. (2012) found that the blast jet waves can have an influence on the average density distribution of the gas in the galaxy affecting the star formation rate of the host galaxy.
The mass of a black hole grows from the accretion gas. If the accretion rate reaches the critical limit, known as the Eddington limit, the radiation pressure from the release of gravitational energy will blow away the nearby material, stopping black hole growth and star formation (Merritt & Quinlan, 1998). Silk & Nusser (2010) showed that a BH on the MBH-σ diagram is not capable of expelling gas out of the galaxy halo only by radiation pressure alone, but an extra mechanism is required. Galaxies in dense environment can remove gas from the galaxy by tidal stripping or ram pressure, therefore, providing the extra energy.
Schawinski et al. (2007), concluded from studying a group of early-type galaxies located in redshift range $0.05 < z < 0.1$, that an evolution sequence from SF by means of AGN to quiescent may have happened. Reuland et al. (2007), support this conclusion with their work at

high redshift z > 3. The impact of AGN on galaxy evolution and star formation remains an opine research area.

1.3 Post-starbursts galaxies (PSB)

The work of Dressler & Gunn (1983) first identified what are now known as Post-starbursts PSB galaxies. From 15% of their sample of 20 galaxies, they noticed the absence of emission lines and a distinguishing strong Balmer absorption lines in the sample spectra. They concluded that these galaxies have a general population of old stars seen in the 4000 Å break, still in the main sequence K giant type stars, with a higher younger and brighter population of A-type stars that are distinguished by having a strong Balmer absorption lines in their spectrum figure (1.4).

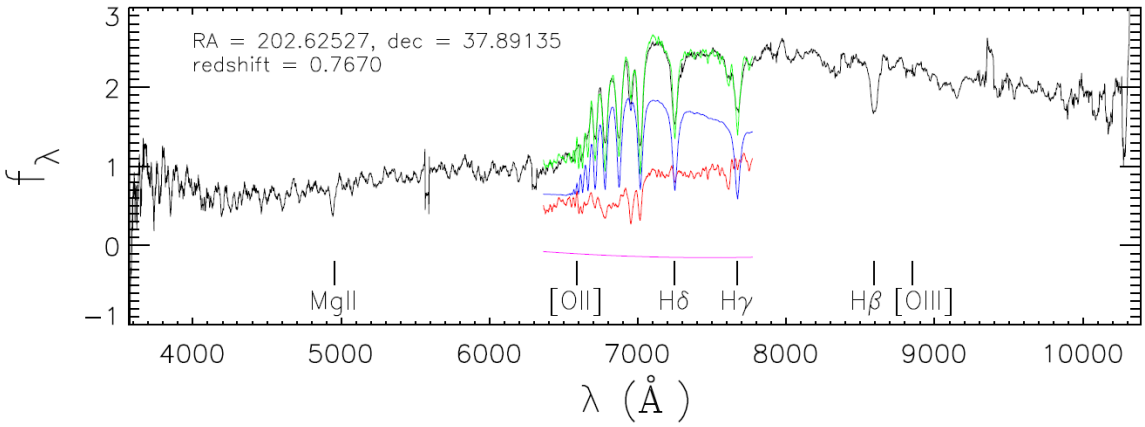

Figure 1.4: PSB galaxy's spectrum (black) from BOSS, ID:3984-233-55333, which has been smoothed to increasing visibility and is normalised, arbitrary unit, having the total flex over the rest frame wavelength 3600-4400 is the same. The spectrum shown is at observed frame. The spectrum has no emission lines and strong Balmer absorption lines from the A-type stars. The redshift, right ascension (RA) and declination (Dec) for the observed galaxy are shown on the plot. The polynomial component (magenta), a dominating K-type population galaxy (red), A-type star (blue) and the best fitted model spectrum (green). The positions of several major lines are shown at the bottom. Figure taken from Pattarakijwanich et al. (2016).

It were only later that these types of galaxies were recognized to be a link in galaxy evolution from the star-forming blue cloud to the red sequence passive galaxies. The PSB phase indicates a strong starburst has happened in the last 100 Myrs to 1.5 Gyrs of the galaxy's life (Couch & Sharples, 1987). Simulations have shown that starbursts producing about 5% to 10% of the total stellar mass of a galaxy within less than 10^8 yr are required to see a PSB spectral

signatures in low resolution spectra (Wild et al., 2009).

A star-forming galaxy that encounters a mechanism that may shut off the star formation temporarily, only to ignite later, can also show moderate Balmer lines and the absence of any emission lines. Also, when working with galaxies spectra, one should always account for the effect of dust in the interstellar media (ISM) and the dust that surrounds newborn stars. It has been argued by Poggianti et al. (1999)that the emission from young stars with temperatures $>$ 10000 K, O and B type can be entirely obscured due to the surrounding dust, leaving old, A-type stars that have dispersed their surrounding dust already . The selective extinction phenomena mean that the younger population of stars will be on average strongly depressed by dust in comparison with the old population. This type of situational effect is more prominent in dusty starbursts than in a typical star-forming galaxy (Liu & Kennicutt, 1995; Poggianti & Wu, 2000). Dusty saturate galaxies can be confused with PSB galaxies and have been observed in both clusters and the field between redshift 0.3 and 0.5 (Dressler et al., 1999; Poggianti et al., 1999).

A fundamental question regarding PSB galaxies is which mechanisms lead to PSB galaxies, and how these mechanism vary in importance throughout cosmic time, and with stellar mass.

1.3.1 Environment

Butcher & Oemler, A. (1984) showed in their study of 33 massive clusters that late-type galaxies fraction has been declining significantly from 25% to 3% from redshift 0.5 to 0.1 respectively, implying the transformation of spiral galaxies to quenched galaxies. This also implies that the number of PSB galaxies has also declined in the same redshift range, since PSB galaxies are to be an intermediary phase between the late and early type galaxies. A number of spectroscopic surveys of massive intermediate redshift clusters show that 25% of the clusters contain PSB galaxies (Barger et al., 1996; Dressler et al., 1999; Swinbank et al., 2007). Furthermore, studies within the redshift range 0.3 - 0.6 showed that PSB galaxies are more prevalent in massive clusters than in the field (Tran et al., 2003; Poggianti et al., 1999). In both clusters and field at z $\backsim$ 0.1 PSB galaxies are rare. Zabludoff et al. (1996) showed from a sample of 21 nearby galaxies that where spectroscopically confirmed of being PSB galaxies, in which 75% of the sample is located within the field. The fraction of PSB galaxies is higher in the field than in clusters for the local Universe (Goto, 2005; Yan et al. (2008)). They also suggested that the primary mechanism that produced these galaxies is mergers as other mechanisms are

mainly associated with clusters. The gas-rich merger may be the primary mechanism that have formed the PSB phase in field (Yang et al., 2004; Nolan et al., 2007). Yan et al. (2008) showed from using both the Sloan Digital Sky Survey (SDSS) at redshift $\backsim$ 0.1 and DEEP2 which was the densest and largest high-precision redshift survey of galaxies at redshift $\backsim$ 0.8 at that time that the PSB galaxies are more prevalent within massive clusters at high redshift and in the field at low redshift.

Ram pressure stripping, harassment, and strangulation are among the mechanisms that can shut down star formation within a galaxy located in massive clusters that can cause PSB signatures.

1.3.2 Redshift

For the nearby galaxies, low redshift, it is easy to observe and classify PSB galaxies, as the main distinguishing features, strong Balmer absorption lines and lack of emission lines, can be observed without difficulty in the rest frame wavelength. The observed frame spectra information provided from massive star-forming galaxies at high redshift > 4, is from the rest frame UV region. Therefore, making ground-based spectral surveys for PSB is not possible at high redshift. Ground-based observations can show the the strong Balmer absorption line, Hδ 4101 Å for a galaxy that has a redshift no more than 1.4. This redshift limit astronomers from classifying PSB galaxies at higher redshift.

The star formation rate can be used as a tracer of a galaxy's evaltion throughout cosmic time. Madau & Dickinson (2014) showed that almost 50% of the total stellar mass in the Universe was formed around redshift 2. At redshift $\sim$ 2.3 Cimatti et al. (2008) showed that a strong star forming burst might be behind galaxy evolution. From redshift of one to the present day, we see the growth in the red sequence, which doubles in mass size through quenching of star-forming galaxies. Wild et al. (2009), showed that the mass density for PSB at redshift 0.07 is 230 less than at 0.7. From all the previous research and knowing that PSB galaxies are a transition phase from star forming to quench galaxies in a relatively short time, 1 Gyr, implied that there are a higher number of PSB galaxies at high redshift than at low.

Whitaker et al. (2012), also showed that the PSB galaxies number density at redshift 2 is higher by a factor of 10 higher than at redshift 0.5. They also found that the majority of their sample galaxies that had recently undergone the PSB phase are smaller in size compared to the older ones. The study shows that PSB galaxies are more compact at high redshift than low. In a more

recent work Almaini et al. (2017), also shows from the Ultra Deep Survey (UDS) data that PSB galaxies with masses $> 10^{10.5}$ $M_\odot$ at redshift >1 are a highly compact spheroid, referring to them as "red nuggets". They also argued that PSB galaxies are a result of gas-rich merger or compaction caused by gas inflow onto a massive galaxy disc. The two previous papers also suggest the majority of the morphology of elliptical galaxy is already established during the quenching of star forming.

1.3.3 Mass

Unlike high mass luminous PSB galaxies, low mass PSB galaxies are hard to detect even in the nearby Universe. The first look at the low redshift Coma cluster, Poggianti et al. (2004) found that PSB galaxies are uncommon in the cluster, but later on the study show that low mass PSB galaxies are more prevalent than known. Wong et al. (2012) from photometric and spectra showed that there are more PSBs galaxies with a mass between log(mass) of 9.5 - 10.5 $M_\odot$ than these between 10.5 - 11.5 $M_\odot$.

The PSB is more abundance at high than low redshift. It is between the observation difficulties, not been able to detect the low mass PSB galaxies, and distinguishing them, the strong Baler absorption lines, from other types of galaxies at high redshift makes this galaxy's underestimated.

1.4 The ingredients for building a model's spectrum

One method of obtaining physical information from a galaxy's spectrum is by fitting it with synthetic model spectra. By fitting the model spectrum to the galaxy's spectrum, we can infer the properties of the galaxy from the model properties. The primary component that build a galaxy spectrum, in the optical region, are stars of various types, age, temperature and metallicity. A simple stellar population (SSP) is a group of stars with the same initial metallicity at a specific age used to build up the synthetic model of the stellar component. Constructing the galaxy spectrum from these SSP models requires knowledge of the initial mass function (IMF), stellar population isochrones, stars formation history and dust content of the galaxy.

1.4.1 Initial Mass Function

The IMF gives the number of stars, $\xi(M)$ $[M^{-1}]$ as a function of mass. The IMF gives a statistic distribution for the numbers of stars within a range of masses. This function estimates initial

number of stars with a given mass in SSP.

Many functions have been suggested to estimate IMF in the literature. Salpeter (1955), gave his version of the IMF equation (1.1) power law, that showed that the number of stars is in a negative correlation with the log(mass) of the star, low mass stars are more numerous than massive stars.

$$\xi(m) \propto m^{-1.35} \tag{1.1}$$

There is evidence that the Salpeter function predicts too many low mass stars. Recent studies have shown that IMF can be multiple power law function or may have a cut at low and high mass ends or log-normal shape. These new IMFs do not suffer the same problem as the Salpeter function at low mass. Some of these IMF are Kennicutt, R. C. (1983); Kroupa et al. (1993); Kroupa (2001); Baldry & Glazebrook (2003) and Chabrier (2003), shown in figure 1.5.

In this work the modelling used is the Chabrier (2003) IMF, which accounts for the various components in a galaxy, e.g. bulge, disk, young stars, and globular clusters. This function uses a log-normal segment and a power-law segment 1.2.

$$\xi(log(m)) \propto \begin{cases} \dfrac{1}{m}\ \mathrm{Exp}\left[-\dfrac{\left[\log(\dfrac{m}{m_c})\right]^2}{2\sigma} \right] & \text{for m} < 1 \\ m^{-1.35} & \text{for m} \geq 1 \end{cases} \tag{1.2}$$

where m is the mass($m/M_\odot$), m_c is Jeans mass at mean density for individual stars $m_c = 0.08$, for stellar systems $m_c = 0.22$, and σ is the dispersion at the high mass break of the function, which for individual stars is roughly 0.69, or stellar systems 0.57.

1.4.2 Isochrones

In the Hertzsprung-Russel (H-R) diagram an isochrone is a curve that represents a stellar population with the same age and metallicity. The isochrone shows the predicted location on the H-R diagram of a population of stars with different masses, estimated from the IMF, at a specific time. With the evolution of this population with the time that location is changed see figure (1.6). The isochrones curve changes as a function of age.

The new isochrone will have different physical properties from its progenitor. High mass stars have a much shorter lifetime compared with the lower mass stars, which can be almost as old as the Universe. A change in metallicity can also affect the population isochrones as it

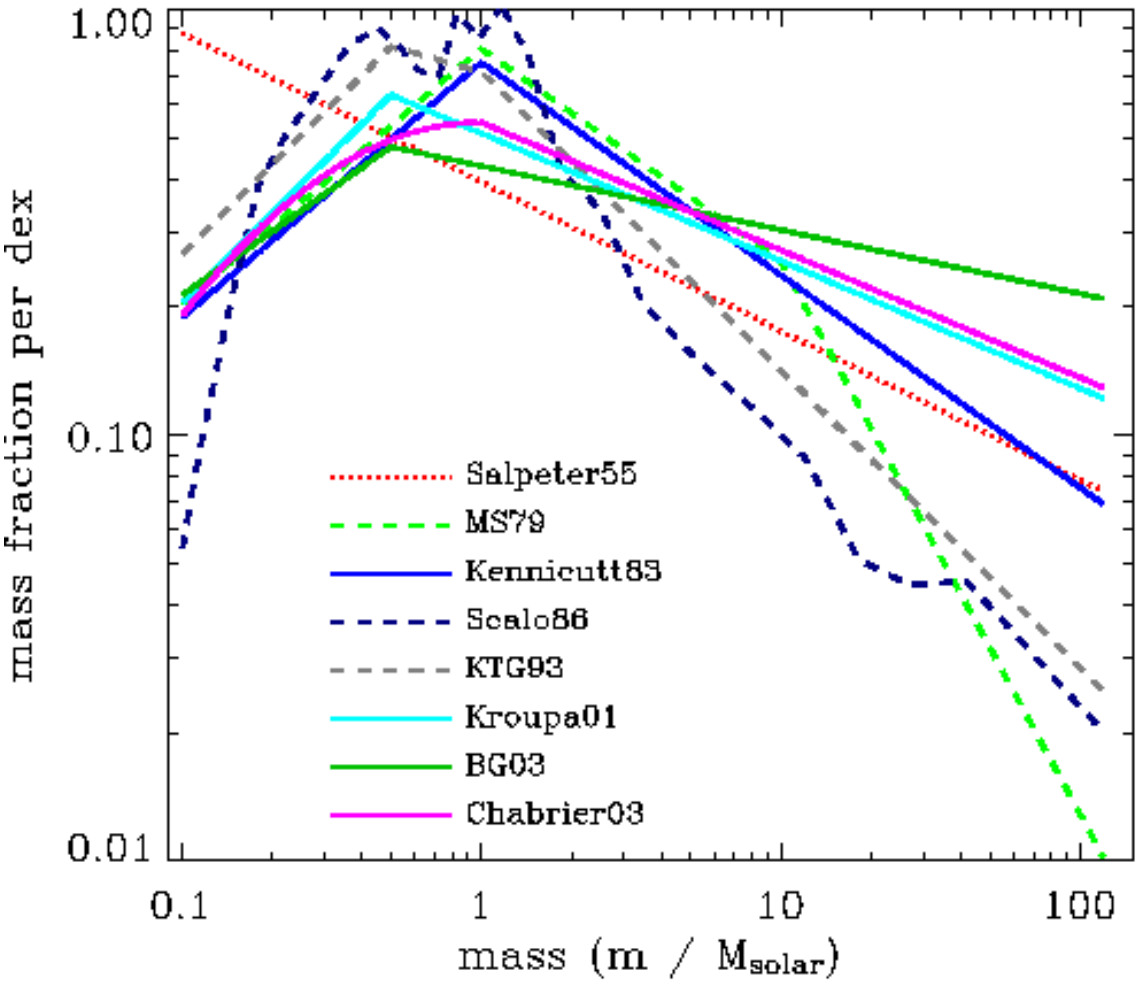

Figure 1.5: The Initial Mass Function as proposed by various authors. Figure from Ivan Baldry's research page at http://www.astro.ljmu.ac.uk/ikb/research

correlates with the age of the population, therefore metallicity needs to be well understood (Choi et al., 2016). Old age SSP tend to have high metallicity than the younger SSP.

1.4.3 Stellar population

Every point on the isochrone represents a star with a specific age, mass and metallicity with a unique spectrum. The stellar library is the collection of all the individual spectrum of stars in an isochrone. It is important to calculate the spectra of the SSPs as accurately as possible. The galaxy history can be reconstructed by combining multiple SSPs together. Different SSPs have been built by a variety of authors (Kurucz 1979; Bruzual & Charlot 2003; Jimenez et al. 2004; Vazdekis et al. (2010); Meneses-Goytia et al. 2015). There are many stellar libraries that are used in astronomy studies.

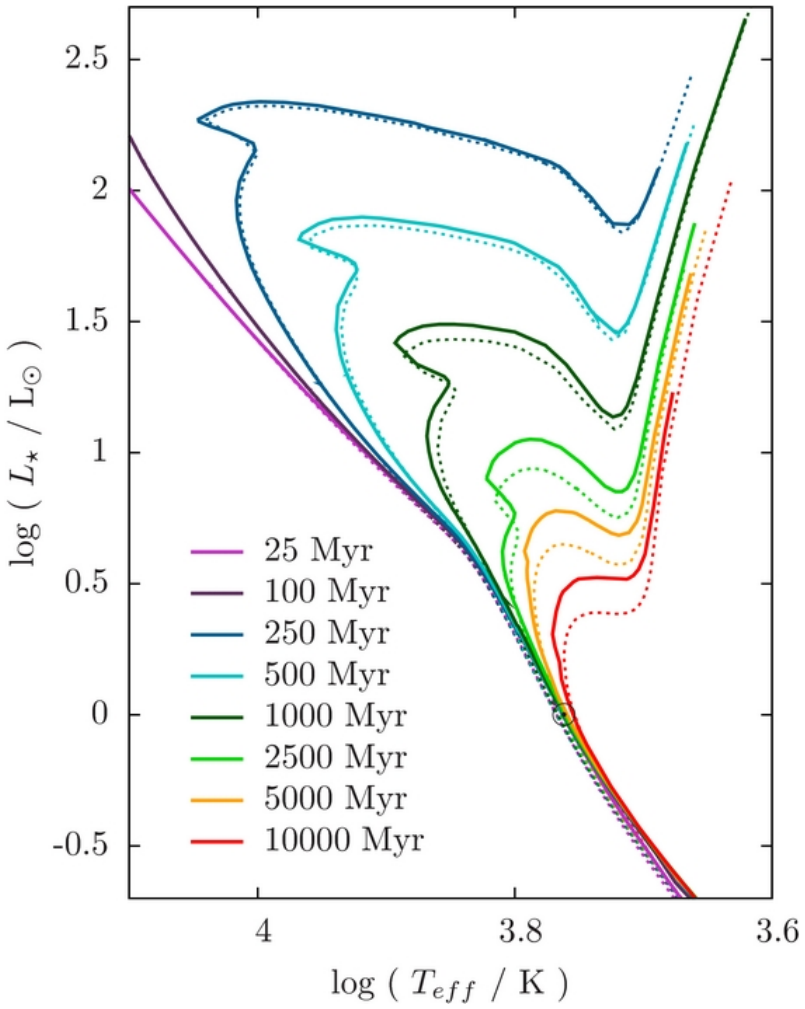

Figure 1.6: The evolution of the isochrones for a population of stars with masses between 0.7-3.5 $M_\odot$ at different ages in the life of the population. Figure taken from Casanellas & Lopes (2011).

The Indo-US empirical library is a spectral library of 1273 stars with a resolution of $\sim$ 1 Å FWHM. The library spectrum covers the wavelength between 3460-9464 Å, but only 885 stars have complete coverage in that wavelength range. This library contains physical information of its stars, e.g. metallicity, surface gravity, stellar atmospheric parameters, effective temperature, and spectral type (Valdes et al., 2004).

The ELODIE empirical library has 908 spectra of 709 stars, observed at high and low spectral resolution, R = 42 000 and R=10 000, in the wavelength range 4100 - 6800 Å. The low-resolution spectra are preferable for the modelling of the stellar population of galaxies and clusters (Prugniel & Soubiran, 2001). This library has been updated to ELODIE v.3.1, with 1962 spectra of 1388 stars and range 3900 - 6800 Å (Prugniel et al., 2007).

The MILES empirical library has 1000 stars, whose spectra were observed with the 2.5m INT telescope. It has a resolution of 2.5 Å FWHM with a range between 3525 - 7500 Å. The MILES

empirical library also has spectra for the near-IR range 8350 - 9020 Å and resolution 1.5 Å FWHM (Sanchez-Blazquez et al. 2006; Falcón-Barroso et al. 2011). Vazdekis et al. (2016), presented the new MILES library known as E-MILES that covers the spectral range 1680 - 50 000 Å at a resolution between 2.5 - 23.5 Å. The MILES library is used to build up the single stellar populations (SSPs) that we use in this work.

Each isochrone is a collection of spectra of a population of stars with same age and metallicity. A SSP is built up from the integrated flux from an isochrone. The synthetic SSPs are used to extract properties from the stellar population of a galaxy.

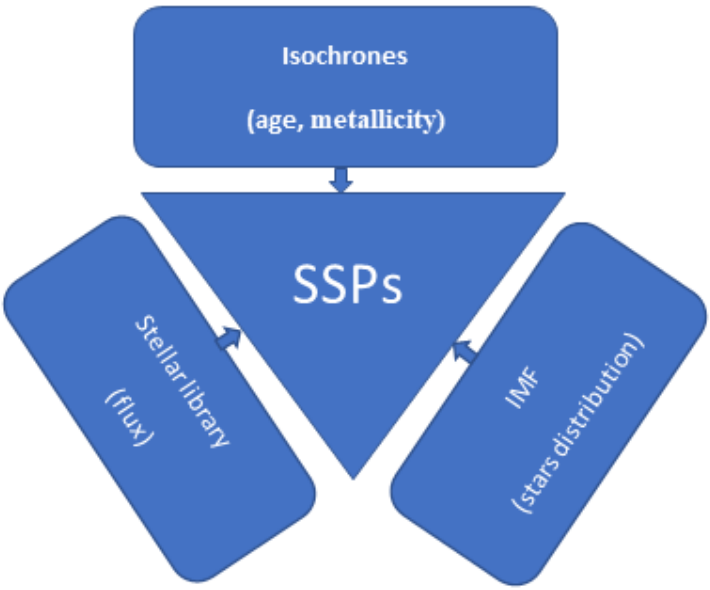

Figure 1.7: Basic ingredient for SSPs models.

1.4.4 Dust

Modelling the dust in a galaxy is another parameter that must be considered when constructing a model galaxy spectrum. Dust grains are heated by the high energy photons from O and B type of stars, causing the light to be absorbed and scattered. Dust effect is strong in the UV region, where the wavelength coming from hot stars is almost the same size, $\sim 0.1\mu$m as the dust grains and weaker in redder wavelengths. The presence of dust in a galaxy effects the calculation of some of the physical properties of a galaxy. Properties like stellar mass and SFR can by miscalculated if dust content in a galaxy is not properly uncounted for (Calzetti

et al., 2007). The luminosity function and the colour-magnitude digram, which are stander diagnostics, can be greatly affected by the presence of dust, altering the results. Young stars have a higher concentration of dust surrounding them than old stars, therefore younger and massive stars look older than they actually are.

Extinction and attenuation are two terminologies used to describe the geometrical distribution of dust for the observed galaxy. Dust extinction is the light that is absorbed and scattered out of the line of sight and is known as the optical depth, whereas dust attenuation is referring to the light that is absorbed and scattered into and out of the line of sight in a complex geometrical distribution and is known as the effective optical depth (Calzetti et al., 2000). These two terminologies summarises the one and two parameter dust models.

The one parameter dust screen model is where the dust is evenly distributed as if it is in a screen in front of the galaxy. This model affects all the stars in the model spectrum equally and considers the galaxy as a point source in the background of the dust screen. The dust screen effect on the flux intensity in the galaxy is given by:

$$\mathrm{I_e}(\lambda) = \mathrm{I_o}(\lambda) e^{-\tau(\lambda)} \tag{1.3}$$

where $\mathrm{I_o}$ is the observed flux intensity, $\mathrm{I_e}(\lambda)$ emitted flux intensity,τ optical depth of the dust screen. The extinction , A_λ, is the difference in magnitudes between the observed and emitted light:

$$\mathrm{A}_\lambda = -2.5 \log_{10}\left(\frac{\mathrm{I_e}(\lambda)}{\mathrm{I_o}(\lambda)}\right) \tag{1.4}$$

Or:

$$\mathrm{A}_\lambda = 1.086\tau(\lambda) \tag{1.5}$$

In the UBV photometric system, the colour excess, E(B-V), is related to the B-V colour by:

$$\mathrm{E(B\text{-}V)} = \mathrm{(B\text{-}V)}_{observed}\text{-}\mathrm{(B\text{-}V)}_{intrinsic} = \mathrm{A_B}\text{-}\mathrm{A_V}.$$

The normalized selective extinction is given by $\mathrm{E}(\lambda,\mathrm{V})/\mathrm{E(B\text{-}V)}$, and the normalized extinction by $\mathrm{R_V} = \mathrm{A_V}/\mathrm{A_B}\text{-}\mathrm{A_V}$, where $\mathrm{R_V} = 3.1$ for low density ISM and in dense clouds $4 < \mathrm{R_V} < 6$. (Fitzpatrick 1999; Jenkins 1987).

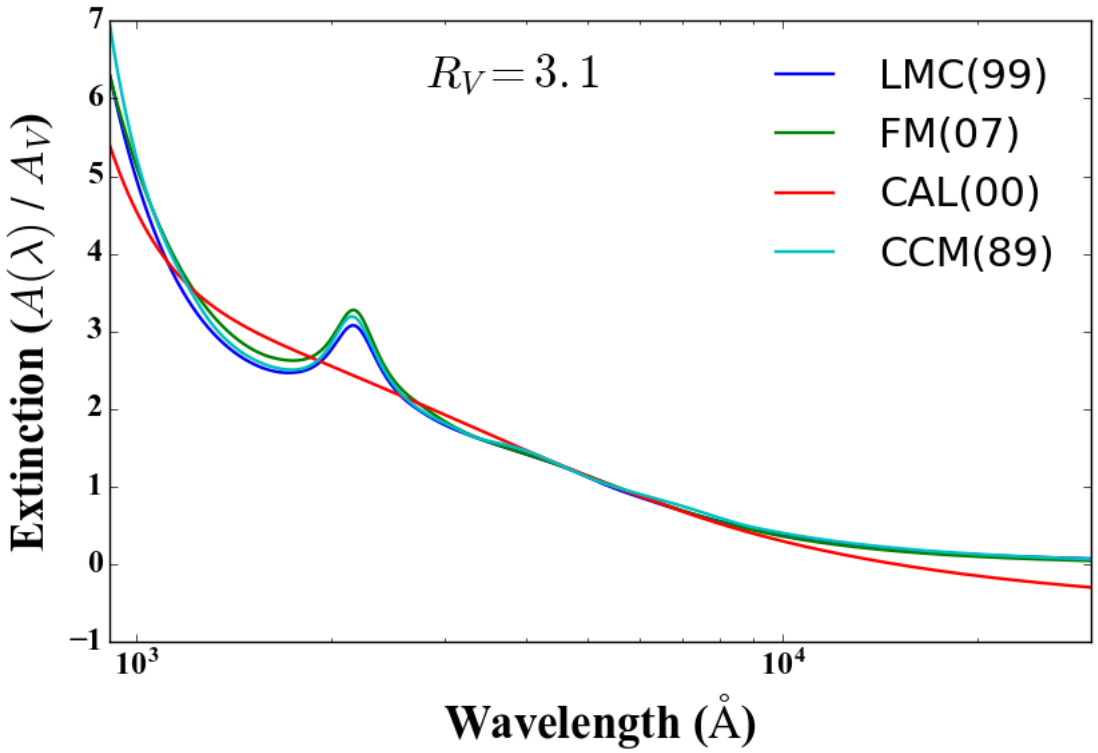

Figure 1.8: Dust curve for different screen laws from top to bottom (LMC(99) from Fitzpatrick 1999; FM(07) from Fitzpatrick & Massa 2007; CAL(00) from Calzetti et al. 2000; CCM(89) from Cardelli et al. 1989) created using code from https://pypi.python.org/pypi/extinction.

Different dust curves are demonstrated in figure(1.8). Calzetti et al. (2000) dust curve in red was determined by observations of starburst galaxies.

In a homogeneous mixture of dust and stars in a galaxy

$$\mathrm{I_e}(\lambda) = \mathrm{I_o}(\lambda)\frac{1 - e^{-\tau'(\lambda)}}{\tau'(\lambda)} \tag{1.6}$$

where τ' is the effective optical depth, which requires to include the mean effects of scattering into the line of sight (Mathis, 1983). This homogeneous mixture model provides us with a more accurate result than the screen model. In reality dust distribution throughout a galaxy is more complicated.

The two component dust model is gives a more realistic model of dust attenuation within a galaxy (Calzetti et al. 1994; Charlot & Fall 2000; Wild et al. 2011; Kriek & Conroy 2013). In this model dust is embedded within the galaxy surrounding the stars. Newborn stars have

a higher concentration of dust surrounding them then the old stars (Boissier et al. (2004); Muñoz-Mateos et al. (2009)).

In this thesis we assume a cosmology with $\Omega_M = 0.3$, $\Omega_\Lambda = 0.7$ and $h = 0.7$. All magnitudes are on the AB system.

2

STARLIGHT

2.1 Fitting codes

Quantifying information from a galaxy spectrum or photometry observation is a somewhat difficult procedure. The advances in computing have enabled astronomers to overcome major obstacles in fitting galaxy's observation data. When fitting spectra various codes are presented, either doing a photometric fitting or a spectroscopic fitting or both. Another distinction between codes is the mathematical method used to do the fitting. To illustrate, the rudimentary diagram in figure (2.1) shows the general methods used in fitting, which are found in almost all codes used. The code either obtains the physical parameters without uncertainties through a χ^2 fitting between the models and the observed spectra, or an extra Bayesian analysis step is obtained to gain the uncertainties on the physical parameters. From Bayesian probability:

$$P(A \mid B) = \frac{(P(B \mid A).P(A))}{(P(B))}, \tag{2.1}$$

where P(A) is known as the prior distribution, (P(B|A))/(P(B)) is the likelihood function (L), $\ln L = constant - \frac{\chi^2}{2}$. This probability is known as Bayes Theorem (Feigelson & Babu, 2013). The percentiles on the distribution gives the uncertainties on the physical parameters.

Some of the codes that we had access to are either found on-line or from a private correspondence with the others: penalized pixel-fitting (pPXF, Cappellari & Emsellem 2004), Bayesian Analysis of Galaxies for Physical Inference and Parameter EStimation (Bagpipes, Carnall et al. 2017) and (STARLIGHT, Gomes et al. 2004).

Figure 2.1: An illustration showing the fitting methods, either maximum likelihood or Basyesion.

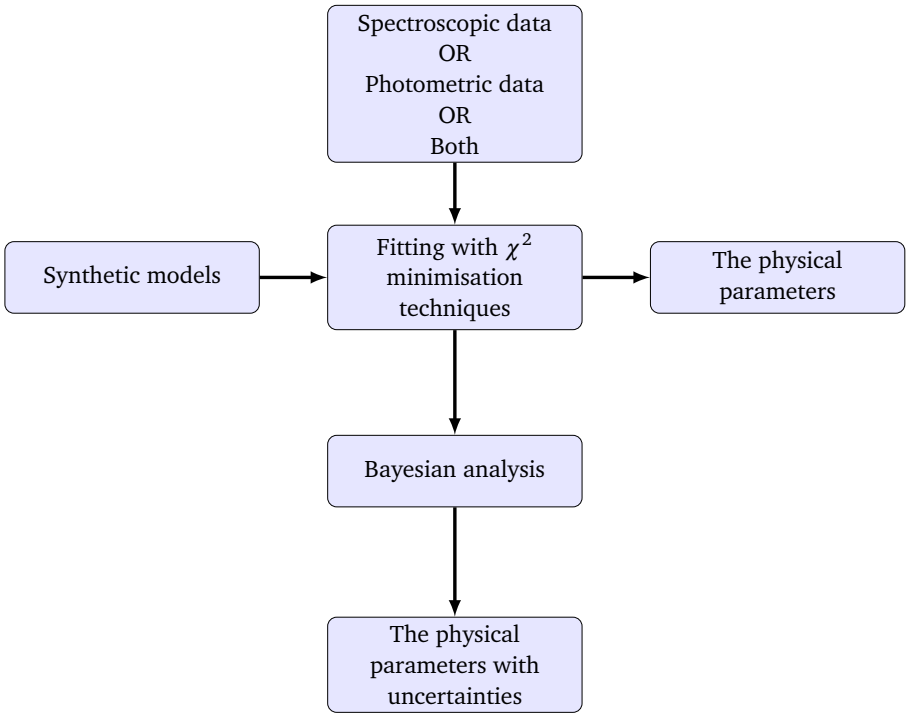

pPXF has traditionally been used in constraining stellar kinematics by using a Gauss-Hermite series in pixel space. This code recovers the line of sight velocity distribution by convolving the model spectra and fitting it in pixel space with the observed spectra. It has proven to be a powerful tool in obtaining galaxy stellar or gas kinematics. Recently it has been updated to provide stellar population from absorption-line spectrum.Allen et al. (2015); Ho et al. (2016) and Cappellari (2017) are some examples on the work done with pPXF code.

The Bagpipes code is used to fit the spectrum of a rapidly generated model, galaxy with spectrum and photometric data of an observed galaxy. The code uses the MULTI NEST algorithm (Feroz et al., 2009), which is the Bayesian analysis method used to calculate the parameter

and the error on it, as well as producing a posteriori samples from the distributions that may contain multiple modes, to fit the arbitrary combination of the spectrum and photometric data. Bagpipes includes gas emission lines, warm dust emission, ionized continuum emission and absorption lines to be fitted in the code. The star formation history (SFH) predicted from this code for quiescent galaxies is a double power law and not an exponentially declining model. The double power law explains the presence of red galaxies at high redshift with SFH that rises an declines rapidly time-scale $\lesssim$ 1 Gyr.

As for STARLIGHT, it combines multiple SSPs into a model spectrum and fits it with the observed spectrum, this method is more reliable than having a single SSP to be fitted. For STARLIGHT code, Mateus et al. (2006) showed that their algorithm is improved compared with earlier release of the code and it is running more efficiently with a multiple Markov Chain in parallel. Cid Fernandas et al. (2005) tested STARLIGHT code on 50,000 SDSS galaxies and abtained high quality results from fitting a synthetic model with the observed spectrum giving an accurate parameter measurement. STARLIGHT has also been compared with other codes such as the MPA/JHU group (Kauffmann et al. 2003b; Brinchmann et al. 2004) and shows very competitive results. Many astrophysical correlations have been reproduced using STARLIGHT, proving it to be a reliable tool for studying the evolution of galaxies. The main disadvantage of using STARLIGHT as described by Panter et al. (2004) is that it is slow and uses brute force and is not using a Bayesian technique, unlike more modern codes. A recent version of the code has combined the fitting spectra and photometric. In this work, STARLIGHT has been modified to the special properties of post starbursts (PSB) galaxies. PSB may have a strong burst in the last 1 Gyr or 1.5 Gyr, therefore we adjusted STARLIGHT to show that feature in the SFH of the galaxy.

In the next sections, we will address the statistical method used by STARLIGHT, the input files and the adjustments done on the input spectrum, the emission line file and the wavelength range used to mask over the emission lines for the SDSS data, the base file, the grid file and we show the information obtained from the STARLIGHT code. We will also use the new STARLIGHT code fitting both the spectrum and photometric data at the same time.

2.2 STARLIGHT

2.2.1 Fitting spectra

In this work we use the Bruzual & Charlot (2003) [here on referred to as BC03] synthesis models. From STARLIGHT we gain the stellar population properties of the fitted model, which is used to determine galaxy properties. STARLIGHT basically revolves around finding the maximum likelihood. The model spectrum is a sum of a random sequence of N* simple stellar populations (SSPs) that are combined to create the fitted model spectrum. The model spectrum M_λ is composite:

$$M_\lambda(\overrightarrow{x}, A_V, \upsilon_*, \sigma_*) = M_{\lambda_\circ}[\sum_{j=1}^{N^*} b_{j,\lambda} 10^{-0.4(A_\lambda - A_{\lambda_\circ})}] \otimes G_{(\upsilon_*, \sigma_*)}, \tag{2.2}$$

where $G_{(\upsilon_*,\sigma_*)}$ is the stellar motion in the line-of-sight that can be calculated by using a Gaussian filter, with mean velocity υ_* and the standard deviation for the dispersion σ_* both in km/s. A_λ is the galaxy's attenuation and is modelled as uniform dust screen from Cardelli et al. (1989) with R_V=3.1, R_V is the ratio of the total to the selective extintion, and is parametrized by A_V. $b_{j,\lambda}$ is the spectrum of the j-th SSP normalized at $\lambda_\circ$. $M_{\lambda_\circ}$is the synthetic model flux spectrum which is normalized at 4020 Å. $\overrightarrow{x}$ is a vector with components x_j that represent the contribution of each individual SSP in the base to the total synthetic flux at $\lambda_\circ$. The SSP, are a combination of stellar spectra at stars that are born at the same time and have the same initial metallicity with the Chabrier (2003) initial mass function (IMF) with a range between 0.1 and 100 $M_\odot$, see section 1.4.1. STARLIGHT operates with the full resolution of the spectrum. The code works over many dimensions of parameters, N*, that are added up to be fit with the observed data (Cid Fernandas et al., 2005) using the maximum likelihood fitting method.

$$\chi^2_{Spec} = \sum_\lambda [(O_\lambda - M_\lambda)\omega_\lambda]^2, \tag{2.3}$$

where the minimal χ^2_{Spec} gives the best spectrum fitted model, ω_λ is the inverse of the errors for the observed data, also known as the weight of the spectrum at a specific wavelength. O_λ is the observed spectra and M_λ is the model spectrum (Gomes et al., 2004). STARLIGHT code can be downloaded at http://www.starlight.ufsc.br.

2.2.1.1 Properties of the input spectrum

The input spectrum data file contains the wavelength, flux, error and mask arrays. The data point of the observed file has been processed:

- The observed galaxies wavelength is shifted to rest frame wavelength in the ranges 3600 to 9000 Å. It is recommended to work with $\triangle\lambda = 1$ for the observed galaxies wavelength, which is the same as the model spectrum in the optical wavelength. Nevertheless if the observed data resolution is not as the model, STARLIGHT will interpolate the model spectrum to match it.
- The observed SDSS spectrum is in vacuum wavelength, whereas the model spectra is in air wavelengths. Therefore, we convert the wavelength from vacuum, SDSS spectrum, to air wavelength (Morton, 1991).
- The observed flux can be in either (erg/s/cm^2/Å) or ($L_\odot$/Å) units.
- The observed spectra flux must be calibrated properly so that any bad pixels are removed, we flag them so that STARLIGHT does not take them into account while doing the fitting. Bad pixels in the observed data are included in the input file to have a flag of 99 that will be assigned a weight, ω_λ, equal to zero. The good pixels are flagged to be zero or one.
- The observed flux has also been cleared to remove residual sky features and strong OH sky emission lines, between 6700 to 9000 Å (Wild & Hewett, 2005), to improve the signal to noise ratio, of the spectrum in that area.
- The observed spectrum is also corrected for the Galactic extinction.
- We flag the region of sky lines that appear in the spectra at the observed wavelength and two region wavelengths that are considered as telluric contamination, the wavelengths are in table (2.1) .

Table 2.1: The mask region prominent for sky emission lines, which we flag as bad pixel in the galaxy spectrum input file.

Beginning wavelength for the sky line Å	Ending wavelength for the sky line Å
4276.0	4282.0
5574.0	5590.0
6297.0	6305.0
6364.0	6368.0
6845.0	6945.0
7550.0	7725.0

2.2.1.2 Emission and interstellar medium (ISM) line mask

The spectrum continuum is the only component that STARLIGHT is fitting, therefore we mask all emission and ISM lines. Masking out a region in the spectra can be either enforced by flagging it in the input file or by using the mask file, which contains the wavelength ranges we mask to exclude in Å . Although we exclude the same set of emission lines as (Asari et al. 2007; Cid Fernandes et al. 2005; Mateus et al. 2006), nevertheless we alter the spectra wavelength range masked, gaining a more precise masking of the emission lines. We preform a preliminery run of STARLIGHT on the spectra then stack the residuals for the various types of galaxies used in this study. The stacked residuals show a clear marker for the beginning and the ending of the emission lines. Figure (2.2), shows the residuals of most of the well known emission lines in the optical region. The grey areas are the altered mask limits used in this work and the red lines is the mask used is in Cid Fernandas et al. (2005).

Table 2.2: shows the emission line areas, the begining and the ending, that were masked and used with StarLight and the emission line chemical symbol and the equivalent emission line wavelength in Å.

Beginning wavelength Å	Ending wavelength Å	Chemical symbol for the emission line	Notes
3863.0	3873.0	[NeIII]	3869 emission line
3967.0	3976.0	H_ϵ	3970 emission line
4099.0	4110.0	H_δ	4102 emission line
4335.0	4345.0	H_γ	4340 emission line
4855.0	4867.0	H_β	4861 emission line
4952.0	4966.0	[OIII]	4959 emission line
4994.0	5019.0	[OIII]	5007 emission line
5869.0	5879.0	HeI	5876 emission line
5882.0	5903.5	NaD	5890 ISM absorption line
6290.0	6310.0	[OI]	6300 emission line
6540.0	6597.0	H_α & [NII]	6563,6548 & 6583 emission lines
6706.0	6741.0	[SII]	6717 & 6731 emission lines

The new mask emission line regions are included in the table (2.2). We use two different masks, one for the galaxies with emission lines, and one for galaxies without. Both mask files remove the telluric features, wavelengths in 2.2, because the BC03 library has synthetically built-up this region with a poor resolution.

2.2.1.3 SSPs

We initially used the SSPs library obtained from the same website as STARLIGHT. The library uses the Padova evolutionary tracks (Bertelli et al., 1994), from the BC03. It includes six metallicities 0.0001, 0.0004, 0.004, 0.008, 0.02 and 0.05, $0.02 = Z_\odot$, with 221 ages, ranging from 0 to 20 Gyr. The whole library covers a total of 1326 SSPs spectra models. An improvement in STARLIGHT from its early launch has been achieved by increase in the number of SSPs that can be fitted the "base", N^*, going from 45 to 150, and in the current work we use 300 SSPs. The high number of base enable us to include 60 ages of SSPs ranging from 180×10^3 to

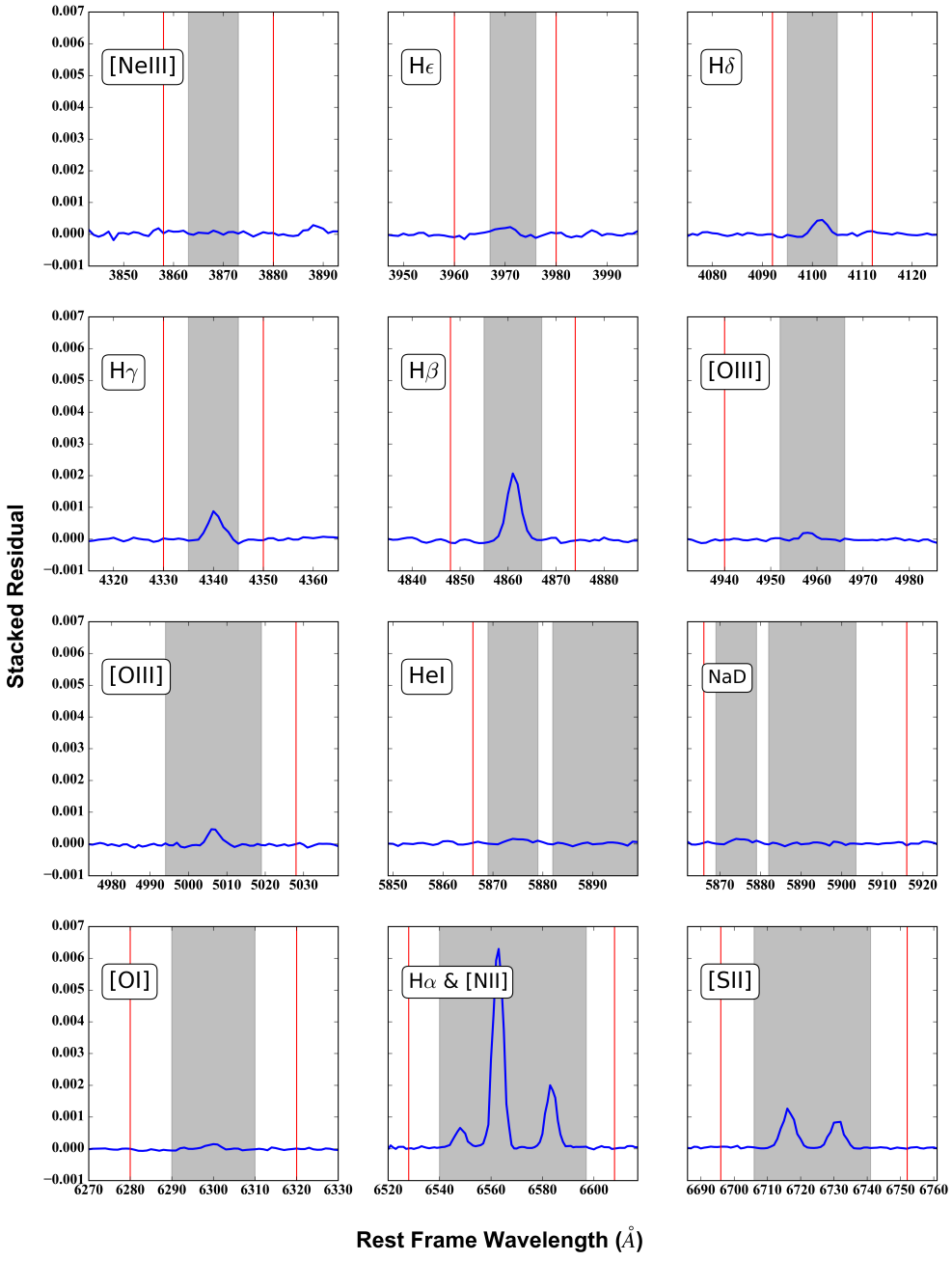

Figure 2.2: The stacked residuals for the star forming galaxies in the low mass bin of our SDSS sample. The stacked residuals are on the y-axis and the rest frame wavelength is on the x-axis for the emission lines from top left to bottom right ([NeIII], H_ϵ, H_δ, H_γ, H_β, [OIII] at 4959Å [OIII] at 5007Å HeI, NaD ISM absorption line, [OI], H_α and [SII]). The red lines show the mask limits used to fit the SDSS sample in Cid Fernandes et al. (2005). The grey area is mask limits used in this work.

13.75×10^9 years, but including only the highest five metallicities'. We reject the lowest metallicity provided from the library, because there are not so many, if not none, stars at low redshift with this low metallicitiy. In the base file, most of the SSPs ages are concentrated in the region between 10^8 and 2×10^9 years, so that we are able to notice the star formation burst considered to be a distinguishing signature of PSB galaxies. By using this specific concentration, we aim to see the declining star formation history and the starbursts that may be observed around 1Gyr. The used base gave acceptable results for the SFH for individual galaxies. Nevertheless, the stacked star formation history for almost all the sample type used in this work showed an artificial, has no physical meaning, increase in the fraction of mass higher at the ages of 1.60, 1.67, 1.69 and 1.79 Gyrs than the usual fraction of mass produced from the declining of the continuum of the star formation history. Figure (2.3) shows the artificial bump which is noticed with this library.

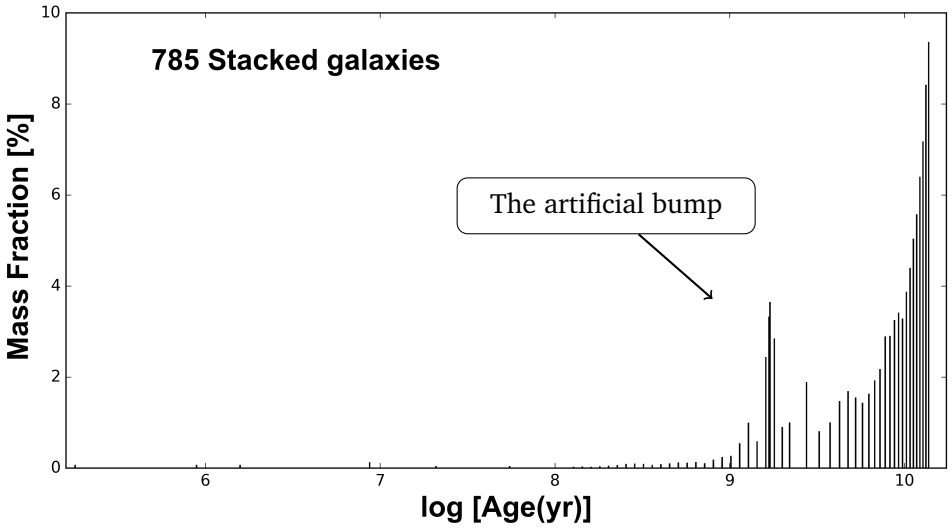

Figure 2.3: The star formation history where the mass fraction of 785 star forming galaxies are stacked in black for the SSPs at different times in the galaxy's age. We use 60 ages of SSPs from 180×10^3 to 13.75×10^9 years and the highest five metallicities in the stelib stellar library. We can notice the artificial bump in the SSPs ages 1.6, 1.67, 1.69 and 1.79 Gyrs. The library is from http://www.starlight.ufsc.br/node/3.

The location of this inaccurate increase in the fraction of mass contaminates any required results, in particular the actual burst we aim to gain throughout the samples. Due to this unwanted feature, we used the second library. The library was provided from MILES (Vazdekis et al., 2010). In this library extra metallicity was adding to the higher end, $0.1 = 5\ Z_{\odot}$, in-

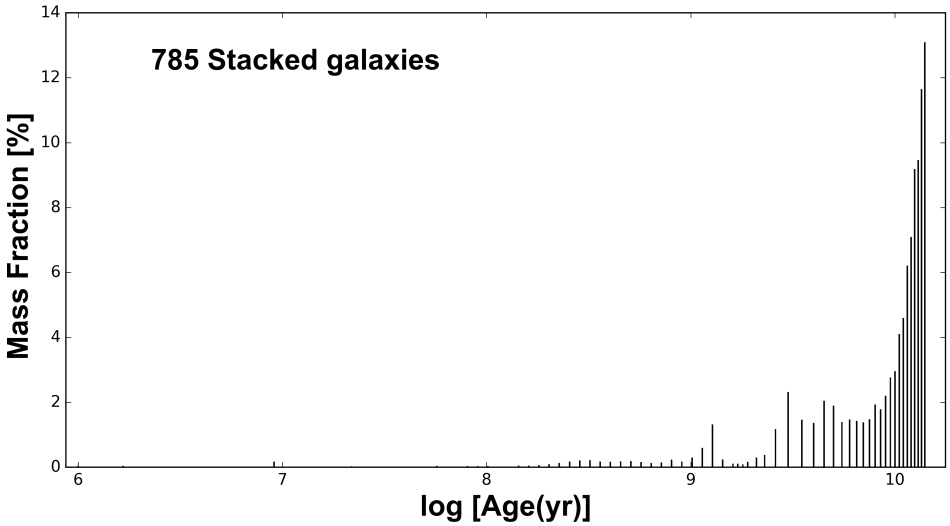

Figure 2.4: The star formation history where the mass fraction of 785 star forming galaxies are stacked in (black) for 60 SSPs ages from 1×10^6 to 14×10^9 years. MILES stellar library is used here, where the artificial bump is highly improved, but not entirely resolved, as we have some slight increase in the mass fraction for the SSPs at 1.276 and 2.576 Gyrs.

creasing the total number of metallicities used in this library from the first library, but this metallicity is not used here. For this new library, we used the ages of 220 SSPs, which are arranged from 100,000 years to 20Gyr. The MILES library cover a total of 1540 SSPs spectra models. Building up the base by using this library, we use the same configuration as before, where the artificial feature is significantly weaker. Figure (2.4) shows the stacked SFH of 783 star forming galaxies fit with the new library, showing the reduced artificial bump.

2.2.1.4 Dust law

We were able to change between two extinction laws the CCM (Cardelli et al., 1989) and the CAL (Calzetti et al., 2000) to see if the dust laws has any effect on the output results from the fitting. The CCM is a polynomial extensions laws that of Cardelli et al. (1989). The CCM law can have a value of Rv from 2.75 to 5.3, STARLIGHT uses $R_V = 3.1$. The R_V is the ratio of the total to the selective extinction as $R_V = A_V$ / (A_B - A_V). Where A_V and A_B are the extinction in the V and B bands. The CAL law from Calzetti et al. (2000) is valid between 912 to 22000 Å . They show that for this law that it works in a reasonably good way for spectra of galaxies that have dominating massive stars in their population. The CAL law has a value of $R_V = 4.05$. The high R_V for the CAL law is observed for the starburst galaxies, which have a higher concentration of dust from the relatively high number of birth and death of massive stars.

2.2.1.5 Output

The top and bottom of figure (2.5) shows the normalized of both the spectrum of the fitted galaxy and the best fit model, the noise and the residual, all shifted to the rest frame wavelength in Å . The top left of the plot shows the ID number for the observed galaxy. We have the log of the galaxies' mass shown in the top middle of the plot, this is the mass calculated for only the spectra that is observed from the fibre optics. The top right number is the galaxy attenuation from the dust, averaged throughout the galaxy, in magnitude units. The primary results that are being used in this work were obtained from the figure (2.6).

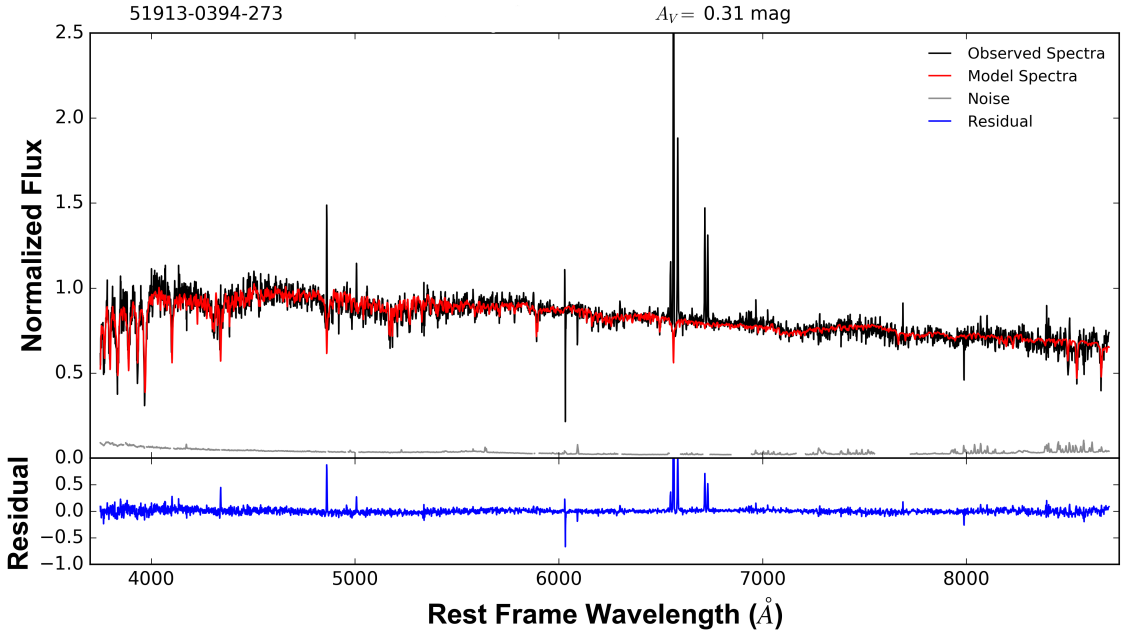

Figure 2.5: The normalized flux of the observed spectrum for a star forming galaxy (Black) the galaxy's ID (top left) with its noise in grey and the best fit model in red. The residual in blue is the difference between the observed and best fit model. The galaxy attenuation due to dust Av (top right) is for a uniform screen dust law model.

The two figures in the plot show the light fraction (top) and the mass fraction (bottom) that has been produced throughout the galaxy star formation history. The fraction of light is colour-coded showing the metallicities that have been implemented from the SSPs library. Whereas the fraction of mass shows only the stellar mass throughout the galaxy lifetime until the observation time. We also obtained the signal-to-noise ratio and has been shown in the plots. STARLIGHT calculates the S/N from calculating the mean for the observed spectra over the root mean square. We also show the reduce chi-square, which implies the goodness of the fit.

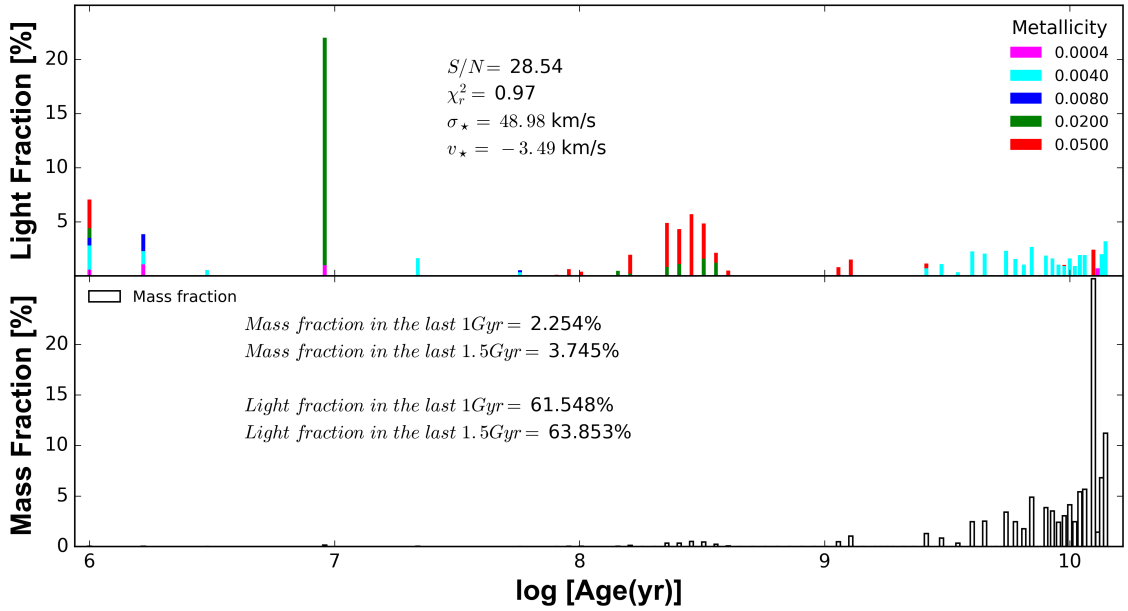

Figure 2.6: The output data from STARLIGHT is shown here: the light fraction (top), colour coded based on the metallicity, and the stellar mass fraction (bottom) that has been produced throughout the galaxy star formation history (SFH). The reduced chi-square, χ^2_r, gives the accuracy of the fit. The velocity dispersion σ_* and the velocity v_* are both in km/s. We calculated the fraction of light and mass produced in the last 1 and 1.5 Gyrs since the time of observation.

A reduce chi-square number around one is the somewhat considered a good fit. The velocity v_* for the observed galaxy will range around zero for a well redshifted galaxy and σ_* the velocity dispersion both in Km/s units.

2.2.1.6 Testing the recovery of recent SFH with STARLIGHT

From the output file, we can calculate the mass fraction and the light fraction that has been transformed into stars in the last 1 and 1.5 Gyrs of the galaxy SFH.

In this work, despite the various information provided from the output file our main interest is the SFH of the galaxy and the fraction of mass accumulated in the last 1 and 1.5 Gyrs. Therefore, and despite being STARLIGHT well tested, we conducted an input vs. output test to see how good STARLIGHT is in retrieving the mass fraction produced in the last 1 and 2 Gyrs. The test excluded the 1.5 Gyr limit due to having only 1 and 2 Gyr in the stochastic mock galaxies that are used for the test. These synthetic galaxies have the properties:

- 13.7 ≥ age (Gyrs) ≥ 5.0.
- Number of star bursts = 1.
- Time of the bursts from the observation $1{\times}10^6$ years ⩽ time < 1 Gyr.
- The fraction of mass formed in the burst 1% to 20%.

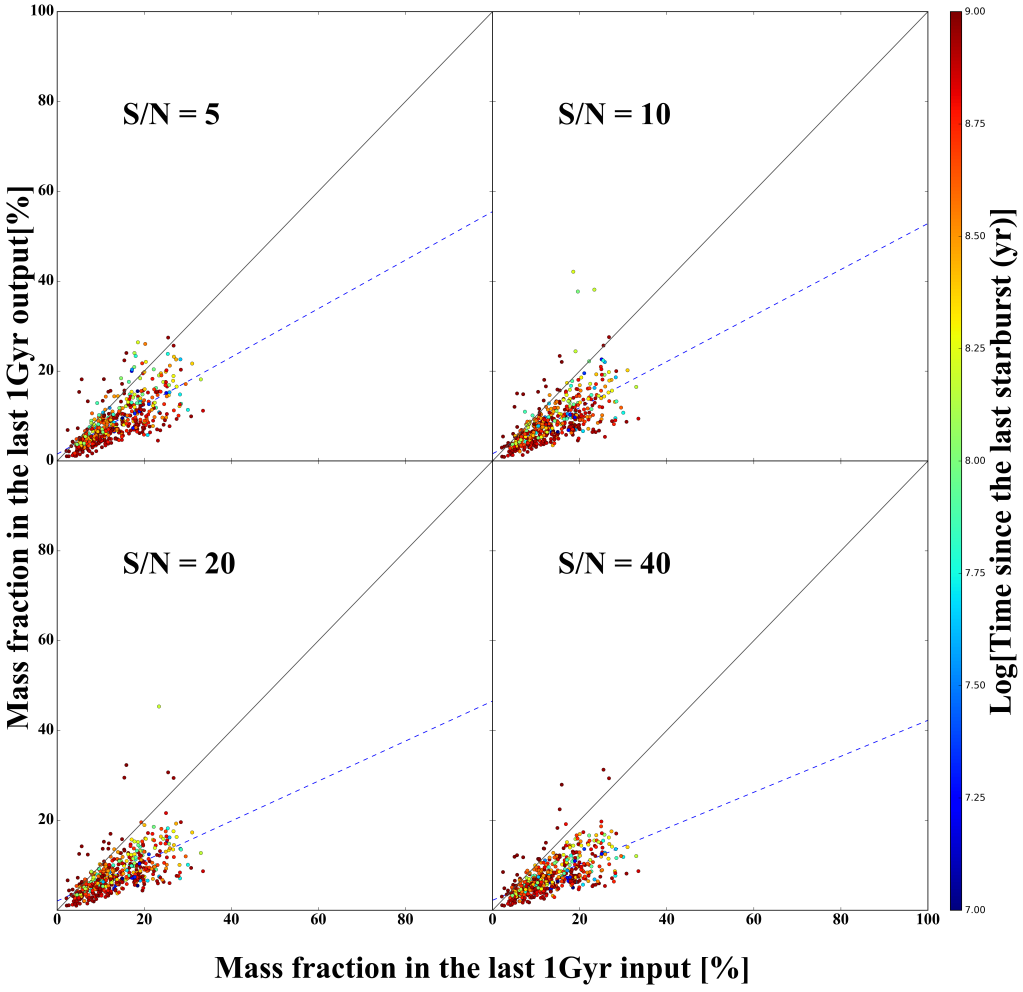

Figure 2.7: Output vs Input values for the simulated data as fitted by STARLIGHT. We see the fraction of mass retrieved from the spectrum of synthetic model galaxies with signal to noise ratio of 5, 10, 20 and 40. The plot shows the fraction of stellar mass that has been accumulated in the last 1 Gyr. The (Blue) dashed line is the linear regression for the points. The color-coded is based on the time since the last burst in a log scale ranging between 10 million years in dark blue to 1 Gyr in dark red.

We fit 492 mock galaxies spectrum with STARLIGHT. Figure (2.7) and (2.8), shows the fraction of mass input and output results with signal to noise ratio of 5, 10, 20 and 40. The black line is the one to one ratio, the line where the data point should be on, and the blue dashed line is the linear regression line for the mock galaxies. Fig. 2.7 shows an underestimation of the retrieved information which may be caused by STARLIGHT not considering the dust obscuring young, massive stars, having to use a screen dust law in its fitting. Thereby slightly miscalculate the actual fraction of mass that has been produced during the last 1 Gyr. Whereas for the mass fraction in the last 2 Gyrs, fig. 2.8, we see that STARLIGHT slightly less underestimates the

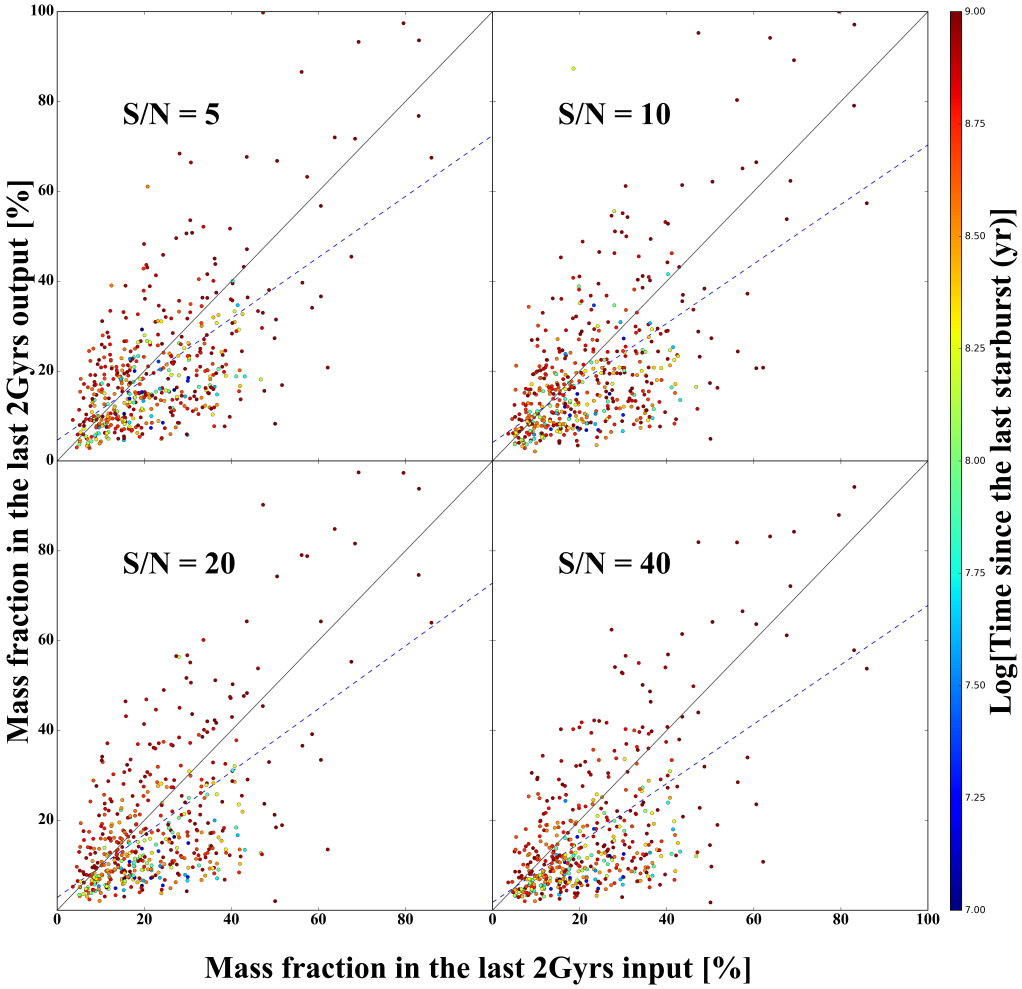

Figure 2.8: The same as the 1 Gyr plot above, but the mass fraction is for the last 2 Gyrs.

mass fraction that has been produced. The fraction of mass at 2 Gyrs is the combination of the mass from the starburst, young stars, and the typical star forming, old population, which is less effected by the dust. The old stellar populations is overwhelming the mass fraction for the last 2 Gyrs, therefore less affected by the dust. The test has been done on both the CCM and CAL dust laws with almost the same conclusion.

2.3 The new STARLIGHT

The new STARLIGHT code combines spectra and photometry in its fitting, requires minor adjustments to STARLIGHT original spectroscopic fitting files. López Fernández et al. (2016), shows the adjustments made on these files and the mathematics applied to STARLIGHT. In this new version it is possible to use an arbitrary combination of spectra and photometry data, in which the maximum likelihood is calculated for each one of the data types, spectrum and

photometry, then combined in a total χ^2_{Tot}.

$$\chi^2_{Tot} = \chi^2_{Spec} + \chi^2_{Phot}, \tag{2.4}$$

where χ^2_{Spec} is shown in equation 2.3. The photometric χ^2_{Phot} is weight with a factor than added to the total maximum likelihood [New STARLIGHT user manual, Werle, A. and Gid Fernande, R., private correspondence]. Spectral observation has a higher number of data points than the photometric observation. And each point is in a specific wavelength containing information regarding that wavelength. Whereas the photometric observation point contain information from a broad region that may extending to a multiple wavelengths. χ^2_{Phot} is calculated from

$$\chi^2_{Phot} = \sum_{i=1}^{N_i} \left(\frac{m_i^{obs} - m_i}{\sigma_i} \right)^2, \tag{2.5}$$

where N_i is the number of photometric points used in the fitting. m_i^{obs} is the observed magnitude for a specific filter and σ_i is the error on it. m_i is the model magnitude. The spectrum input file requires the spectra to be shifted to the rest-frame wavelength. whereas the photometric data points are at observed frame. Thereby not requiring to do any K-corrections on the observed filter points. As STARLIGHT shifts the model spectrum to the observed frame than calculate the magnitude for the filter point from using a filters transmission curves.

2.3.1 Adjustments to STARLIGHT

To fit the ultra deep survey spectrum (UDSz) and its photometric data points, UDS, we adjusted some of the new STARLIGHT input files.

- In the executable file of the code we expand the limit of the new STARLIGHT code to include 3.6 μm photometric filter.
- As for the base file with the SSP ages, we removed the old SSP age for the high redshift galaxies, $1.05 < z \leqslant 1.2$, for the information gained from fitting that age will exceed the age of the Universe.

2.3.2 The mask file for the UDSz

From the stacked spectrum from each type of galaxy in the UDSz, we determine the emission lines region and adjusted the masked range that is applied in the mask file as we include an

individual file for each type of galaxies. We form four mask files:

1. For the star forming galaxies type we mask emission line in the regions that are included in table 2.3. This file is used to mask the emission lines in SF1, SF2 and SF3 type of galaxies.
2. The dusty type galaxies table 2.3 is also used except for the [OII] emission line range is 3716 - 3736 Å.
3. The PSB type galaxies we mask only the [OII] emission line in the region, 3721 - 3734 Å.
4. The Red type of galaxies we used a mask file having only the [OII] emission line region, 3722.5 - 3735.5 Å.

Table 2.3: shows the emission line areas for the star forming galaxies in the UDSz, SF1,SF2 and SF3 the begining and the ending, that were masked and used with STARLIGHT and the emission line chemical symbol and the equivalent emission line wavelength in Å.

Beginning wavelength Å	Ending wavelength Å	Chemical symbol for the emission line	Notes
3712.0	3743.0	[OII]	3727 + 3729 emission line
3881.0	3895.0	H8	3890 emission line
4094.0	4109.0	H_δ	4102 emission line

All these limits are calculated from the stack spectrum of each type of galaxies, fig. 2.9.

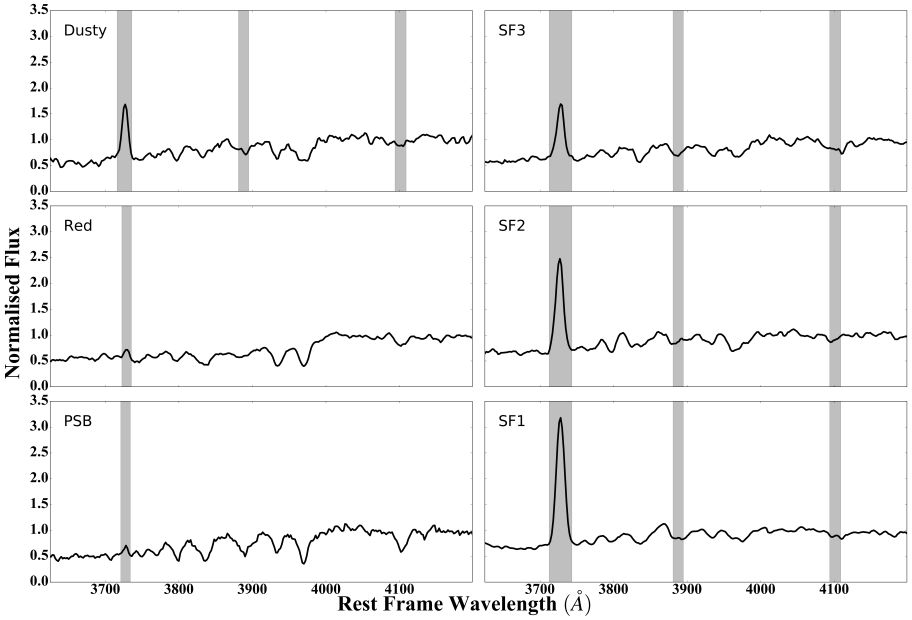

Figure 2.9: The stacked spectrum for 10 PSB, 63 Red, 30 Dusty, 122 SF1, 52 SF2 and 46 SF3 galaxies from the UDSz data. THe flux has been normalised at 4020 Å. The masked regions are in grey.

3

Post Starburst Galaxies in the SDSS

3.1 The Sloan Digital Sky Survey (SDSS)

The SDSS was initiated in 2000, covering an area of 10,000 deg^2 in the Northern Galactic cap and an additional three strips in the South Galactic cap. It covered more than a third of the sky and had spectra for more than three million objects chosen from more than 500 million photometric targets. The survey was conducted with the 2.5m Apache Point Observatory telescope. The survey includes images with u, g, r, i and z filters and spectroscopic observations. It provided a 3D image that can be as deep as redshift $= 6$ for some quasars, whereas the primary galaxy sample has an average redshift $= 0.1$. For further information on SDSS see Stoughton et al. (2002).

The seventh Data Release (DR7), one of many data releases in the SDSS, has been used in this study (Abazajian et al., 2009). The DR7 spectroscopy survey covers two areas: Legacy field surveys with 8032 deg^2, which is the primary galaxies survey and SEGUE field survey with 1348 deg^2. The Legacy survey used 1802 plates with 640 fibres each. Each fibre has an

aperture of 3″ in diameter. The spectrum data has 4096 pixel points for a wavelength range of 3800 - 9200 Å. Galaxies are observed with a resolution of 1800, ∼167 km/s, between 3800 - 6150 Å and 2000, ∼150 km/s, between 5800 - 9200 Å. Galaxies were chosen for a followup spectroscpic survey based on the photometry survey. The spectrocopic survey has a magnitude limit in the r-band = 17.77 and two more deeper fields with a magnitude in the r-band = 19.2 and 19.5 taking into consideration galactic extinction in Schlegel et al. (1998). In the Legacy survey, the total number of spectra spectroscopically classified as galaxies is 929,555; their sky distribution is seen in figure (3.1).

We used the high number of spectroscopy observed galaxies in the DR7, which increases the probability of detecting a statistically significant number of PSB galaxies to use in this work.

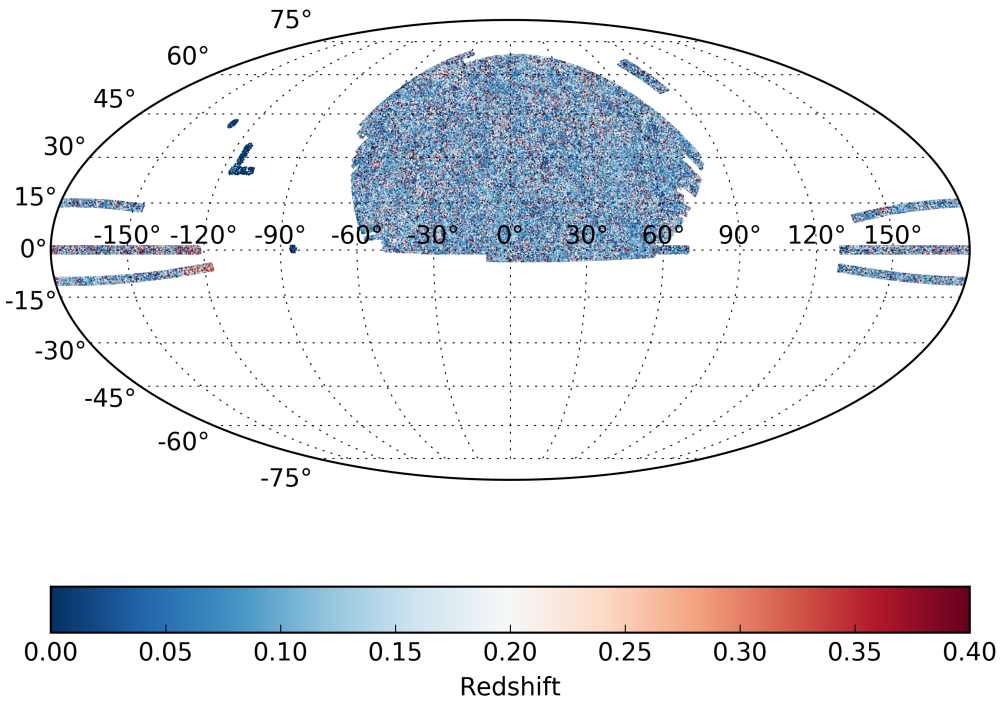

Figure 3.1: An Aitoff projection of the galaxies in SDSS DR7 showing 929,555 galaxies, which are colour-coded based on each galaxy's redshift range 0 <z <0.4.

3.2 Sample selection

3.2.1 Selection criteria and spectra processing

Our sample was selected from the Legacy survey based on the following critera from Pawlik et al. (2018):

- A magnitude cut between 17.7 and 14.5 in the r-band.
- A maximum and minimum redshift of 0.05 and 0.01, respectively.
- We select galaxies that are statistically complete in the red sequence with mass higher than $\log(M/M_{\odot}) > 9.5$.
- The sample selection of PSB galaxies and the control sample, passive galaxies (PAS) and star forming (SF) galaxies was from the spectral characteristics. All edge-on galaxies having a projective axis ratio greater than 0.32, 75° inclination angle, are removed.
- A spectrum signal to noise ratio (SNR) ≥ 8 in the g-band.

The sample is divided into two mass bins ($M/M_{\odot}$) $>3 \times 10^{10}$ high mass bin and ($M/M_{\odot}$) $<3 \times 10^{10}$ low mass bin. The 3×10^{10} cut limit on the $M/M_{\odot}$ is the mass at which galaxies split predominantly in to red spheroids or blue disks in the local Universe (e.g. Kauffmann et al. 2003a). The stellar mass for each galaxy is calculated from the SDSS-MPA/JHU catalogue, from fitting stellar populations models to the 5-band photometry. The models include two component dust attenuation, changing metallicity and include stochastic starbursts (Brinchmann et al., 2004).

The galaxy spectra used in this study are processed to remove any skyline residuals in the red end of the spectra. Wild & Hewett (2005) provides a detailed description of the method used to discard the prevailing OH skylines from the sample spectra. The spectra are also amended for Galactic, Milky Way, dust reddening. The spectral observation is limited for the low redshift and massive galaxies to the centre area of the galaxies, 0.6 - 3 kpc, as the observations are done with a fixed $3''$ aperture fibre. It has been found from merger simulations that gas falling to the center of the galaxy due to the merger, (Barnes & Hernquist, 1991), will cause a central starburst, which would be detected in the observation and our main interest.

3.2.2 Method of selection

The Principal Component Analysis (PCA) method is a standard multivariate analysis technique, utilized to identify the PSB candidates and separate them and the control sample galaxies used in this work (Wild et al., 2007). This technique combines features in the galaxy's optical spectra that vary together. Galaxy spectra can be visualised as a one dimension flux array with n-values or as one point in an n-dimensional space. A set of galaxy spectra can be imagined as a group a of points in n-dimensions. For these points the line of greatest variance is computed, and forms the first principal. The subsequent line of greatest variance, constrained to be orthogonal to the first is the second principal component (and so on). A stochastic burst BC03 library is used to calculate the components, similer to that used in Gallazzi et al. (2005).
This method is applied to the spectra wavelength in range between 3750 and 4150 Å . In this range the PCA method identifies the first principal component (PC1) as the strength of the 4000 Å break, and the second principal component (PC2) is related to strength of Balmer absorption lines. Both PC1 and PC2 depend on the stellar population, star formation history, of the galaxy. High specific star formation rate galaxies are seen at the left area of the distribution. Whereas PC1 with high values shows galaxies that are dominated by an old population of stars and low star formation rate and PSB galaxies with a strong Balmer absorption lines have a high PC2. The top row figure (3.2) shows the PC1 - PC2 distribution for our sample. The sample used, PAS, SF and PSB galaxies was selected from PC1 and PC2 regions:

- SF galaxies have -1.0 < PC2 < -0.5, and this sample is split by PC1 depending on the mass limit -4.5 < PC1 < -3.4 for the low mass bin and -3.5 < PC1 < -2.4 high mass bin. A Balmer decrement constrain is put on the SF sample. A BPT digram is used to identify AGN sample separated from SF sample, see the bottom row fig. (3.2).

- PAS galaxies have PC2 < 0.8 × PC1 - 0.6 and PC2 > 0.8× PC1 - 0.2, and this sample is split by having low mass bin -1.0 < PC1 < -0.2 and high mass bin -0.8 < PC1 < 0.0 .

- PSB galaxies have -6 > PC2 > -1.5 and 3 > PC2 > 0.0. Galaxies in this area have a starburst age more than 0.6 Gyr (Wild et al., 2010). Both the Balmer decrement and BPT diagram have been used to obtain the sub samples used in this work.

The control samples are chosen from the high density regions in the plot, as PCA method has no clear limits to separate galaxies types. The selection of 5 random galaxies from each SF and

PAS samples is made for every one PSB galaxy. Rapid change happens in the stellar population of a galaxy after 1 Gyr from the time of a starburst, where the O and B type star die leaving the A and F type stars with strong Balmer absorption lines. These strong lines are seen in the PC1-PC2 distribution plot at the high top, making the PCA method very effective tool to identify PSB phase.

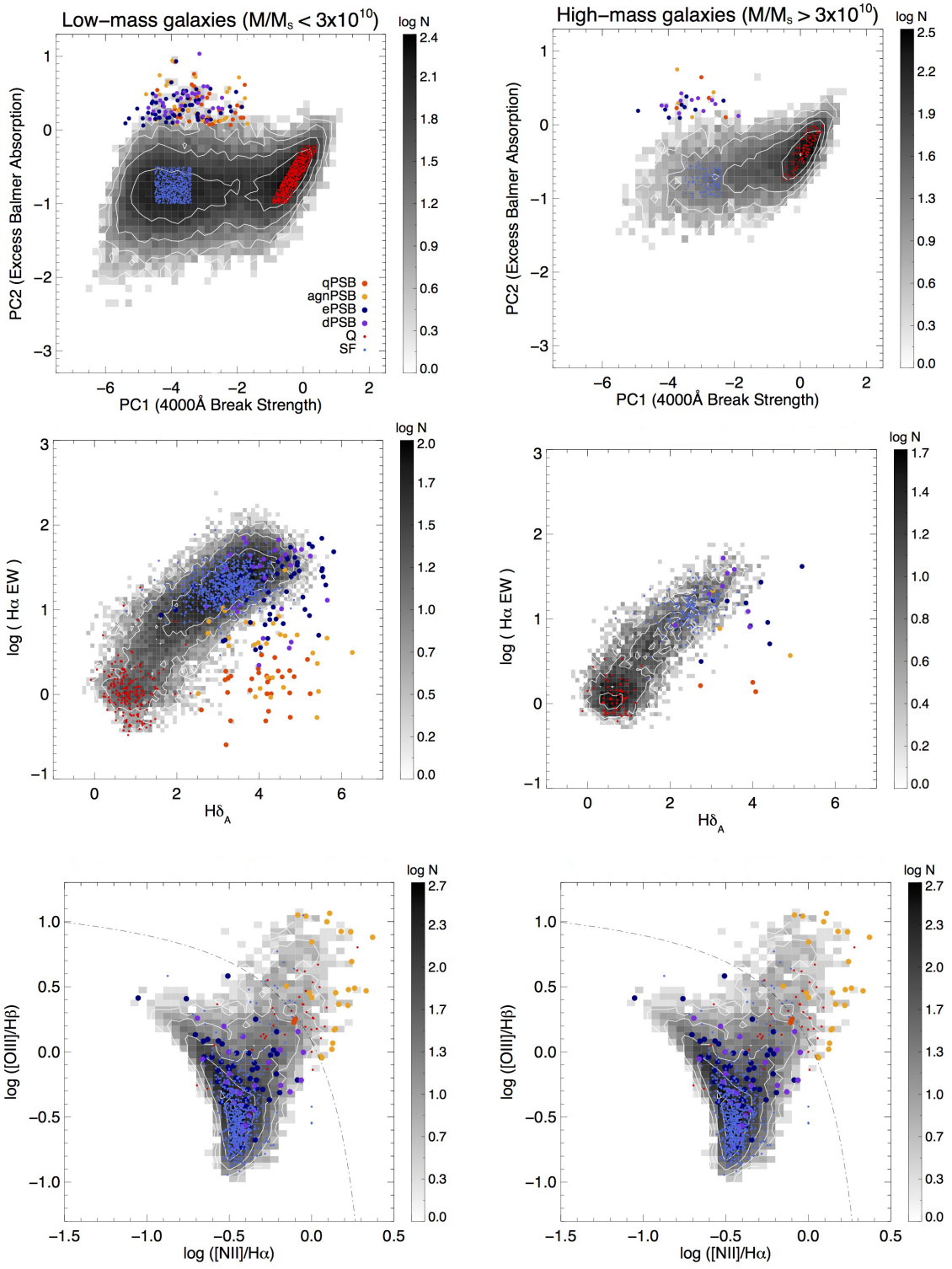

Figure 3.2: The strong Balmer absorption line galaxies: galaxies that show the classical PSB features are referred to as qPSB (orange), galaxies that show an AGN as well as the strong Balmer absorption line features are referred to as agnPSB (yellow), galaxies that show an emission lines as well as the strong Balmer absorption line features are referred to as ePSB (dark blue) and galaxies that show high concentration of dust as well as the strong Balmer absorption line features are referred to as dPSB (purple) plotted over the distribution of all the parent galaxy sample spectral indicators in grayscale. The SF (light blue) and the quiescent (Q) in red are the control sample. The top row are the PC1 and PC2 amplitudes, that are used for selection of PSB candidate galaxies. The middle row, shows the traditional Hδ_A lick absorption line index and H$_\alpha$ emission line equivalent with. The bottom row, shows the BPT digram for the two mass bins (Baldwin et al., 1981). log([OIII]/H$_\beta$) is on the y-axis and log([NII]/H$_\alpha$) on the x-axis. The dashed dotted line separates between the galaxies that have AGN and only star forming galaxies (Kewley et al., 2001). The grey colour-coded bar shows the number density of the observed galaxies in a log scale. Figure taken from Pawlik et al. (2018).

The final sample number of galaxies that have been use in this work are seen in table (3.1).

Table 3.1: The final number of galaxies PSB, SF, PAS, dusty-SF and AGN fitted by STARLIGHT.

$M/M_{\odot}$	PSB	SF	PAS	dusty-SF	AGN
Low mass bin	157	785	783	149	418
High mass bin	32	154	155	31	155

The dusty-SF and AGN galaxies fitting results are not presented here as they are not relevant to our purpose of understanding PSB galaxies.
The PSB galaxies are divided into sub samples based on their emission line characteristics see table (3.2) Quenched PSB (qPSB), star forming PSB (ePSB), dusty PSB (dPSB) and AGN PSB (agnPSB).

3.2.3 qPSB sample

The qPSB are galaxies traditionally identified as PSB galaxies in their spectrum. They have strong Balmer absorption lines and EQW of H_{α} in emission < 3Å . These aspects imply that the galaxy experienced a recent starburst, around 1 Gyr ago, that quenched the galaxy and may have forced it to join the red sequence. We expect PSB galaxies to be limited in their dust content, as Type 1a Supernovae stars (SNe) do not produce dust, and it is well beyond the timescale for Type II to be contributing significantly to the dust content (beyond that expected for a normal star forming galaxy).

3.2.4 ePSB sample

As we initially select our PSB-candidates from their steller continuum features, we notice many of the PSB-candidates have clear emission lines, with measurable H_{α}, which are not classical PSB. These galaxies are referred to as ePSBs. The ePSB type are distinguished from AGN by using the BPT diagram and are not highly contaminated with dust. Having emission lines suggest a reservoir of gas and an ongoing star formation after the starburst. PSB galaxies are traditionally suggested to be progenitors of early-type galaxies. Quenched galaxies show no evidence of any reasonable amount of star formation going on. Therefore, having emission lines in the PSB-candidates imply that it may be that after the starburst, a reasonable amount

of gas was conserved to maintain some level of star formation.

3.2.5 dPSB sample

The Hydrogen Balmer series are observed in the optical wavelength and are well studied in Astronomy. The relative intensity of these lines is well known and are calculated accurately as the atomic structure of hydrogen is well understood. The ratios of these lines in emission are known as the Balmer decrement (i.e. the ratio of H_α/H_β). The standard ratios for H_α/H_β = 2.87 and H_γ/H_β = 0.47. The difference between the observed ratios of the Balmer lines and the standard ratios is used to measure the dust contents of galaxies (Groves et al., 2012). In this work, we use the Balmer decrement to distinguish the dustier galaxies from all the galaxies that have recognisable Balmer emission lines. dPSB galaxies are top 10% dustiest galaxies with $H_\alpha/H_\beta > 5.2$ for the low mass bin and $H_\alpha/H_\beta > 6.6$ for the high mass bin. The Balmer decrement limit is applied to all star forming galaxies in the sample.

3.2.6 agnPSB sample

The ionisation state of the emission line presents us with a reasonable method to seperate AGN from star formation. For separation between the AGN and star forming galaxies we use the BPT diagram (Baldwin et al. 1981). The BPT is an optical diagnostic diagram that distinguishes between AGN galaxies which have a higher ionized spectrum and star forming galaxies that are ionised by hot stara alone. AGN galaxies can either be ionized from the photons coming from the accretion disc (Koski, 1978) or by strong shock waves (Dopita & Sutherland, 1995), while HII areas are ionized from the ongoing star formation (Huchra, 1977). The most common emission lines used to distinguish between these two types of galaxies are the ratios of [OIII]/H_β and [NII]/H_α. The ionization level of log([OIII]/H_β) and log([NII]/H_α) are stronger in AGN than that of a star forming galaxies. In this work Kewley et al. (2001), demarcation is used to separate the AGN type from the star forming type galaxies. Considering that these galaxies also have strong Balmer absorption lines, we referred to them as agnPSB type galaxies.

Table 3.2: The numbers of subsample galaxies and their percentage, in brackets, in the PSB sample for qPSB, agnPSB, ePSB and dPSB in the two mass bins.

Sample	Counts (%) $M/M_{\odot} < 3 \times 10^{10}$	Counts (%) $M/M_{\odot} > 3 \times 10^{10}$
qPSB	36(23)	5(16)
ePSB	57(36)	10(32)
dPSB	31(20)	12(37)
agnPSB	33(21)	5(15)

3.3 SDSS results

3.3.1 Sample fitting

The PSB candidates, qPSB, ePSB, agnPSB and dPSB with the control sample SF and PAS galaxies spectrum were fitted with STARLIGHT as described in Chapter 2. An example of the output fitting results are shown in figures (3.3, 3.4 and 3.5). The example galaxies were picked out from each group for having higher quality observations. The figures shows the observed spectra with the best fitting model spectra and residual (left) the STARLIGHT star formation history for the mass and light (center) and a three-colour image of the observed galaxy (right). The total number of all the galaxies that were fitted is shown in table (3.1) for the two mass bins. The low mass bin contains 2292 and the high mass bin 527 galaxies. In this work we will show the results obtained from PSB candidates and the comparison groups SF and PAS galaxies. The figure shows the results from fitting with CCM dust law. The results that we will show are for CCM dust law. These these are roughly the same as using CAL dust law.

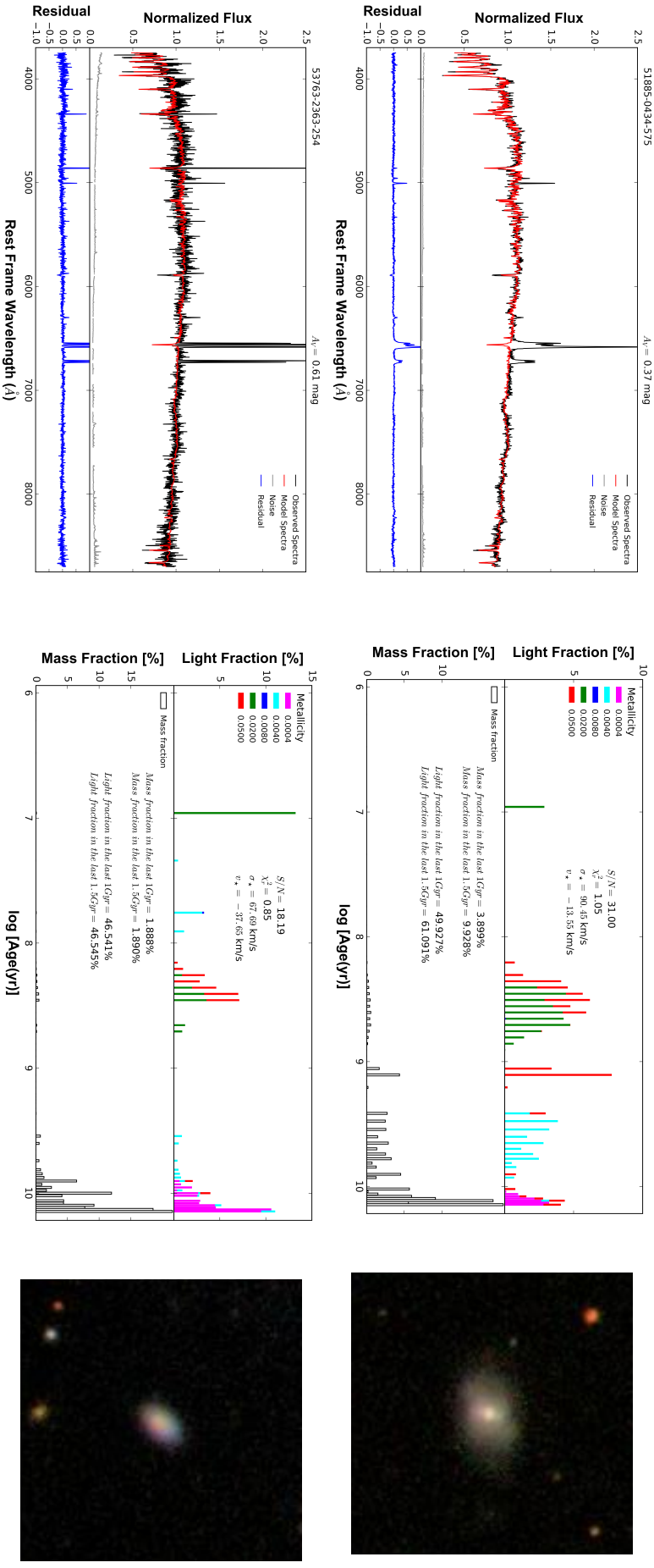

Figure 3.3: Random examples of agnPSB (top row) and dPSB (bottom row) types galaxies that were used in this work. The examples were selected with high SNR. For each row the left plot shows the observed spectrum normalized at $\lambda_0 = 4020$ in black, with the best fitting model in red and the observed noise in grey and the residual in blue. We mask any bad pixels and emission lines present in the observed spectrum. In the middle plot the lower half shows the fraction of mass formed during the lifetime of the galaxy and the upper half is shows the fraction of light produced by the stellar populations, colour coded by the metallicity. The right plot is the observed SDSS image of the example

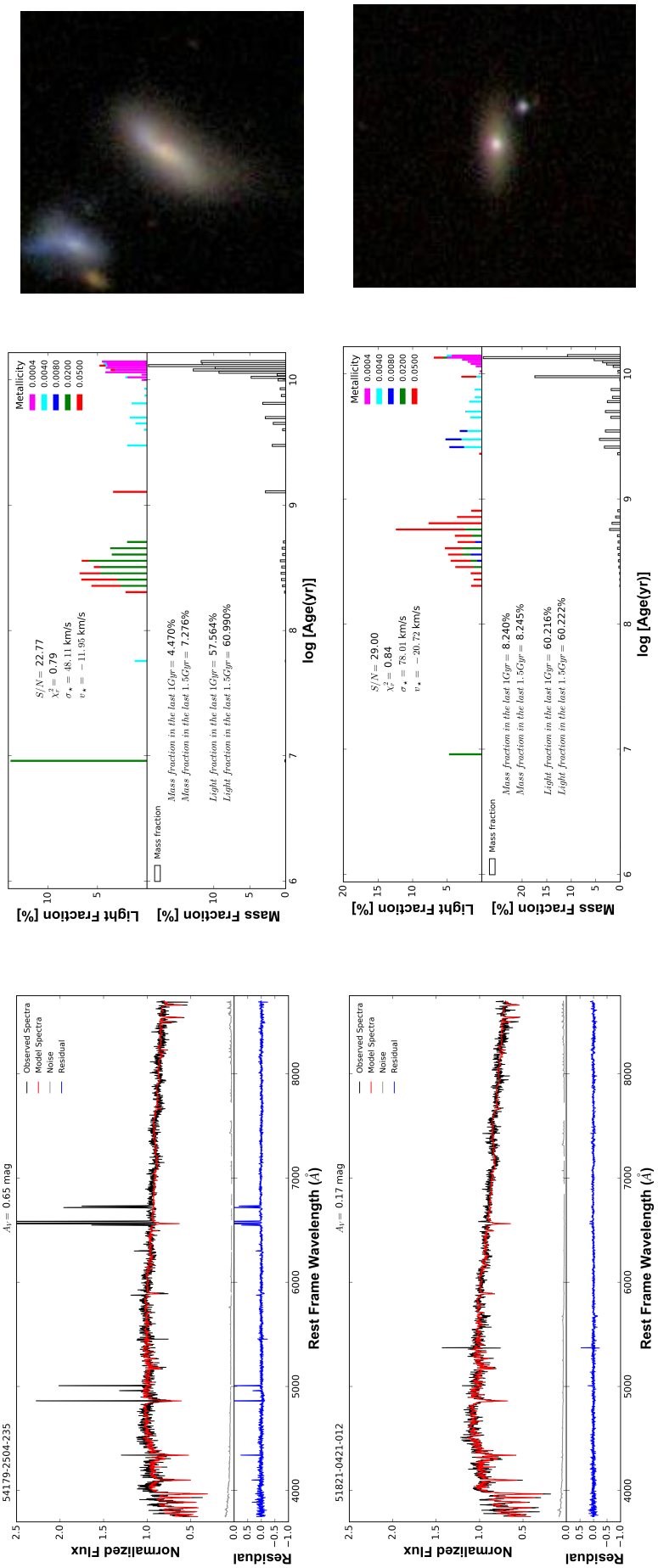

Figure 3.4: Random examples of ePSB (top row) and qPSB (bottom row) types galaxies that were used in this work. See figure 3.3 for more detalis

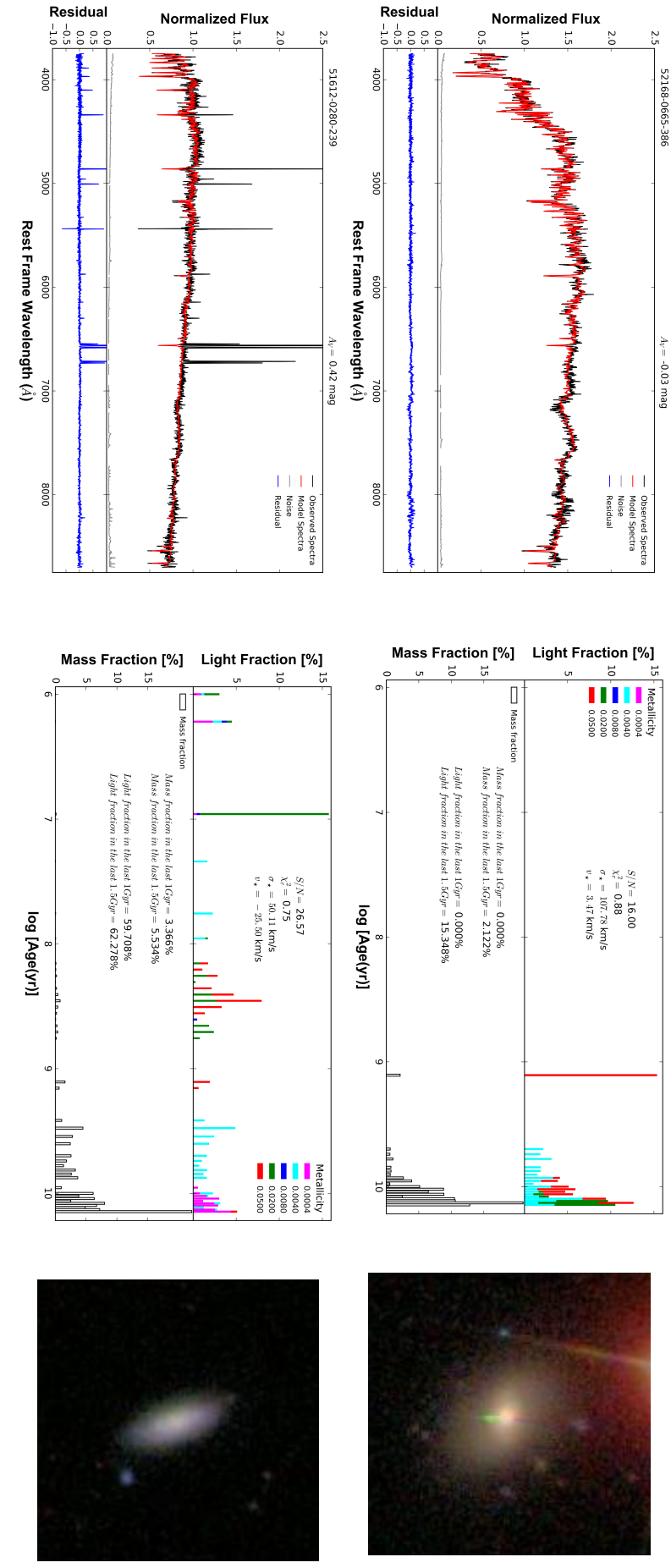

Figure 3.5: Random examples of SF (top row) and PAS (bottom row) types galaxies that were used in this work. See figure 3.3 for more detalis

3.3.2 Mass Fraction in the last 1 and 1.5 Gyr

We expect that PSB galaxies have formed more of their mass fraction in the last 1 and 1.5 Gyr than PAS and SF galaxies have in the same period. Therefore, to distinguish the PSB galaxy from other various types of galaxies, one can look at the stellar mass fraction produced in the last 1Gyr and 1.5 Gyr.

Figures (3.6) and (3.7), show the fraction of mass that has been produced in the last 1 Gyr and 1.5 Gyr respectively for the low mass bin of the PSB candidates and the control samples.

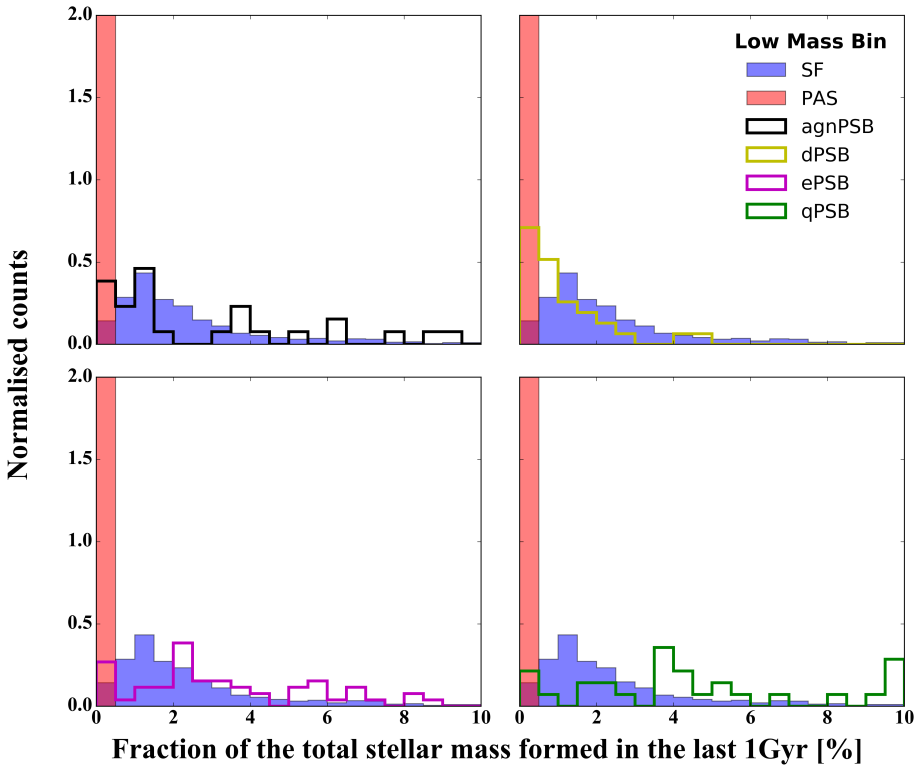

Figure 3.6: The fraction of mass produced in the last 1 Gyr as calculated by STARLIGHT, for galaxies in the low mass bin. The plots show the fraction of stellar mass that has been accumulated in the last 1 Gyr for agnPSB (black), dPSB (yellow), ePSB (purple), qPSB (green), PAS (red) and SF(blue) galaxies. Quiescent galaxies, PAS, have a fraction of mass around zero and the y-axis has been shortened to focus on the other samples.

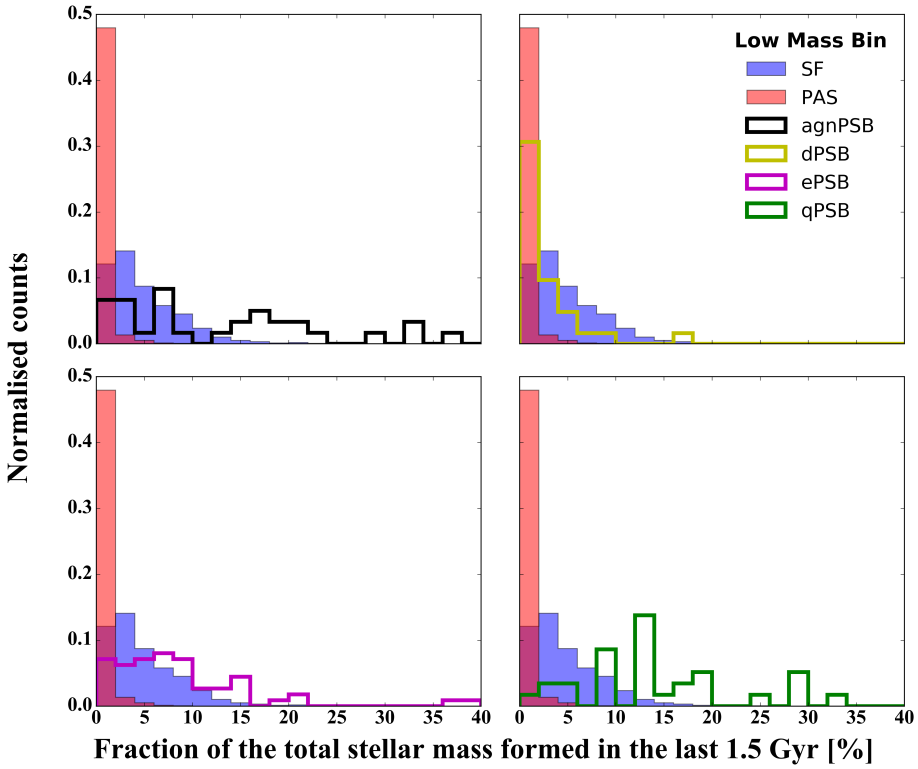

Figure 3.7: The fraction of mass produced in the last 1.5 Gyr as calculated by STARLIGHT, for galaxies in the low mass bin. See figure 3.6 for more details.

Figures (3.8) and (3.9), shows the fraction of mass that has been produced in the last 1 Gyr and 1.5 Gyr respectively for the high mass bin of the PSB candidates and the control sample. Also table (3.3), shows the percentage of PSB candidates with fraction of mass in the last 1 and 1.5 Gyr in a limits.

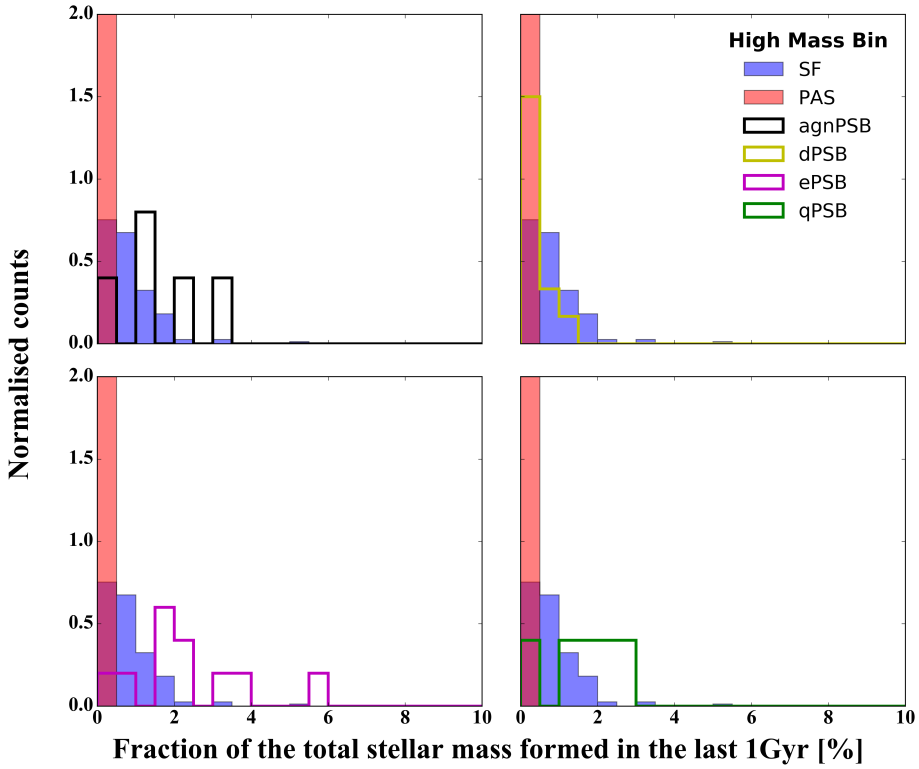

Figure 3.8: The fraction of mass produced in the last 1 Gyr as calculated by STARLIGHT, for galaxies in the high mass bin. See figure 3.6 for more details.

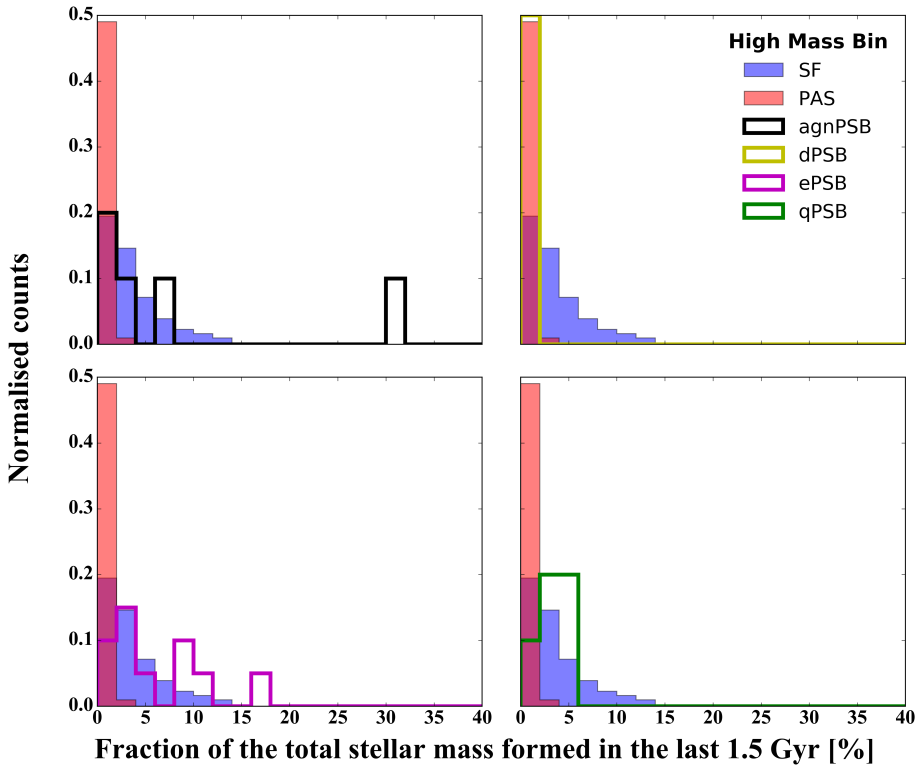

Figure 3.9: The fraction of mass produced in the last 1.5 Gyr as calculated by STARLIGHT, for galaxies in the high mass bin. See figure 3.6 for more details.

Table 3.3: The percentage of PSB candidates and control sample galaxies that formed the given percentage of their stellar mass in the last 1 and 1.5 Gyr.

Low Mass Bin	qPSB %	agnPSB %	ePSB %	dPSB %	SF %	PAS %
Fraction of mass 1 Gyr $< 5\%$	50	60	64	100	88	100
Fraction of mass 1 Gyr $> 10\%$	22	21	8	0	1	0
Fraction of mass 1.5 Gyr $< 12\%$	27	45	75	96	95	100
Fraction of mass 1.5 Gyr $> 20\%$	33	30	8	0	0.8	0
High Mass Bin	**qPSB %**	**agnPSB %**	**ePSB %**	**dPSB %**	**SF %**	**PAS %**
Fraction of mass 1 Gyr $< 1\%$	40	20	20	100	71	91
Fraction of mass 1 Gyr $> 1.5\%$	60	40	80	0	12	0
Fraction of mass 1.5 Gyr $< 2\%$	20	60	20	100	40	98
Fraction of mass 1.5 Gyr $> 5\%$	40	40	50	0	22	0

The x-axis range changes between the figures, as the high limit is cut off to show the plots more clearly. The y-axis is the normalised number of the galaxies.

To clarify and quantify whether the galaxy types are significantly different or not we conducted a Kolmogorov - Smirnov test (KS-test), on the low mass galaxy sample. We do not provide results for the high mass bin as the galaxies number is low, making the results unreliable. In the K-S test we cross correlate each sample with all the others, the KS-test finds the maximum difference in the cumulative fraction (D) and how significant is the difference (P-value).

1. In the low mass bin, comparing the mass fraction from 1 and 1.5 Gyr between control and PSB candidates agnPSB, ePSB and qPSB not including the highly dusty dPSB galaxy type we see that there is a shift to a higher fraction of mass in the PSB candidates than the control sample. The agnPSB and the qPSB almost show the same amount of mass fraction produced in the last 1 Gyr, more than double the mass fraction produced from the SF galaxies. While most dPSB type galaxies do not show any increase in their mass fraction above SF galaxies and have a mass fraction mainly concentrated around zero. The ePSB type reveal a slight increase in mass formation compared to the SF galaxies, at no time approaching the enhancement produced in the agnPSB or the qPSB galaxies.
   - Table (3.3), shows:
     - $\sim$90% of the SF control galaxies have a mass fraction $< 5\%$ and $< 12\%$ formed in the last 1 and 1.5 Gyr respectively, and only $\leq 1\%$ have a mass fraction $> 10\%$ and $> 20\%$.
     - Between (27 - 75) % of qPSB, agnPSB and ePSB galaxies $< 5\%$ and $< 12\%$ of their mass in the last 1 and 1.5 Gyr respectively and between (8-33)% of their populating to have a mass fraction $> 10\%$ and $> 20\%$ respectively.
     - PAS and dPSB are consistent with $\sim$ forming more of their mass in the last 1.5 Gyr.
   - Tables (3.4) shows:
     - The PAS galaxies have a high D and P-value, KS-test, significantly different from all the other galaxies types.
     - For the SF galaxies, it has a D roughly around 0.4 for all the PSB candidates and a P-value that is significantly different for all the PSB candidates except with the dPSB type.
     - The PAS and SF galaxies have a high 0.96 , D value, and 9.8E-323 ,P-value, showing how different they are.
     - As for the PSB candidates with each other, we see that the D is ranging from 0.23 between ePSB and agnPSB to 0.70 between qPSB and dPSB. The P-value shows that agnPSB and qPSB are not significantly different, but the ePSB and dPSB with qPSB and angPSB are significantly different.
   - Table (3.5), shows the same conclusions as in tables (3.4).
2. In the high mass bin, the mass fraction accumulated in the last 1 and 1.5 Gyr is less than

the low mass bin. The low numbers in this mass bin makes it difficult to retrieve any meaningful information from the KS-test.

- Table (3.3), shows:
  - (20 - 80)% of the PSB galaxies have formed $> 1.5\%$ of their mass in the last 1 Gyr and (40-50)% of PSB galaxies have formed $> 5\%$ of their mass fraction in the last 1.5 Gyr.
  - $\sim$ (0.8 and 22)% of the SF galaxies have formed $> 20\%$ and 5% of their mass in the last 1 and 1.5 Gyr respectively.

Table 3.4: The KS-Test results comparing the mass fraction distribtions produced in the last 1 Gyr in the low mass bin.

D						
	agnPSB	ePSB	dPSB	qPSB	SF	PAS
agnPSB	-	0.23	0.48	0.26	0.39	0.90
ePSB	-	-	0.62	0.24	0.45	0.92
dPSB	-	-	-	0.70	0.33	0.82
qPSB	-	-	-	-	0.55	0.91
SF	-	-	-	-	-	0.96
PAS	-	-	-	-	-	-
P-value						
	agnPSB	ePSB	dPSB	qPSB	SF	PAS
agnPSB	-	1.85E-01	7.05E-04	1.65E-01	7.54E-05	2.68E-24
ePSB	-	-	9.28E-08	1.31E-04	2.93E-10	1.05E-41
dPSB	-	-	-	3.16E-08	1.67E-03	3.83E-19
qPSB	-	-	-	-	4.92E-10	9.53E-27
SF	-	-	-	-	-	0
PAS	-	-	-	-	-	-

Table 3.5: The KS-Test results comparing the mass fraction distribtions produced in the last 1.5 Gyr in the low mass bin.

D						
	agnPSB	ePSB	dPSB	qPSB	SF	PAS
agnPSB	-	0.34	0.65	0.25	0.51	0.89
ePSB	-	-	0.59	0.44	0.40	0.85
dPSB	-	-	-	0.79	0.34	0.73
qPSB	-	-	-	-	0.70	0.94
SF	-	-	-	-	-	0.85
PAS	-	-	-	-	-	-
P-value						
	agnPSB	ePSB	dPSB	qPSB	SF	PAS
agnPSB	-	3.35E-03	8.64E-07	1.73E-01	3.69E-08	1.04E-23
ePSB	-	-	4.35E-07	2.15E-04	2.05E-08	8.99E-36
dPSB	-	-	-	2.80E-10	9.35E-04	3.40E-15
qPSB	-	-	-	-	8.18E-16	1.42E-28
SF	-	-	-	-	-	1.09E-250
PAS	-	-	-	-	-	-

3.3.3 The Dust Attenuation

One of the main parameters that STARLIGHT output from fitting the galaxy spectra is a dust attenuation. Figures (3.10) and (3.11), show the dust attenuation results A_v in magnitude, from STARLIGHT, for the low and high mass bin respectively. The left plot in the figures shows the agnPSB and qPSB, whereas the right shows the dPSB and ePSB, and both have the SF and PAS for comparison.

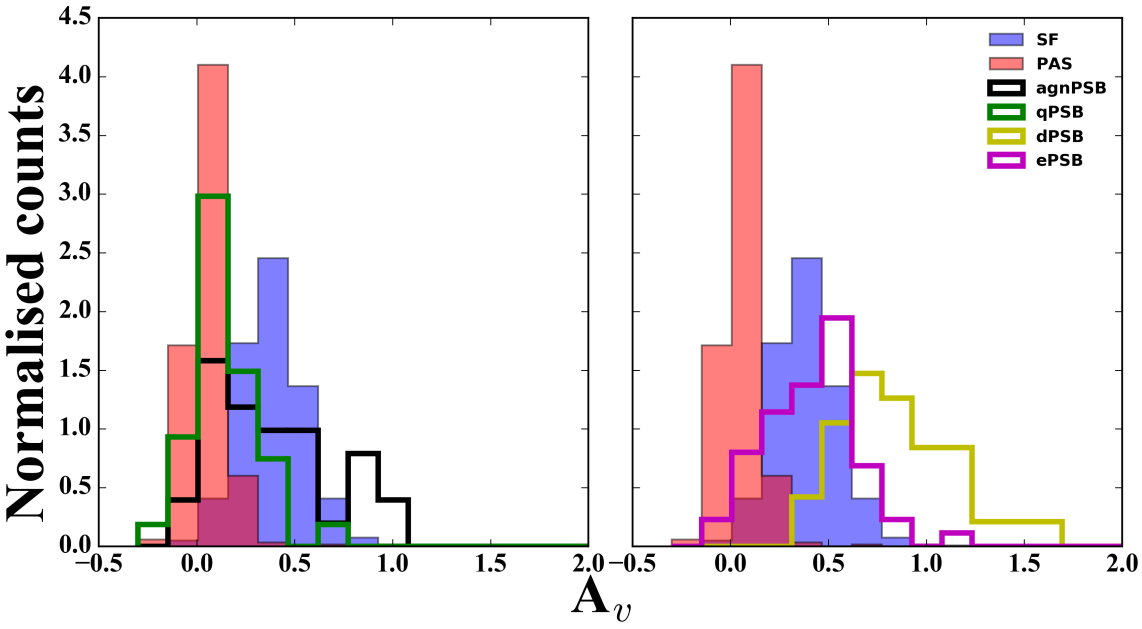

Figure 3.10: The dust attenuation, from CCM dust law, for all the galaxies in the low mass sample. Normalized number is on the y-axis and the dust attenuation is on the x-axis. The left plot shows the qPSB (green) and agnPSB (black) galaxies, whereas the right shows the dPSB (yellow) and ePSB (purple) they are presented as an empty histogram. The PAS (orange) and SF (blue) galaxies are shown as filled histograms for comparison.

We used CAL (Calzetti et al., 2000) and CCM Cardelli et al. 1989 dust laws to fit both the low and high mass samples, as the CCM, $R_V = 3.1$, is used to test the low dust density and CAL, $R_V = 4.05$, to test the dense dust clouds . As The figures shown are for the CCM screen dust law, as the fitting results have no crucial difference between the use of CCM and CAL dust law. STARLIGHT uses an open parameter fitting method, therefore we see some A_v having a negative result, which should be considered for this parameter as zero.

- The PAS galaxies have the least dust compared with the other sample types, consistent with no dust.
- In both low and high mass bins the dPSB galaxies exceed all other sample types with the amount of attenuation they suffer from. This confirms the classification method used.
- The agnPSB galaxies are slightly shifted to a higher A_v even more than the ePSB galaxies, suggesting slightly higher contents of dust.
- qPSB galaxies show the least amount of dust, when compared with the other strong Balmer absorption galaxies. This may be due to the galaxies having lost most of their dust contents during a recent strong starburst.

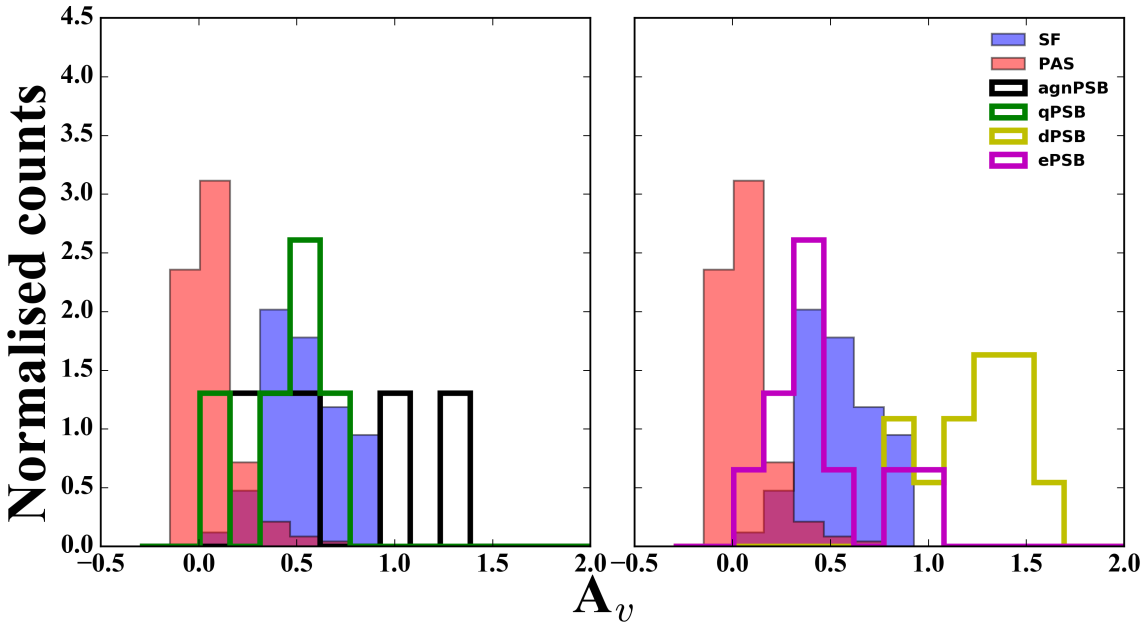

Figure 3.11: The dust attenuation, from CCM dust law, for all the galaxies in the high mass sample. Galaxies in this plot are as in figure (3.10).

The dust contents in a galaxy, if not fully understood and correctly processed, can cause a strong bias that affects the results.

3.3.4 The star formation history

As described in chapter two there is a bump in the star formation history that is caused by the synthetic models library, which affects the SFH around the age 1.5 Gyr. We use the cumulative mass fraction with time prior to 2 Gyrs, to minimise the effect that this bump has on the results. At that time, 2 Gyrs, the total mass of the galaxies has been calculated. The cumulative SFH at 2 Gyrs is used to trace the galaxy history prior to the starburst. Figures (3.12) and (3.13), show the pre-burst SFH for the low and high mass bin galaxies. We used a bootstrap method to calculate the 16th and 84th percentile errors for all the sample types. The high number of galaxies in the low mass bin gives a better constraint on the mean than the high mass bin.

- The differences in SFH between both the SF and PAS samples is hard to miss. As is well known, the PAS galaxies have formed a higher percentage of their mass more rapidly and at an earlier time than the SF galaxies.
- The dPSB SFH for the low and high mass bins is almost the same as the PAS galaxies. This is inconsistent with their emission line properties. We suggest that these SFHs are

unreliable due to the high dust contents of the galaxies.

- The agnPSB, ePSB and qPSB in the low mass bin, are almost identical to the SFH of SF galaxies and clearly distinct from the PAS SFH. This shows that low mass agnPSB, ePSB and qPSB galaxies are descended from gas rich SF progenitors, rather than quiescent galaxies.
- For the high mass bin, we see that agnPSB and ePSB lie between the SF and PAS SFHs. This indicates that they may have an equally mixed population of both PAS and SF galaxies.
- For the qPSB galaxy population in the high mass bin, they overlap with the PAS SFH. This suggests progenitors from the red sequence, that may have rejuvenated from a minor merger with a dwarf with high gas content.

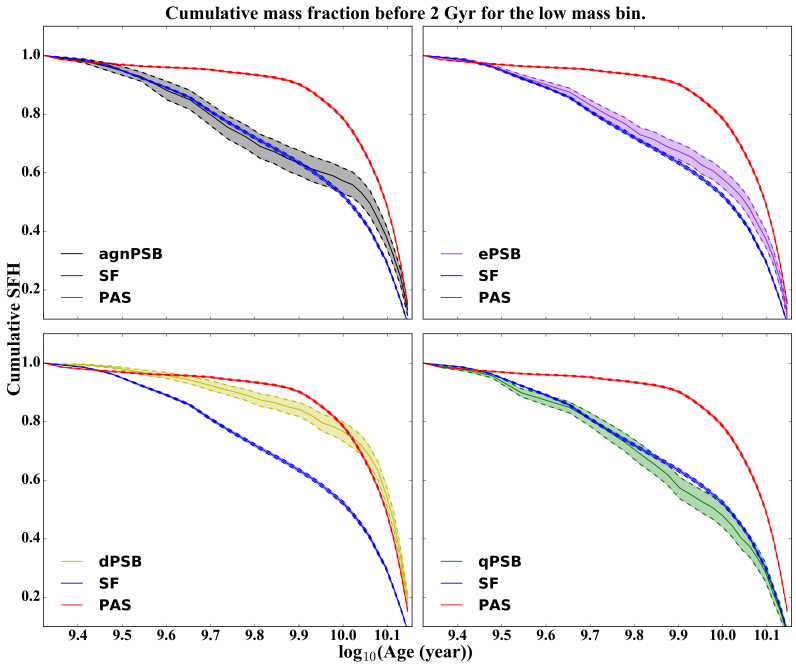

Figure 3.12: The pre-burst SFH of agnPSB (black), ePSB (light purple), dPSB (yellow), qPSB (green) SF (blue) and PAS (red) galaxies for the low mass bin. We plot the stacked normalised cumulative pre-burst SFH, to the total mass formed at 2 Gyrs lookback time on the y-axis and the lookback time on the x-axis. The mean (solid line) and 16th and 84th percentile errors on the mean (dashed lines) are shown, calculated from a bootstrap analysis.

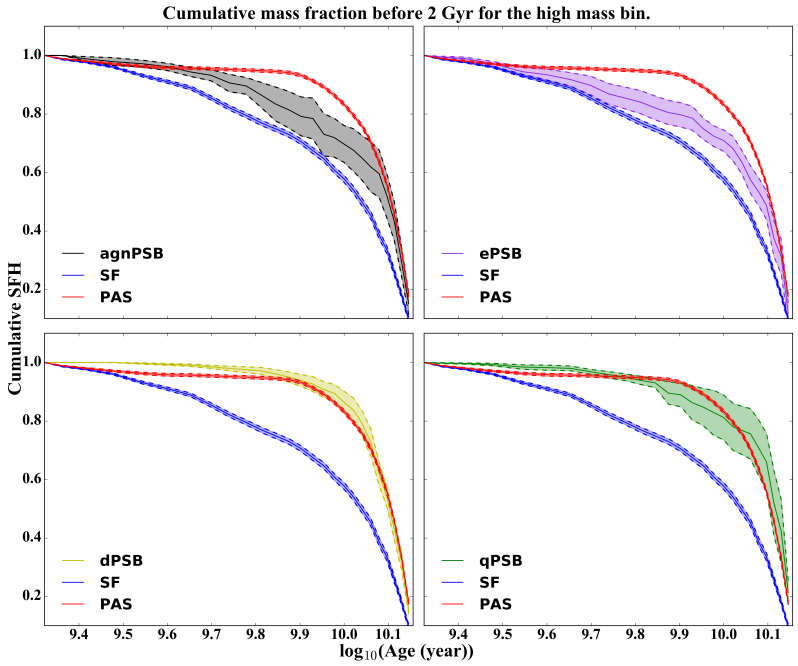

Figure 3.13: The pre-burst SFH for the high mass bin. The galaxies are shown as in figure 3.12.

Figures (3.14) and (3.15), show the full SFH for each sample of galaxies for both mass bins. We show these figures to illustrate the effect of the artificial bump on the stacked cumulative star formation history of the galaxies. In particular, notice the bump in the PAS and SF control samples at $\sim$ 1.9 and 1.2 Gyr respectively.

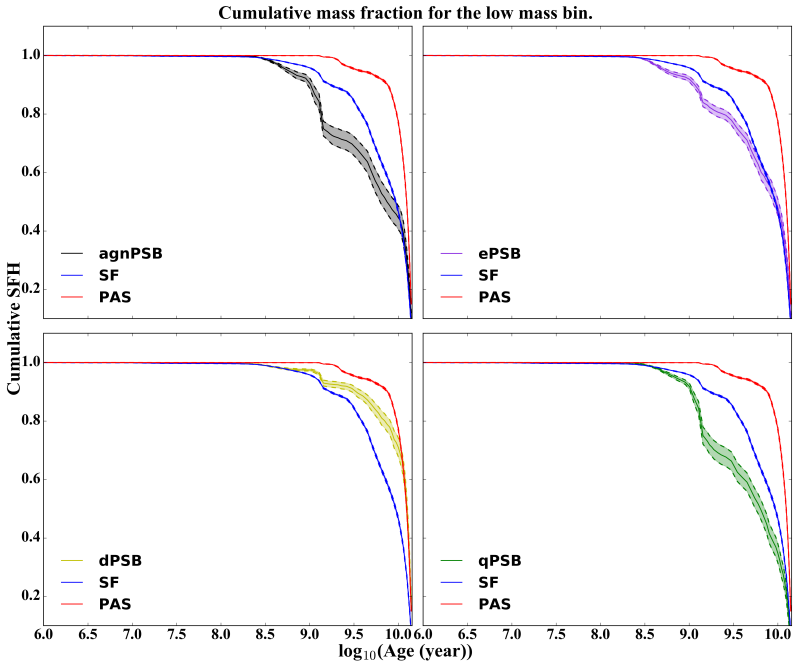

Figure 3.14: The full SFH for the low mass bin. The galaxies are as shown in figure 3.12.

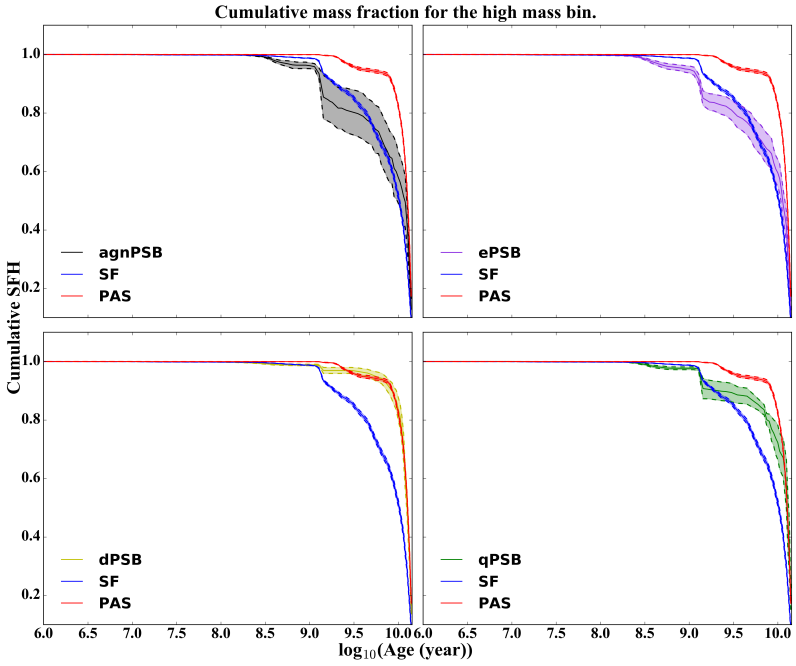

Figure 3.15: The full SFH for the high mass bin. The galaxies are as shown in figure 3.12.

While the former is out of the age range that we are interested in for PSB galaxies, the latter means that exct burst mans fractions are not possible to obtain. However, despite this bump,

we can still very clearly see the difference between the PSB classes and the control samples.

3.4 Conclusions

We have derived star formation histories and accumulated mass fractions for post-starburst and control samples, in two bins in stellar mass.

For the low mass bin, our star formation histories show that the progenitors of the post-starburst galaxies are consistent with being gas rich star-forming disks. However, additional morphology information presented in Pawlik et al. (2018), shows that the event that leads to the starburst may or may not alter the galaxy morphology to be elliptical, as many of the PSB galaxies have disky morphologies. It is possible that some of the ePSB galaxies may be an intermediate phase between the starburst and agnPSB/qPSB phases. The similarities between the agnPSB and qPSB samples, in everything other than their emission line ratios, show that the starburst phase is often followed by AGN activity, as the galaxy is transformed to join the red sequence. While some low mass PSBs may be caused by a gas rich major merger of star-forming galaxies which causes a violent starburst, the disk morphology of the majority of ePSB galaxies, as well as the ongoing star formation indicated by the emission lines, suggests that these galaxies will return to the blue-sequence and continue forming stars. We cannot rule out that a less violent event has led to the post-starburst features in most of the ePSB galaxies. This is supported by the typically weaker accumulated mass fractions that we find in the ePSB galaxies.

The high mass bin has fewer galaxies, making strong constraints difficult. A clear difference between the high and low mass bins is the pre-burst star formation history of the qPSB sample, which resembles the quiescent control sample. This indicates that a minor merger between a passive and low-mas gas-rich galaxy may lead to a short PSB phase, before cycling back to the red sequence. The star formation histories of the ePSB high mass galaxies is intermediate between the star-forming and passive control samples, and the ePSB sample has a higher mass fraction formed in the last 1Gyr than the agnPSB and qPSB samples. It is possible that these galaxies were recently massive disks that have merged leading to a violent starburst and transformation into a passive galaxies through the ePSB then agnPSB/qPSB phases.

4

Post Starburst Galaxies in the UDS

4.1 High Redshift Surveys

To study galaxies at high redshift in the optical area of the spectrum requires observations in the near-infrared wavelength range. Figure (4.1) shows model galaxy spectra at three redshifts 0, 0.4 and 0.7. For an elliptical galaxy at z ∼0.4 we can observe the 4000 Å break in between the g and r bands, wavelength ∼ 5600 Å . Whereas it is observed at z ∼ 0.7 in the r band, wavelength ∼ 6800 Å . So to observe the 4000 Å break in this elliptical galaxy at z ∼1.5, we need to observe at a wavelength ∼10000 Å .

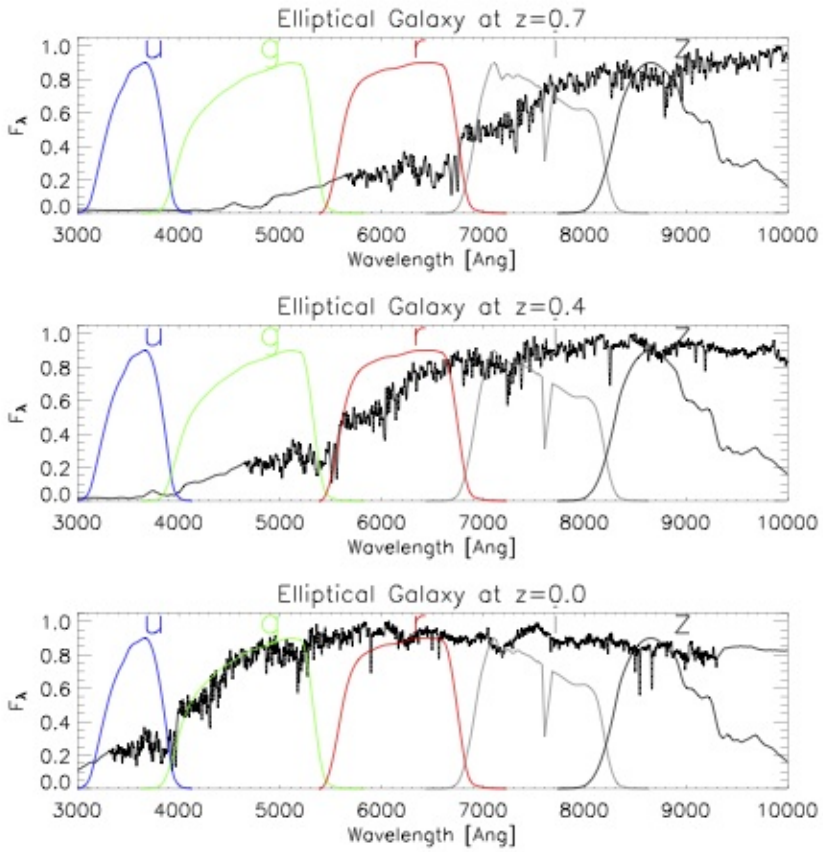

Figure 4.1: A BC03 model spectrum (black)of an early type galaxy. The spectrum is shown at three redshifts: 0, 0.4 and 0.7. Five SDSS filters are shown: u (blue), g (green), r (red), i (grey) and z (black). The 4000 Å break is seen to be shifted from g to r band as the galaxy go from redshift 0.0 to 0.7. Figure reproduced from Padmanabhan et al. (2007).

The UKIRT Infrared Deep Sky Survey (UKIDSS) (Lawrence et al., 2007), was started in September 2005 and has three fields of observation with depths in the K band of 18, 21 and 23 covering an area of $\sim$ 7000, 35 and 0.77 deg^2 respectively, in the first data release (DR1). The survey at the time of release of DR1, had up to five bands Z, Y, J, H and K, with wavelength ranging from 8360 to 23800 Å . In our present work we use Ultra Deep Survey (UDS) and its follow up spectroscopy survey (UDSz). Our objective is to investigate the mechanism in which produces the PSB phase at high redshift, also show the effect of adding the photometry data to the fitting of the spectrum on STARLIGHT results.

4.2 The UDS and UDSz surveys

The UDS uses the Wide Field Camera (WFCAM) on the 4m United Kingdom Infrared Telescope (UKIRT). Its first data release DR1 had depth for K∼23 (Lawrence et al., 2007). The DR8 managed to improve the depth and had J ∼ 24.9, H ∼ 24.2 and K ∼ 24.6 (Hartley et al., 2013). Magnitudes are on the AB system, are 2-arcsec aperture values and limit of 5σ. The B, V, R, i′, and z′ band were provided from the deep optical Subaru Suprime-CAM to complement the Near-IR images for the UDS data (Furusawa et al., 2008). The 3.6μm and 4.5μm bands, were provided by the Spitzer UDS Legacy Program (SpUDS; PI: Dunlop). In DR11 the J,H and K depth was increased (see table (4.1)).

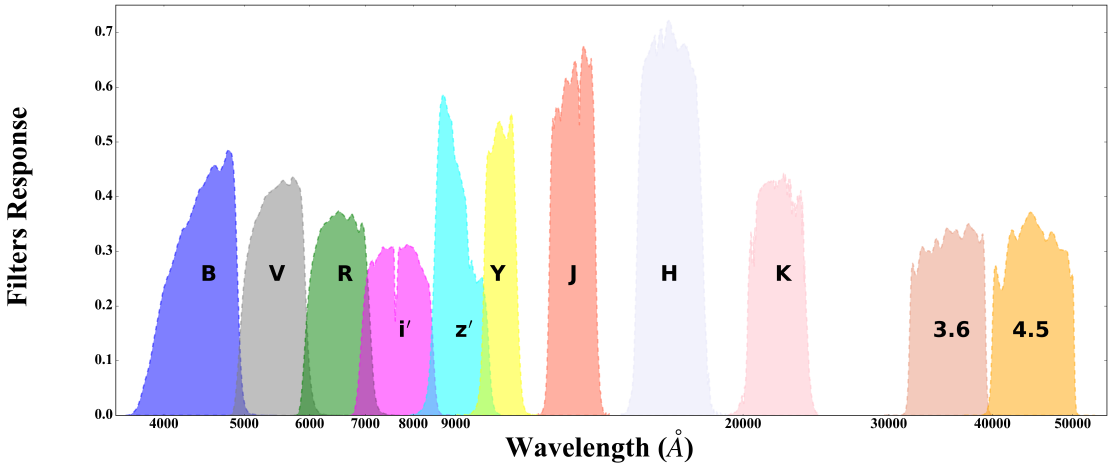

Figure 4.2: Eleven filters out of twelve from the DR11. The filter curves are normalised to have an area under the curve = 1.

Figure 4.2, shows eleven out of the twelve response filters found in DR11. The DR11 has U band in its catalogue, but it is not included in this figure, or used in this work. The objects magnitudes in the DR11 are aperture/point-spread function (PSF)-corrected to total magnitudes. The total number of objects that have been observed in this survey is 295,999. Areas are masked around bright stars, image boundaries and artefacts. The masked regions reduce the number of observed objects to 208,570 (figure (4.3)). The total area for the masked UDS field is ∼0.62 deg^2.

Table 4.1: The broadband filters that are included in the UDS DR11 are shown except for the U band. The columns show the band, the 5σ limiting 2-arcsec aperture magnitude, the effective wavelength and the short and long wavelength range.

Band	AB Magnitude	λ_{eff} Å	Range Å
B	27.6	4427	3600-5480
V	27.2	5454	4780-6572
R	27.0	6507	5760-7689
i′	27.0	7646	6710-8913
z′	26.0	9010	8360-9290
Y	24.0	10305	9790-10810
J	25.4	12483	11690-13280
H	24.8	16313	14920-17840
K	25.3	22010	20290-23800
3.6μm	24.2	35439	29650-41590
4.5μm	25.3	44840	37040-53159

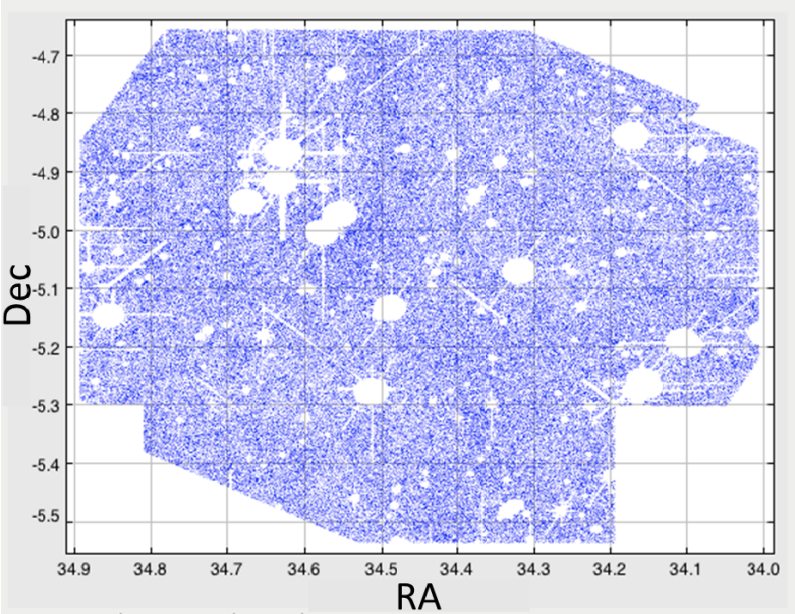

Figure 4.3: The coverage of the UDS field, having 34.0 $\lesssim$ Right ascension (RA) $\lesssim$ 34.9 and -5.55 $\lesssim$ declination (Dec.) $\lesssim$ -4.75. The (blue points are observed objects 208,570), in the UDS field with the masked areas in white for the bright stars, image boundaries and artefacts.

One out of six objects were randomly chosen from the photometric data for spectral observation with the Very Large Telescope (VLT). The main spectrum targets had a photometric redshift > 1 and $K < 23$. A control sample of ~ 500 objects at redshift < 1 was also selected. The targets in this survey were divided between two instruments, the VIsible Muti-object spectrograph (VIMOS) that was assigned the bright objects and the FOcal Reducer and low dispersion spectrograph2 (FORS2), see figure (4.4).

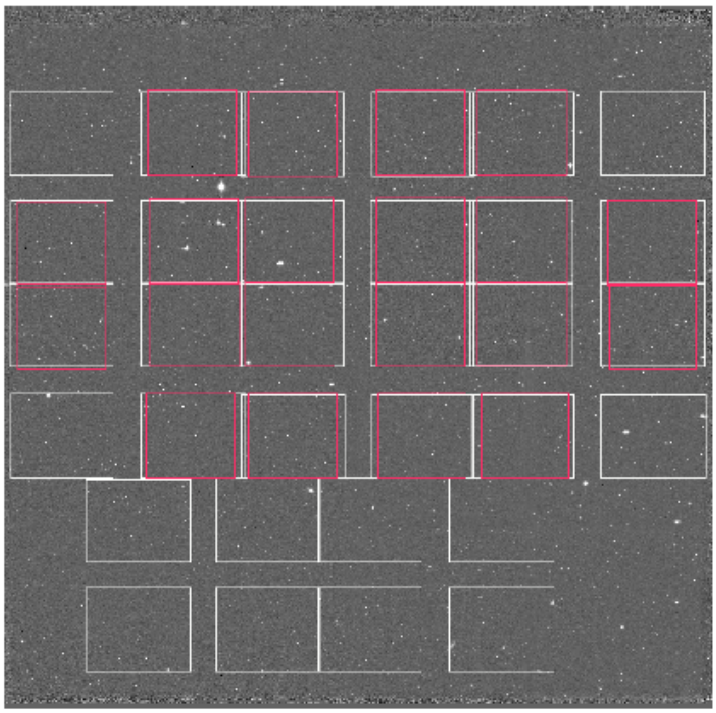

Figure 4.4: The UDS covers an area of 0.8 deg^2 centred on RA = 02:17:48, Dec = -05:05:57. Overplotted are the spectroscopic masks for the UDSz field observed with the FORS2 instrument in red and VIMOS instrument in white. Figure taken from Pearce (2012).

VIMOS is a multi object spectrograph with a wide field of view and a wavelength range, 3600 - 10000 Å and with a spectral resolution of R$\simeq$ 200. It has four identical arms each one has a $7' \times 8'$ field view. The CCD have a $0.205''$ pixel size. VIMOS was used for the brighter and bluer galaxies in the survey. For this survey the total number of observed objects was $\simeq$ 2500, with 93 hours of exposure.

FORS2 was used for the fainter and redder targets. This instrument had 142 hours of exposure for this survey. FORS2 is a multi mode optical instrument working in the wavelength 3300 -

11000 Å . It has two magnifications one with field size $6.8' \times 6.8'$ with $0.25''$/ pixel as a pixel scale and $4.25' \times 4.25'$ field size with 0.125"/pixel. The total targets observed was $\simeq$ 762 objects. Its spectral resolution is R $\simeq$ 600, which is higher than that of VIMOS.
Figure (4.4) shows the VIMOS observed areas in the UDS field as white squares, and FORS2 as red squares (Appenzeller et al., 1998;Pearce, 2012). The UDSz data covers the rest frame UV and optical area of spectrum. The target galaxies from UDSz were processed through various methods to obtain a high accurate redshift (Pearce, 2012).

4.2.1 Sample selection from the UDS

Wild et al. (2014), used a Principal Component Analysis (PCA) technique to classify galaxies from the UDS, $0.5 < z < 2$. The method uses a library of BC03 model spectra with a random distribution of star formation histories. The spectra library is converted to a photometric library, with the filter response curves figure (4.2). Then the library is shifted gradually across the redshift range observed targets $0.5 < z < 2$. A PCA is used on the resulting data array to find the mean flux and a series of eigenspectra (eigenvectors) from which one can rebuild a spectrum with some approximation. The principal component amplitudes uniquely describe the shape of a galaxy SED. The amplitudes indicate the amount of each eigenvector found in a galaxy. This amplitude is named in Wild et al. (2014) work as supercolour (SC), the work shows that only three supercolours are needed to be able to recognise and distinguish the shape of the SEDs of galaxies with high accuracy.
Figure (4.5) shows the UDS sample after being processed through the supercolours method. This method is used to separate the different galaxy types. This types are classified SF, Red, PSB, dusty and low metallicity type galaxies. The SF type is subdivided from high to low specific star formation rate, as SF1 is the highest and SF3 is the lowest. The SC1 correlates with the mean stellar age of the galaxy and also with the dust content in the galaxy. The galaxy's metallicity correlates with SC3 and SC2. SC2 correlates with the fraction of mass formed from a starburst in the last 1 Gyr.
The main population types that we are focusing on are red, SF and PSB. In the figure the red sequence galaxies are seen to the left for having old stellar population low dust constants, low mass fraction formed in the last 1 Gyr and somewhat high metallicity. The SF galaxies has a young population that is plotted to the right and is gradually shifted to the left as the O and B stars dies out. This population ranges widely in age, dust constants, mass fraction formed in

the last 1 Gyr and metllicity. The PSB galaxies are seen to have the highest stellar mass formed in the last 1 Gyr, a mixed youngish and old populations, an average metallicity and low dust content.

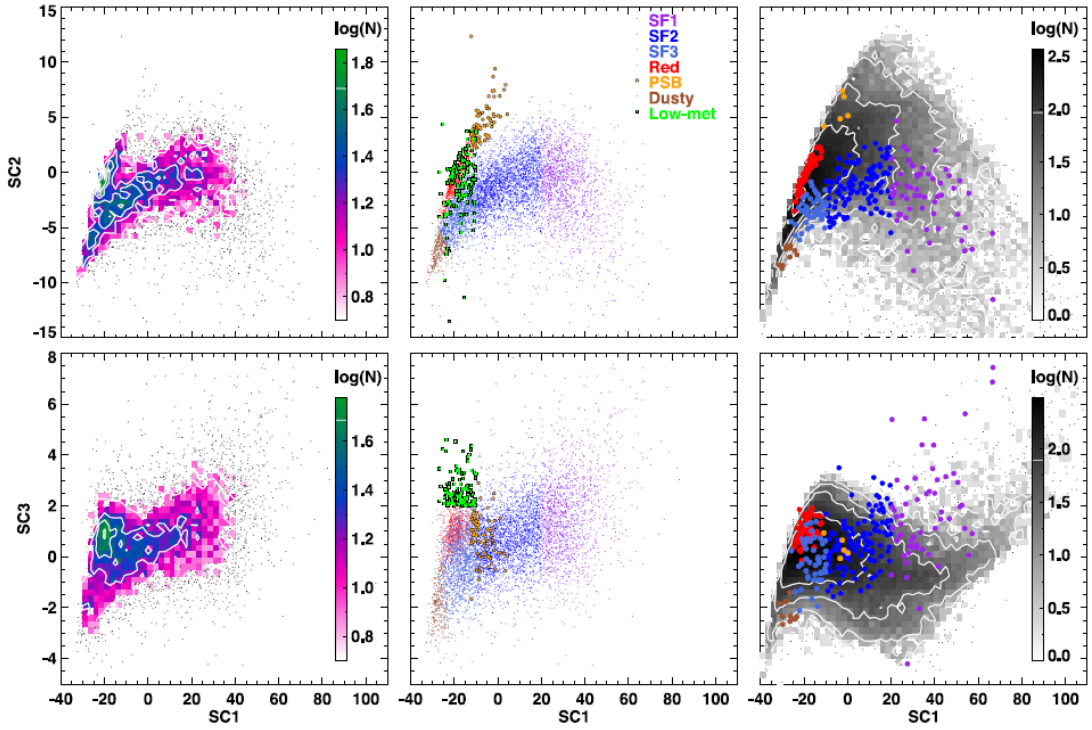

Figure 4.5: Super-colour diagram for the UDS galaxies with their SC1, that correlates with the age of the galaxy, on the x-axis and SC2, that correlates with the fraction of mass formed in the last 1 Gyr from a starburst, (top row) and SC3, that correlates with the galaxy's metallicity, (bottom row) on the y-axis. The galaxies are at $0.5 < z < 2.0$. The left plot shows the red sequence galaxies in the top left and the star forming galaxies are seen from high SC1 to bottom left, the color scale is the number density of the galaxies. In the low density regions single galaxies are shown as gray dots. The central plots show the super colour classification for the UDS field: red-sequence population galaxies (red), blue-cloud which is subdivided (arbitrary boundaries), with the increasing mean stellar age, from SF1 (purple), SF2 (blue) and SF3 (cyan), the PSB galaxies (larger orange circles) are seen in the tail at the top left of the plots, low - metallicity galaxies (larger green squares) and dusty galaxies(brown). The right plots, show the stochastic model galaxies (grey scale). The galaxies with spectroscopic redshift from the UDSz survey are over-plotted in colours for comparison. Figure taken from Wild et al. (2014).

The boundaries that are used to separate between PSB galaxy and the other types of galaxies are:

- The limit between Red and SF galaxies is $SC2 = 0.4 \times SC1 + 3.8$.
- The limit between PSB and SF is $SC2 = 0.18 \times SC1 + 3.5$.
- The limit between Red and PSB is $SC2 = -0.4 \times SC1 + 4.0$.

These limits are set by comparing with spectroscopically classified galaxies [Aaron Wilkinson, private communication].

We use the B,z′, Y, J, H, K and 3.6μm magnitudes, and disregard the three bands that are covered by the spectroscopic observations (V, R and i′). We do not include the 4.5 μm band because this band may be contaminated with hot dust emission at the redshift of our galaxies. We also disregard the U filter, as it is shallower than all the other bands.

4.2.2 The UDSz

We select galaxies with redshift $0.9 < z < 1.2$ in the UDSz catalogue giving 323 galaxies. This sample contains 10 PSB, 63 Red, 30 Dusty, 122 SF1, 52 SF2 and 46 SF3 galaxies as classified by their supercolours. Figure (4.6), shows the stacked spectra of the samples. The average spectral SNR for the stacked SF1, SF2, SF3, Dusty, Red and PSB are 41, 19, 18, 20, 41 and 19 respectively, which is relatively low when compared with the composite SDSS galaxy spectra having an average 132 SNR (Dobos et al., 2012).

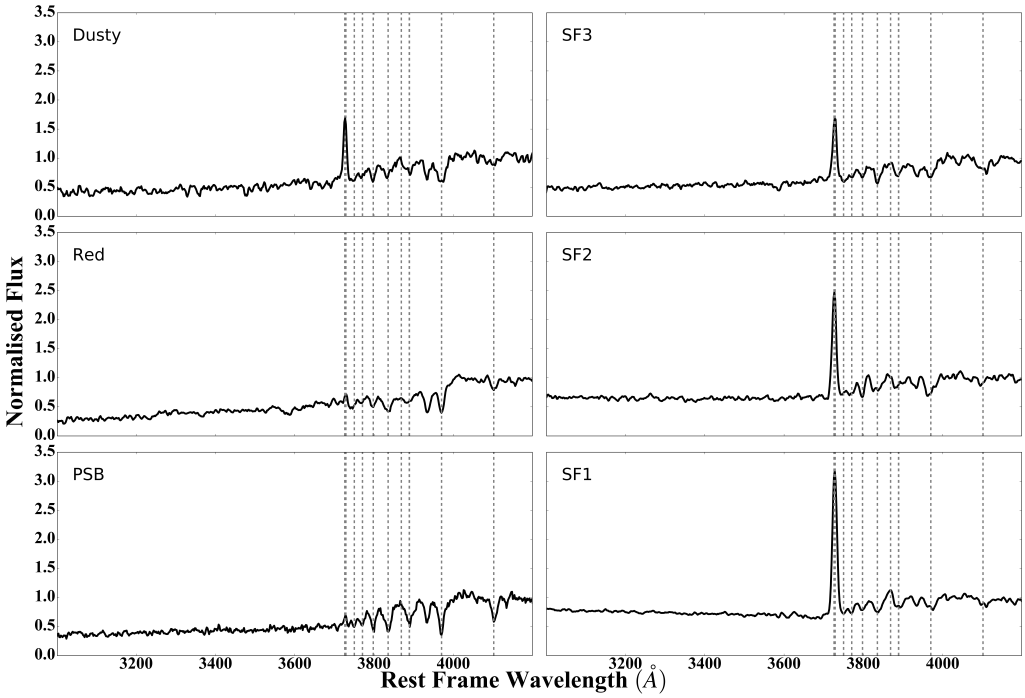

Figure 4.6: The stacked spectrum for 10 PSB, 63 Red, 30 Dusty, 122 SF1, 52 SF2 and 46 SF3 galaxies from the UDSz. The flux has been normalised at 4020 Å. The dash lines are showing the location of some emission or absorption lines from left to right: [OII] (λ λ 3726, 3728 Å), H12 (λ 3750 Å), H11 (λ 3770 Å), H10(λ 3797 Å), H9 (λ 3835 Å), [NeIII] (λ 3868 Å), [HeI] (λ 3888 Å), H8 (λ 3889 Å), [NeIII] (λ 3868 Å), Hϵ (λ 3970 Å) and Hδ (λ 4101 Å).

In it the SF1, SF2 and SF3 are showing the [OII] (λ λ 3726, 3728 Å) emission lines the strength of emission lines is declining as we go from SF1 to SF3 having a declining specific star formation rate. The separating limit for these three subtypes is arbitrary. The PSB sample are showing their classical features no emission lines, and a strong Balmer absorption lines e.g. Hϵ (λ 3970 Å) and Hδ (λ 4101 Å) absorption lines. The Red galaxies have no emission lines and are showing the a strong 4000 Balmer break, which is an accompanied feature with the red sequence. The Dusty sample has an average SNR $\sim$ 3.7, which is the lowest average between the sample, having a SNR$\sim$ 20 when stacked. It shows [OII] (λ λ 3726, 3728 Å) emission line that maybe generated from shock waves.
The stacked samples illustrates how good the supercolour classification is separating of the different types. Also we show the location of some emission lines that we mask over. Other than [OII] (λ λ 3726, 3728 Å) lines it is not that clear to distinguish between the emission lines and the noise.

4.2.3 Processing the UDSz spectrum

In order to fit both the spectrum and the photometric data with the new STARLIGHT code, we need to renormalise the spectra to the photometric data. First we correct the spectrum and the photometry for Milky Way extinction using an E(B-V) = 0.02 (Oesch et al., 2007). Then we remove 200 Å from the low and high end of the spectrum as these regions were highly contaminated either from sky or instrument noise. We convert the magnitude to flux density. The spectra are convolved with the R and i$'$ band filters, where the spectrum covers the filters range. Finally the flux from the convolved spectrum and the flux from the photometric points, are used to calculate the normalisation to be applied to the spectra.
We flagged the telluric absorption due to the sky between 7580 and 7660 Å , in the spectra input file, so that range is not used in the fitting, as this range may be contaminated with sky lines.

4.3 The UDS and UDSz results

Figure (4.7) shows the output results of fitting a PSB galaxy from UDSz data with somewhat high SNR. The new STARLIGHT code can fit both the spectra and photometric data as described in Chapter 2.

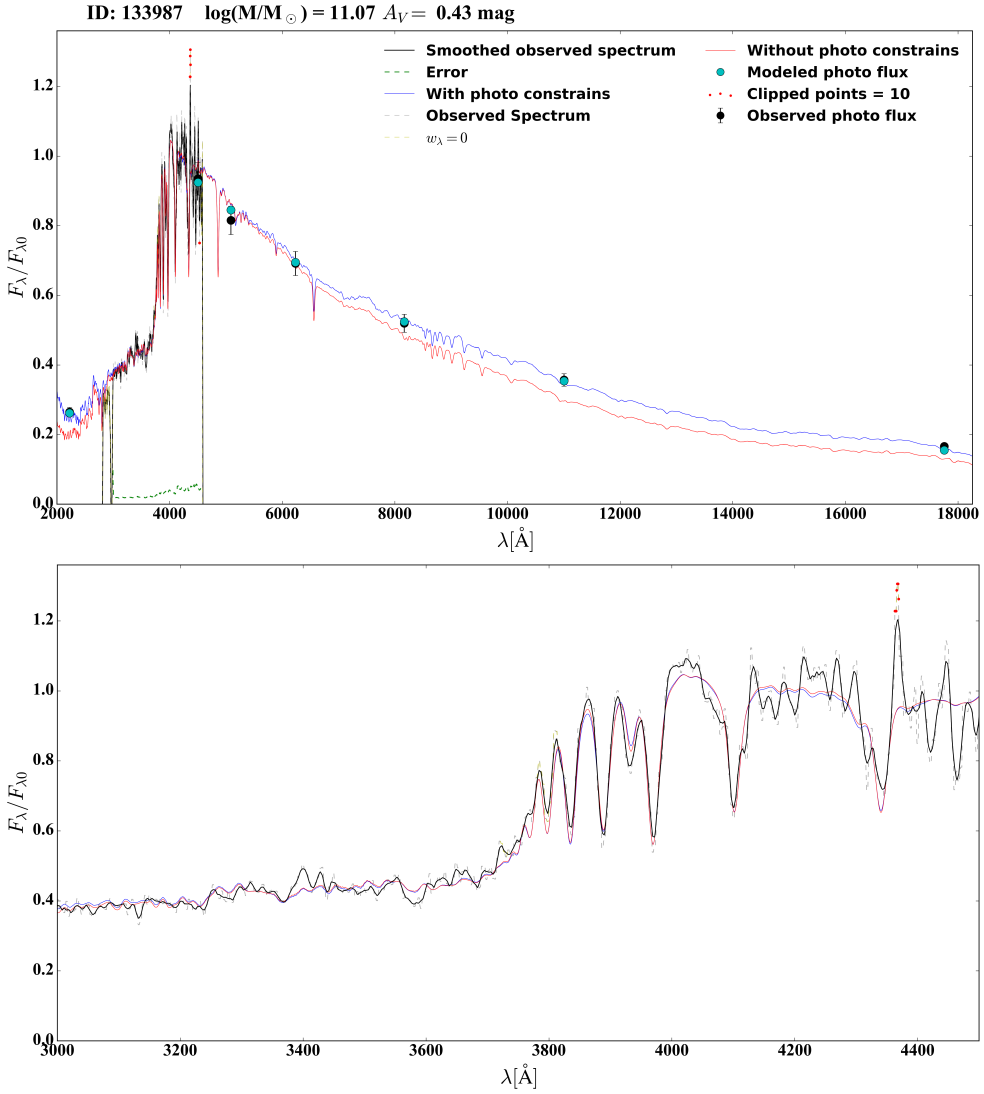

Figure 4.7: A high SNR spectrum and photomety of a PSB galaxy. The DR11 ID is given in the top left, with the resulting log(M/M$_\odot$) and dust extinction A_v in magnitude from the fit with photometry. The spectra and photometric points are normalized at 4020 Å . The observed spectrum (grey dashed line), smoothed spectrum (black line), photometric data with errors (black points), best fit model for the spectrum and photometry (blue line), best fit model for the spectrum (red line), model photometric points (green points), error on the spectrum (green dashed line), clipped points from the spectrum (red points) and masked areas with $w_\lambda = 0$ (yellow). The bottom plot is a zoom in to the region of spectrum.

The figure compares the fitting of both the spectrum and the photometric points with fitting only the spectrum. The spectra covers a range 3000 - 4200 Å , whereas the photometry covers 2000 - 18000 Å . Both the spectra and photometric are normalized at 4020 Å . The best fit model with photometric constraints is seen in blue and without in red. The bottom plot is a zoom in on the galaxy spectrum.

Both fits have a reasonable ${\chi_r}^2$, although the use of photometric constraints give us a better

fit at long wavelength, therefore better constraint on the physical parameters. For almost all galaxy types it is seen that including photometry is important to obtain a good fit, by combining the photometry with the spectra we improve our estimation of the stellar mass in NIR.

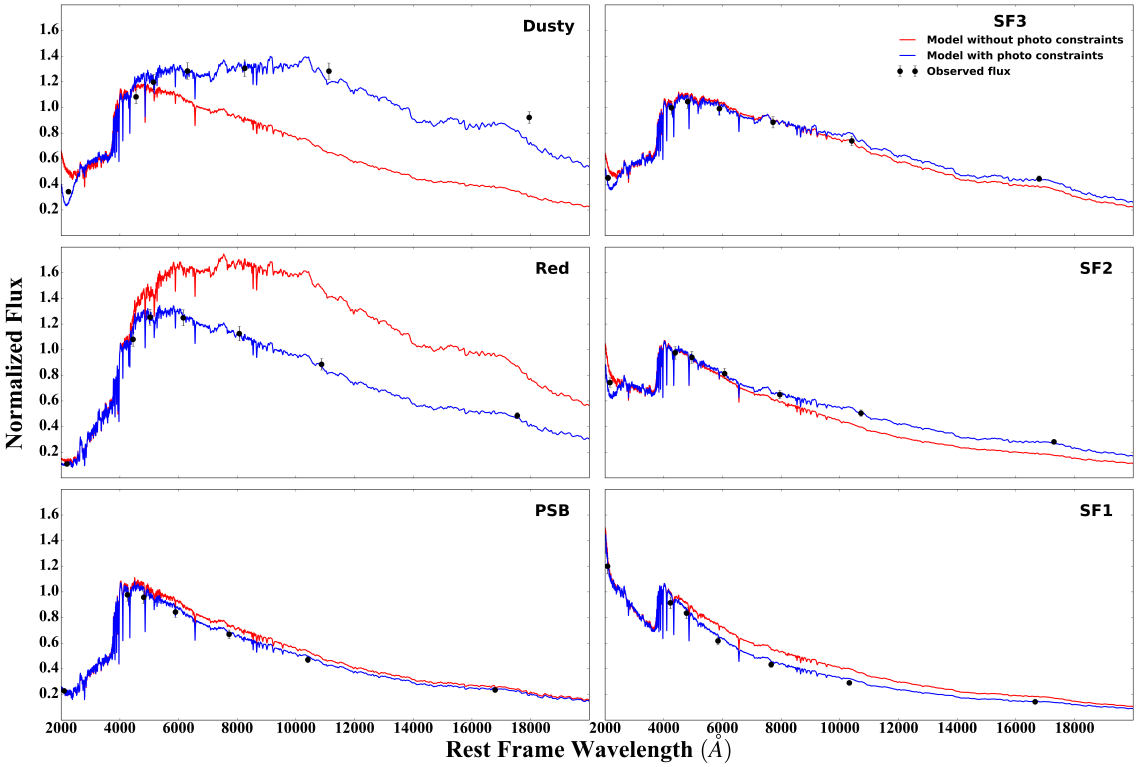

Figure 4.8: The stacked best fit synthetic models when fitting both spectra and photometry (blue) and only spectra (red), the observed photometric flux (black).

In figure (4.8) the SF1, SF2, SF3 and PSB classes are clearly quite well constrained just from the small part of the optical spectrum. The Red and Dusty are not well constrained. This may be from the lack of the young population of stars in the Red type and the blocking of the young stars by bust in the Dusty type. Here the small section of optical spectra that we have is misleading. However, the small difference in the NIR translates into a very significant difference in the SFH. We plot the observed photometry only, as a spectral region is almost identical for both fittings.

Figure (4.9), shows the PSB look very good. The photometry is not adding the huge amount of information. SF1 Spectra only have a tale of higher mass objects and SF2, SF3 spectra only have a tail of low mass objects. When compared with spectra and photometric fit. This matches the direction of difference between the stacked fits in the NIR (4.8). Red have a significant tail to high masses. Dusty have a significant tail to the low masses. Again both as expected from

stacked fits. We show that the NIR is important to constrain M/L of galaxies, however, if you have optical spectra, a reasonable estimation can be made within NIR photometry in the case of SF and PSB galaxies. It is to the flux limited survey that we see different distributions and do not see low mass PSB, Red and Dusty.

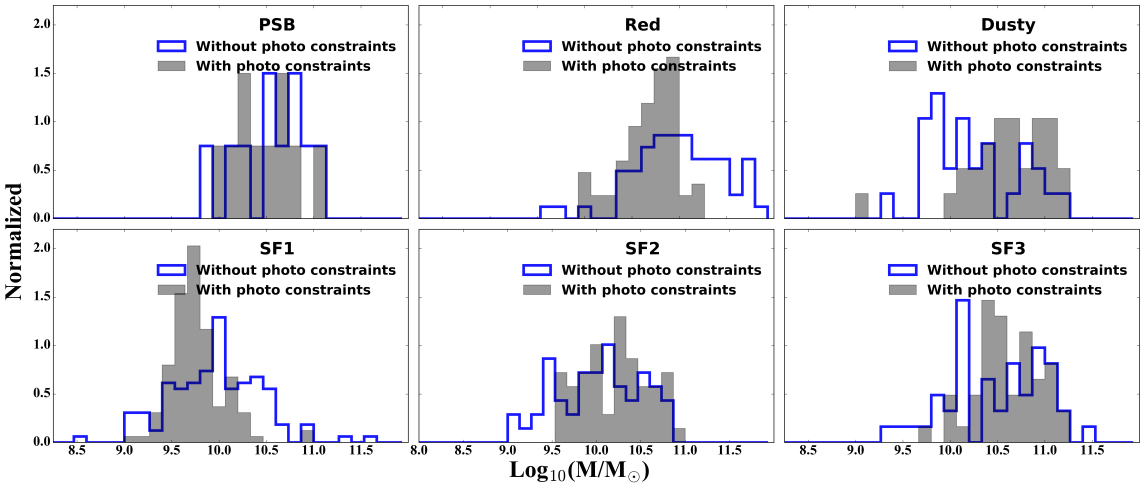

Figure 4.9: The calculated stellar mass for the galaxies in the UDSz, when fittign both photometry and spectra (full grey) and only spectra (blue).

In figure (4.10), we notice that STARLIGHT has a tendency to fit zero dust in the absence of long wavelengths information, when photometry is included dust is required in the fit.

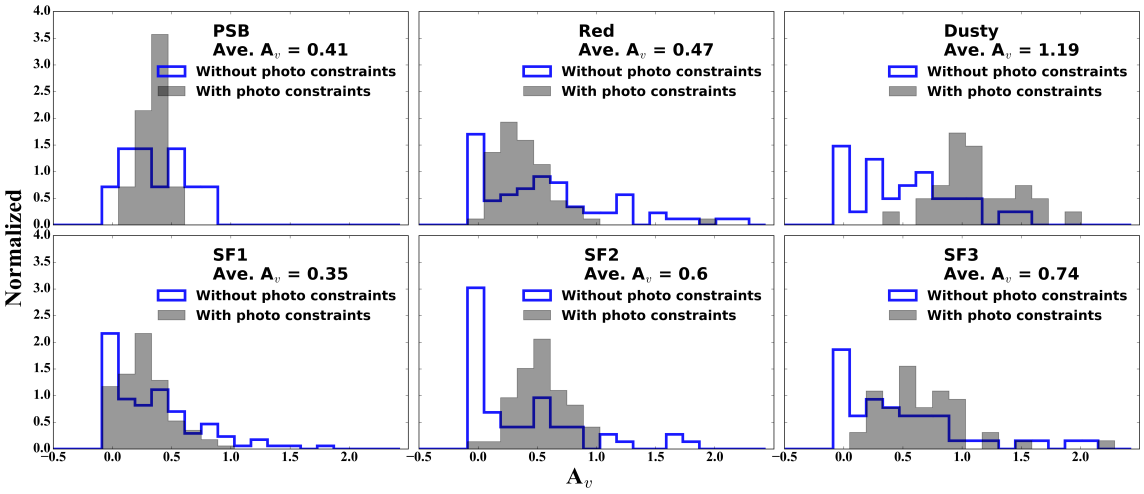

Figure 4.10: The dust attenuation, from CCM dust law, for all the high redshift galaxies in the UDSz sample. Fitting with constraints (full grey) and its averag shown for each class and without constraints (hollow blue). Normalized number is on the y-axis and the dust attenuation is on the x-axis in magnitude.

We see that SF3 is more dusty than SF2 and SF1. This matches how they were selected

with SF1 having high SC1 being very blue. The PSBs show similar dust contents to the red. For figure (4.11), we assume that spectra combined with photometric is more reliable to give correct SFH, giving previous discussion.

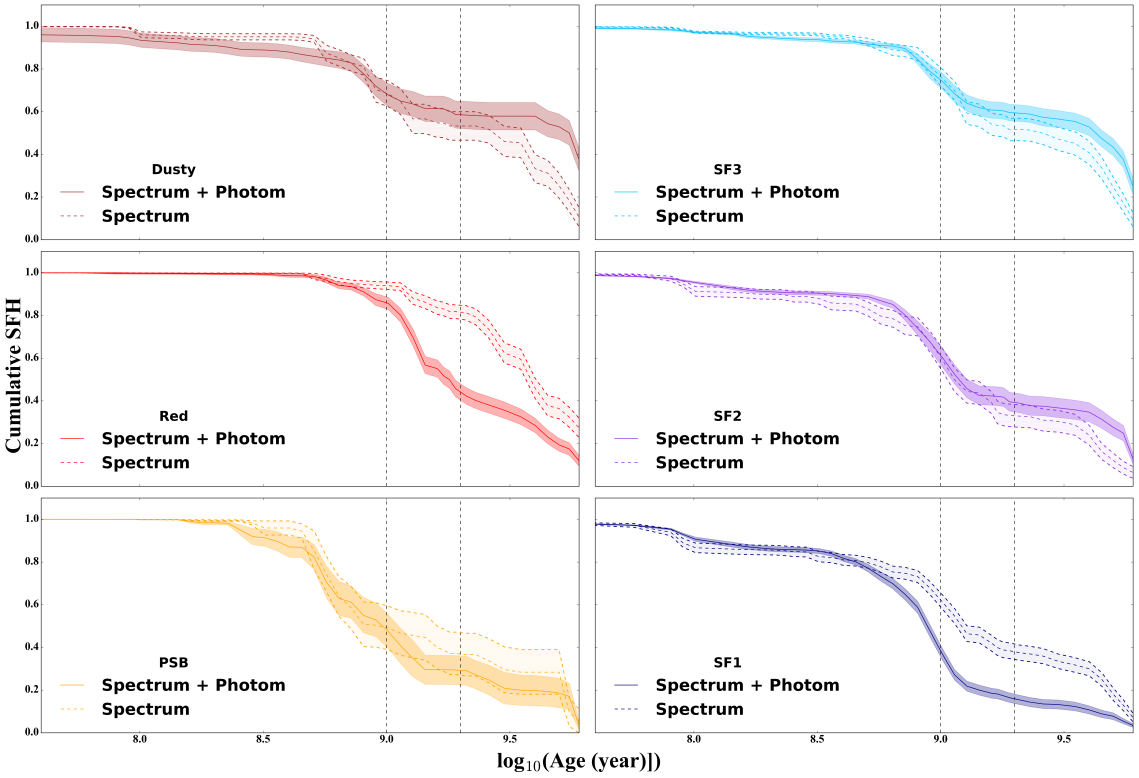

Figure 4.11: The stacked cumulative SFH for the sample selected from the UDSz: dusty (brown), Red (red), SF3 (cyan), SF2 (lilac), SF1 (blue) and PSB (orange) galaxies. The dashed transparent line is the SFH from fitting the galaxy spectra, and the solid line is from fitting both spectra and photometry.The curve for each SFH shows the mean and the 16 and 84 percentile, from Bootstrap method. The dash vertical lines are showing the 1 and 2 Gyrs times respectively. The a lookback time in $\log_{10}$(age(year)) on the x-axis is shortened to better shows the growth of the stellar mass.

So focusing on spectra plus photometry fits alone we see SF1 to SF3 type build up mass from later to earlier. Now accounting for dust, which the supercolours could not do. STARLIGHT shows how the colours progression is predominantly on age effect. The Dusty class looks to be a simple progression from SF3, building mass more steadily. However, we caution that fitting these objects is very difficult with degenerate between SFH and dust. Surprisingly the lack of difference in the SFH between Red and SF3. It looks like the only difference between these classes is the Red have a slopped star forming and SF3 have not. However, it is possible that the additional dust contents may mimic old stars and then effect the SFH. More work is required to test this. The PSBs are shown to be the only galaxies to form $> 60\%$ Of their mass in the last Gyr. This confirms the supercolours methods for selecting PSB.

Figure (4.12) is shows the mass accumulated in the last 1 and 1.5 Gyr for individual galaxies in the different samples. For the moment we focus on filled histograms which show UDSz distribution (we look at the comparison with SDSS below).

- All classes show substantial mass growth in the last 1 and 1.5 Gyr, even the Red class.
- PSBs all show significant mass growth. This shows that the supercolours method has zero contamination.

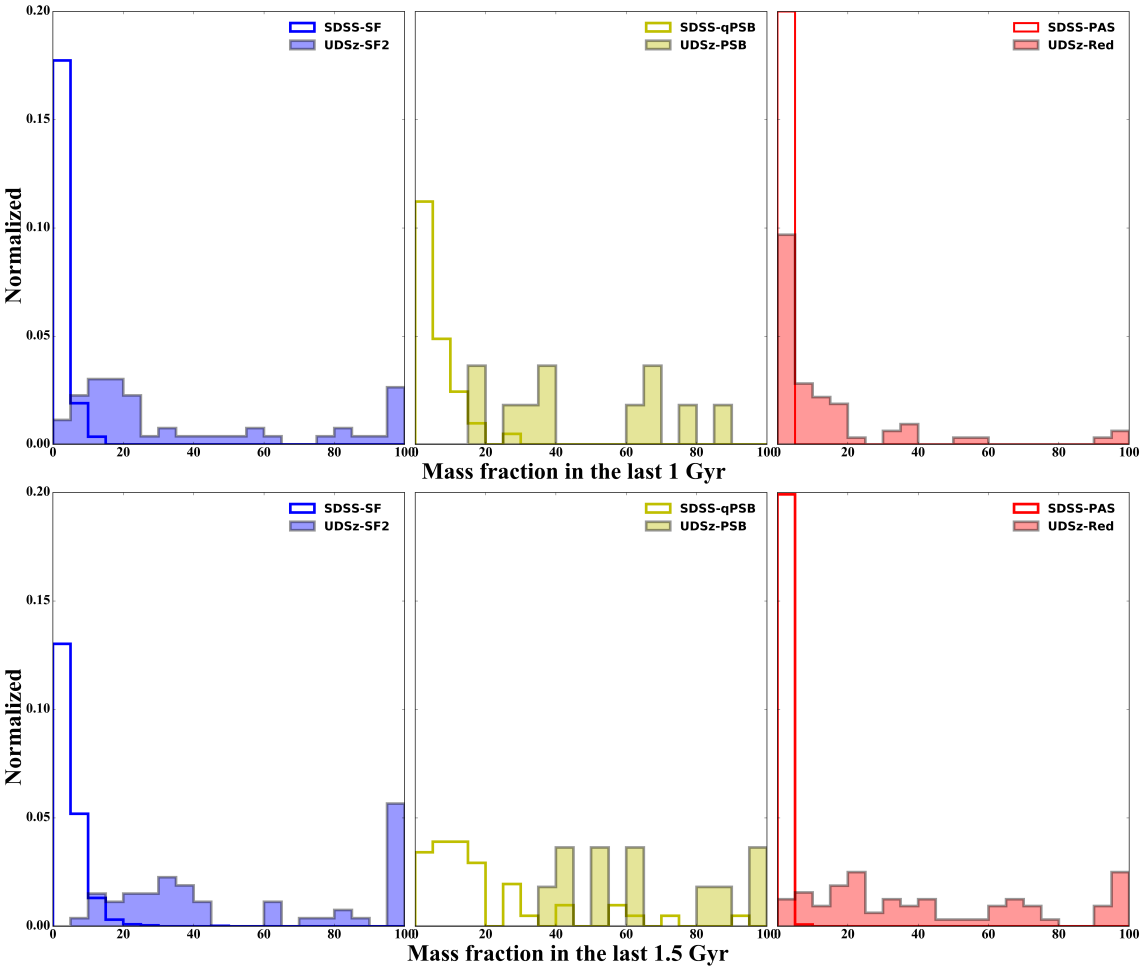

Figure 4.12: The SDSS sample (empty histogram) and the USDz sample (solid histogram). The fraction of mass formed in the last 1 Gyr (top) and 1.5 Gyr (bottom). The SF SDSS and SF2 UDSz samples are shown in the left plot (blue). The qPSB SDSS and PSB UDSz samples are shown in the middle plot (yellow). The PAS SDSS and Red UDSz samples are shown in the right plot (red). The mass fraction accumulated in the last 1 and 1.5 Gyr for the UDSz data is hugely higher than that of the SDSS samples.

4.4 Comparing between UDSz and SDSS

From looking back on figure (4.12), we see that SF shows much higher mass formed, as expected, from SF2. While the Red are showing an interesting high mass fractions. These galax-

ies have only just quenched, whereas SDSS have quenched ages ago. The PSB are showing a much higher burst mass fraction at high-z. This is either selection effect or real. There are cases of high burst mass fractions galaxies at low redshifts, but only $\sim 30\%$ in the last Gyr. Whereas the high-z sample 20-100% for all objects. This suggest a real difference. However, it is not clear that the supercolours method would detect the low burst mass fraction objects seen in SDSS.

It is also interesting to compare the dust content at low and high redshift. From figure (4.13) we see that the SF show less differences between SDSS and UDSz, although still more dust may have an effect on the results (probably not due to mass difference). The Red galaxies are showing significantly higher dust contents at high redshift consistent with the idea that dust hangs around and is destroyed slowly in the ISM. We also note that the PSB have higher dust contents at high redshifts. Possibly due to higher gas fraction. Which would be constant with the higher burst fractions.

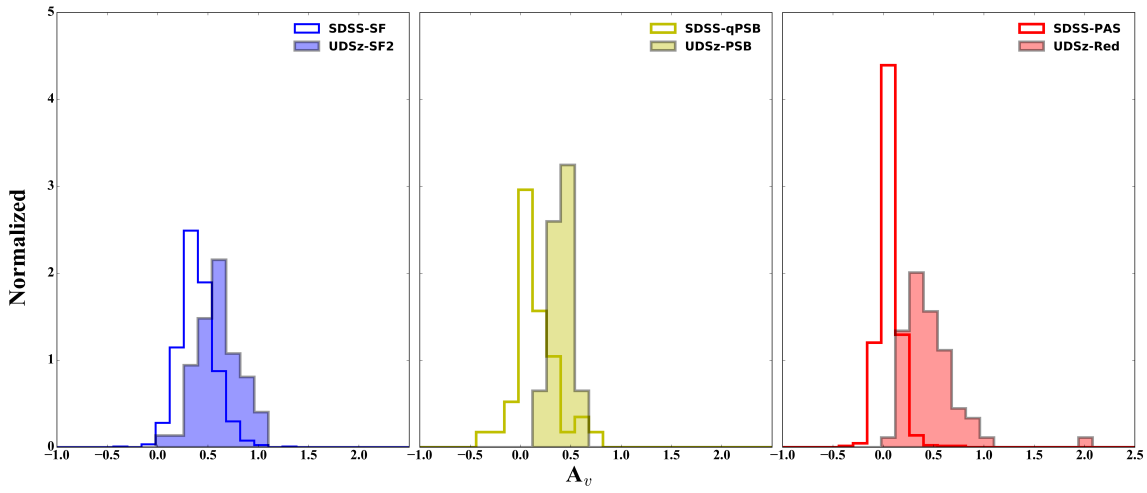

Figure 4.13: The dust contents, A_v in mag., in both the SDSS, the added low and high mass bins, and DSz samples. Fitted with CCM dust law. The SF SDSS and SF2 UDSz are seen on the left (hollow blue) and (full blue) respectively. The qPSB SDSS and PSB UDSz are (hollow yellow) and (full yellow) respectively in the middle. The PAS SDSS and Red UDSz are (hollow red) and (full red)respectively in the right. The dust contents is for the UDSz galaxies are higher, as the are more constrained.

4.5 Comparing new STARLIGHT with Bagpipes

In this paragraph we illustrate the stability of our results even with fitting the sample with an entirely different code using a different method of fitting. We compare the results of the fraction of mass at 1 and 1.5 Gyr from both STARLIGHT and Bagpipes for the PSB and the Red samples.

The PSB sample figure (4.14), shows a resemblance between the results from STARLIGHT and Bagpipes, they covering the whole range in mass fraction. However, Bagpipes shows a higher fraction of galaxies with 100% of the mass formed with 1 or 1.5 Gyr then STARLIGHT. Bagpipes has a constraint on its parameters. The low number of galaxies in this sample may explain the non-continuous in the results.

Figure (4.15), shows the results from the two codes is almost identical for the mass fraction formed in the last 1 Gyr. STARLIGHT is showing a small fraction with 100%, that may be from a sample selection.

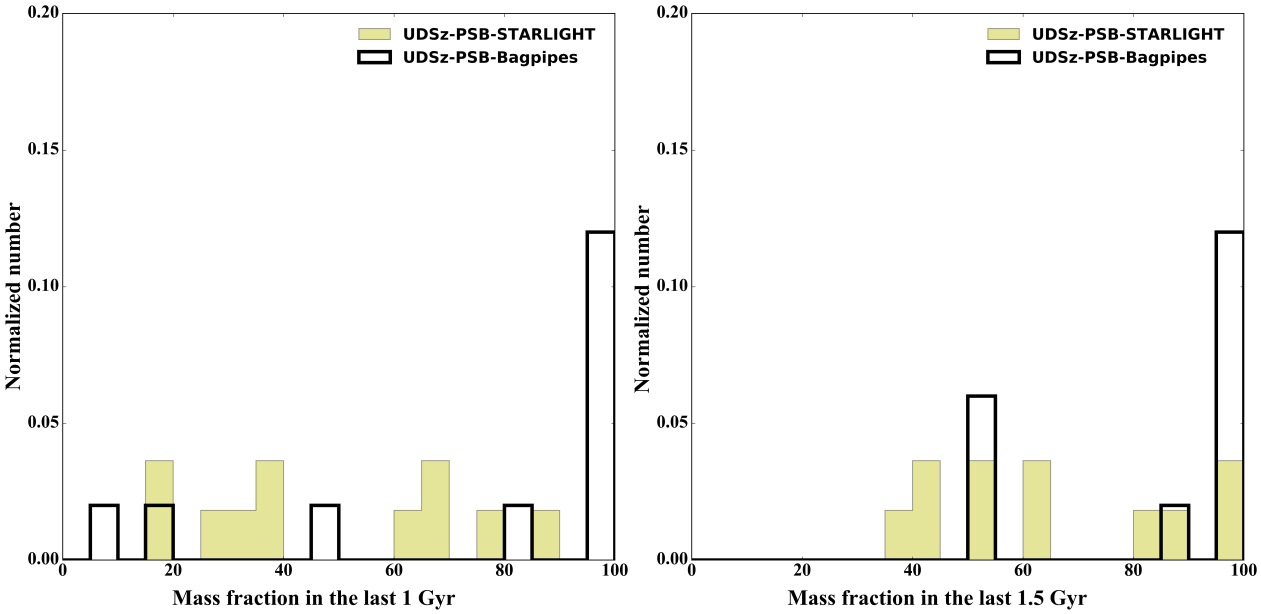

Figure 4.14: The PSB sample for the fraction of mass at 1 Gyr (left) and 1.5 Gyr (right) from both STARLIGHT (full yellow) and Bagpipes (black line) histograms.

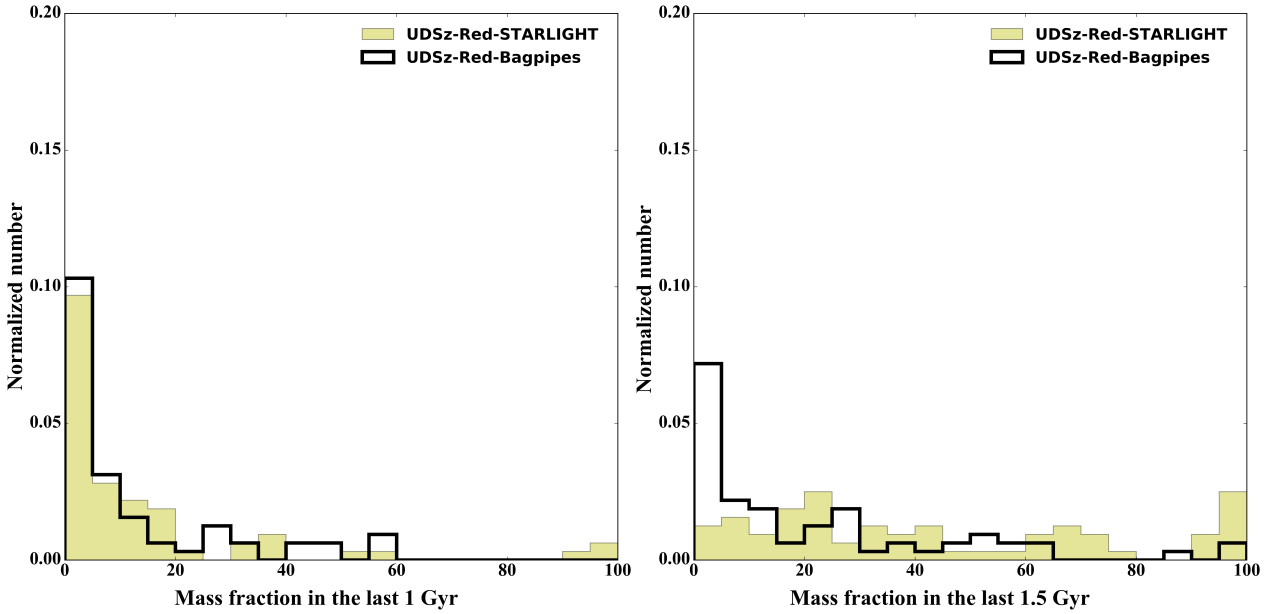

Figure 4.15: The Red sample, see figure (4.14) for more details.

4.6 Conclusions

With SDSS we were able to combine spectral analysis, morphology and environment to build a complete picture of where the PSB galaxies come from and is evolving in to.

With UDS we limit ourselves to discussion more by combining with other work, we may be able to tackle the results from UDS and UDSz in the future. Clearly all galaxies z $\sim$1 have formed a large fraction of mass in the very recent past. This is unsurprising, as this is the epoch of highest star forming in the whole cosmic time. Our results clearly show that the past SFH of the galaxies does not determine their current state of star forming. The quenched galaxies, at low-z, have very similar SFHs to SF3. So we can conclude that some external or internal process has caused some galaxies to shut down star forming over others, regardless of their previous history. This process for galaxy quenching has been much speculated in the literature, and could include environment or AGN. From Hartley et al. (2013) and Socolovsky et al. (2018), we know the UDS galaxies classified as red with the supercolours method are more highly clustered and in dense environments. Therefore, it seems possible that environment has caused the recent quenching event.

Next, we turn to the PSB galaxies. These are being identified by the supercolours as having distinct SFHs than the other classes. However, this is not well captured by the mass fraction in the last 1 and 1.5 Gyr: clearly there are lots of star forming and red galaxies with the same

values. What seems to be distinct about the PSB galaxies that they formed a large fraction of their mass recently and they have had no ongoing star forming for the last $\sim$ 150 Myr. What appears to distinguish the different classes, unlike at low redshift, is the time since they quenched. Our final figure (4.16), shows the time at which a galaxy formed 95% of their mass. This illustrates that the star forming galaxies are ongoing, whereas the red galaxies shut off Star forming at $\sim$ 0.5 Gyr ago. The PSB galaxies are inter media. Unlike at low redshift, where we believe PSB are an unusual event, are results supported the picture in which all red sequence galaxies, these results are formed through an PSB event.

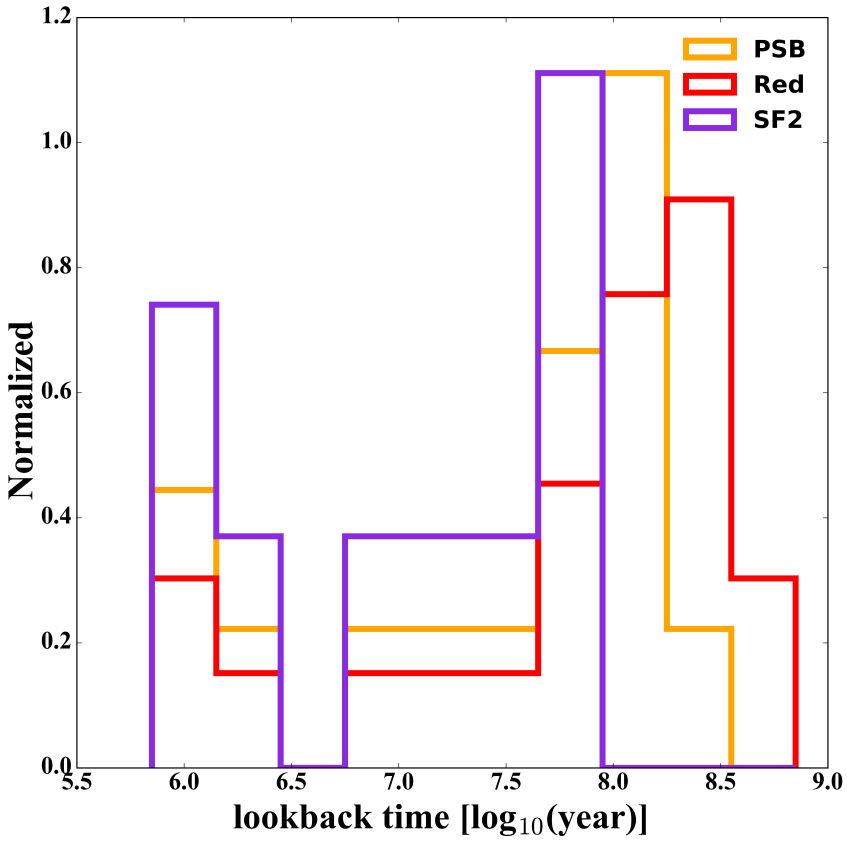

Figure 4.16: The lookback time showing when the galaxies class formed $\geqslant$ 95% of their mass

5

Conclusions

5.1 Summary and Conclusions

Chapter 1 presents a basic description of the spectral energy distribution (SED) of a galaxy. We describe the information that can be obtained from the different regions of an SED. We briefly describe the topic of galaxy evolution and highlight some proposed evolution mechanisms. We focus in particular on our main topic of interest, which is post starburst galaxies and on the elements that contribute in building a synthetic library of model spectra. We end the chapter with a brief look at the main ingredients of building a synthetic spectra model.

Chapter 2 of this thesis is based on the STARLIGHT code. We describe the preparations that are required for the input files and conduct a series of tests on the input base to investigate the reliability of STARLIGHT in retrieving the required information about post-starburst galaxies.

In chapter 3 we use SDSS to identify a sample of post-starburst candidates and fit their spectra with STARLIGHT, alongside control samples of star-forming and quiescent galaxies. The sample is divided into two mass bins. Each mass bin shows a different SFH. The SFH in

the low-mass bin suggests that qPSB are the product of a violent event of gas-rich galaxies that may lead to the quenching. In the proses of quenching the galaxy may pass through ePSB or agnPSB phase. The event, might be a major merger, which may lead to a ePSB phase that may cycle back to SF. The high mass bin, shows a SFH for the qPSB different than the low mass bin. The pre-burst SFH resembles the passive galaxies. A minor merger between PAS and a low mass gas-rich galaxy might have lead to short qPSB phase. Eventually, this may go back to a being PAS.

Chapter 4 describes the fitting of galaxies in the UKIDSS Ultra Deep Survey galaxies (UDS) with spectra from the UDSz and new VIMOS observations (P.I. David Maltby) with the new STARLIGHT code. We show how including the photometric data is important to obtain the correct stellar mass, dust content and star formation histories for some galaxies types. We compare the mass fraction that has been accumulated in the last 1 and 1.5 Gyr for the low-z SDSS and high-z UDSz galaxies. We note that the SFH of SF3 is almost as the PAS in the low-z. This may suggest that an effective event has stopped some galaxies from forming star. The new STARLIGHT results do not distinguish the mass fraction in the last 1 and 1.5 Gyr for the PSB from the Red sample. However, the PSB are distinguished by not having any small stellar mass fraction formed. All the high-z galaxies show they have formed most of their stellar mass in a short time.

5.2 Further work

- Almost a complete picture for SDSS is obtainable from combined morphology, spectra and environment, whereas the UDS at z $\sim$ 1 do not have. This information would complete the picture of the origin of PSB galaxies.
- It will be useful to have the gas contents for PSB galaxies both at low and high redshifts. This is difficult observantly, and various groups are working into it. This will provide us the future evolution of the PSB as gas is crucial for forming stars.
- Investigating the nature of PSBs in cosmological hydrodynamic simulations would help to illustrate the impact of environment.
- At low redshift integrate field survey such as MaNGA have a significant number of PSB galaxies, which may further constrain their formation mechanism.
- Bagpipes unlike STARLIGHT is able to fit photometry only. Do we need spectra?

Bibliography

Abazajian, K. N. et al. 2009, The Astrophysical Journal Supplement Series, 182, 543

Alatalo, K., Cales, S. L., Appleton, P. N., Kewley, L. J., Lacy, M., Lisenfeld, U., Nyland, K., & Rich, J. A. 2014, Astrophysical Journal Letters, 794

Allen, J. T. et al. 2015, Monthly Notices of the Royal Astronomical Society, 451, 2780

Almaini, O. et al. 2017, Monthly Notices of the Royal Astronomical Society, 472, 1401

Appenzeller, I. et al. 1998, The Messenger, 94

Asari, N. V. et al. 2007, Monthly Notices of the Royal Astronomical Society, 381, 263

Bajtlik, S., Duncan, R. C., & Ostriker, J. P. 1988, Astrophys Journal, 327, 570

Baldry, I. K., Balogh, M. L., Bower, R., Glazebrook, K., & Nichol, R. C. 2004, in American Institute of Physics Conference Series, Vol. 743, The New Cosmology: Conference on Strings and Cosmology, ed. R. E. Allen, D. V. Nanopoulos, & C. N. Pope, 106–119

Baldry, I. K., & Glazebrook, K. 2003, The Astrophysical Journal, 593, 258

Baldwin, A., Phillips, M. M., & Terlevich, R. 1981, Publications of the Astronomical Society of the Pacific, 93, 5

Balogh, M. L., Morris, S. L., Yee, H. K. C., Carlberg, R. G., & Ellingson, E. 1999, The Astrophysical Journal, 527, 54

Barger, A. J., Aragón-Salamanca, A., Ellis, R. S., Couch, W. J., Smail, I., & Sharples, R. M. 1996, Monthly Notices of the Royal Astronomical Society, 279, 1

Barnes, J. E., & Hernquist, L. E. 1991, The Astrophysical Journal, 370, L65

Bell, E. F. et al. 2004, The Astrophysical Journal, 608, 752

Bertelli, G., Bressan, a., Chiosi, C., Fagotto, F., & Nasi, E. 1994, Astronomy and Astrophysics Supplement Series, 106, 275

Blanton, M. R., & Moustakas, J. 2009, Annual Review of Astronomy and Astrophysics, 47, 159

Boissier, S., Boselli, a., Buat, V., Donas, J., & Milliard, B. 2004, Astronomy and Astrophysics, 0024, 17

Brinchmann, J., Charlot, S., White, S. D. M., Tremonti, C., Kauffmann, G., Heckman, T., & Brinkmann, J. 2004, Monthly Notices of the Royal Astronomical Society, 351, 1151

Bruzual, G., & Charlot, S. 2003, Monthly Notices of the Royal Astronomical Society, 1028, 1000

Bruzual A., G. 1983, The Astrophysical Journal, 273, 105

Butcher, H., & Oemler, A., J. 1984, The Astrophysical Journal, 285, 426

Calzetti, D., Armus, L., Bohlin, R. C., Kinney, A. L., Koornneef, J., & Storchi-Bergmann, T. 2000, The Astrophysical Journal, 533, 682

Calzetti, D. et al. 2007, The Astrophysical Journal, 666, 870

Calzetti, D., Kinney, A. L., & Storchi-Bergmann, T. 1994, The Astrophysical Journal, 429, 582

Cappellari, M. 2017, Monthly Notices of the Royal Astronomical Society, 466, 798

Cappellari, M., & Emsellem, E. 2004, Publications of the Astronomical Society of the Pacific, 116, 138

Cardelli, J. A., Clayton, G. C., & Mathis, J. S. 1989, The Astrophysical Journal, 345, 245

Carnall, A. C., McLure, R. J., Dunlop, J. S., & Davé, R. 2017, Preprint, 24, 1

Casanellas, J., & Lopes, I. 2011, Astrophysical Journal Letters, 733, 3

Chabrier, G. 2003, Publications of the Astronomical Society of the Pacific, 115, 763

Charlot, S., & Fall, S. M. 2000, The Astrophysical Journal, 539, 718

Choi, J., Dotter, A., Conroy, C., Cantiello, M., Paxton, B., & Johnson, B. D. 2016, The Astrophysical Journal, 823, 102

Chung, A., Van Gorkom, J. H., Kenney, J. D. P., Crowl, H., & Vollmer, B. 2009, Astronomical Journal, 138, 1741

Cid Fernandas, R., Mateus, A., Sodré, L., Stasińska, G., & Gomes, J. M. 2005, Monthly Notices of the Royal Astronomical Society, 358, 363

Cid Fernandes, R., Gonzalez Delgado, R. M., Storchi-Bergmann, T., Martins, L. P., & Schmitt, H. 2005, Monthly Notices of the Royal Astronomical Society, 356, 270

Cimatti, a. et al. 2008, Astronomy & Astrophysics, 42, 1

Couch, W. J., & Sharples, R. M. 1987, Monthly Notices of the Royal Astronomical Society, 229, 423

Cox, T. J., Jonsson, P., Primack, J. R., & Somerville, R. S. 2006, Monthly Notices of the Royal Astronomical Society, 373, 1013

Croton, D. J. et al. 2006, Monthly Notices of the Royal Astronomical Society, 365, 11

da Cunha, E., Charlot, S., & Elbaz, D. 2008, Monthly Notices of the Royal Astronomical Society, 388, 1595

Da Cunha, E., Charlot, S., & Elbaz, D. 2008, PhD thesis

Dobbs, C. 2013, Astronomy & Geophysics, 54, 5.24

Dobos, L., Csabai, I., Yip, C.-W., Budavári, T., Wild, V., & Szalay, A. S. 2012, Monthly Notices of the Royal Astronomical Society, 420, 1217

Dopita, M. A., & Sutherland, R. S. 1995, The Astrophysical Journal, 455, 468

Dressler, A., & Gunn, J. E. 1983, The Astrophysical Journal, 270, 7

Dressler, A., Smail, I., Poggianti, B., Butcher, H., Couch, W., Ellis, R., & Oemler, A. 1999, The Astrophysical Journal Supplement Series, 122, 51

Falcón-Barroso, J., Sánchez-Blázquez, P., Vazdekis, A., Ricciardelli, E., Cardiel, N., Cenarro, A. J., Gorgas, J., & Peletier, R. F. 2011, Astronomy & Astrophysics, 532, A95

Feigelson, E. D., & Babu, G. J. 2013, in Planets, Stars and Stellar Systems (Springer), 445–480

Feroz, F., Hobson, M. P., & Bridges, M. 2009, Monthly Notices of the Royal Astronomical Society, 398, 1601

Fitzpatrick, E. L. 1999, Publications of the Astronomical Society of the Pacific, 111, 63

Fitzpatrick, E. L., & Massa, D. 2007, The Astrophysical Journal, 663, 320

Furusawa, H. et al. 2008, The Astrophysical Journal Supplement Series, 176, 1

Gaibler, V., Khochfar, S., Krause, M., & Silk, J. 2012, Monthly Notices of the Royal Astronomical Society, 425, 438

Gallazzi, A., Charlot, S., Brinchmann, J., White, S. D. M., & Tremonti, C. A. 2005, Monthly Notices of the Royal Astronomical Society, 362, 41

Gomes, J. M., Cid Fernandes, R., & Lacerda, R. R. 2004, Proceedings of the International Astronomical Union, 2004, 173

Goto, T. 2005, Monthly Notices of the Royal Astronomical Society, 357, 937

Groves, B., Brinchmann, J., & Walcher, C. J. 2012, Monthly Notices of the Royal Astronomical Society, 419, 1402

Gunn, J. E., & Gott J. Richard, I. I. I. 1972, The Astrophysical Journal, 176, 1

Güsten, R. 1989, in IAU Symposium, Vol. 136, The Center of the Galaxy, 89

Hartley, W. G. et al. 2013, Monthly Notices of the Royal Astronomical Society, 431, 3045

Hernquist, L., & Mihos, J. C. 1995, The Astrophysical Journal, 448, 41

Hester, J. a. 2006, The Astrophysical Journal, 647, 910

Ho, I. et al. 2016, Astrophysics and Space Science, 361, 280

Hopkins, P. F., & Elvis, M. 2010, Monthly Notices of the Royal Astronomical Society, 401, 7

Hubble, E. 1926, The Astrophysical Journal, 64, 321

Hubble, E., Humason, M. L. 1931, The Asteophysical Journal, 74, 43

Huchra, J. 1977, The Asteophysical Journal, 217, 928

Jenkins, E. B. 1987, Element Abundances in the Interstellar Atomic Material, Vol. 134 (A Series of Books on the Recent Developments of Space Science and of General Geophysics and Astrophysics Published in Connection with the Journal Space Science Reviews), 533

Jimenez, R., MacDonald, J., Dunlop, J. S., Padoan, P., & Peacock, J. A. 2004, Monthly Notices of the Royal Astronomical Society, 349, 240

Johnson, K. E., Kobulnicky, H. A., Massey, P., & Conti, P. S. 2001, The Astrophysical Journal, 559, 864

Kannappan, S. J., Guie, J. M., & Baker, A. J. 2009, The Astronomical Journal, 138, 579

Kauffmann, G. et al. 2003a, Monthly Notices of the Royal Astronomical Society, 341, 33

——. 2003b, Monthly Notices of the Royal Astronomical Society, 341, 54

Kennicutt, R. C., J. 1983, The Astrophysical Journal, 272, 54

Kewley, L. J., Dopita, M. a., Sutherland, R. S., Heisler, C. a., & Trevena, J. 2001, The Astrophysical Journal, 556, 121

Koski, A. T. 1978, The Astrophysical Journal, 223, 56

Kriek, M., & Conroy, C. 2013, The Astrophysical Journal, 775, L16

Kroupa, P. 2001, Monthly Notices of the Royal Astronomical Society, 322, 231

Kroupa, P., Tout, C. a., & Gilmore, G. 1993, Monthly Notices of the Royal Astronomical Society (ISSN 0035-8711), 262, 545

Kurucz, R. L. 1979, The Astrophysical Journal Supplement Series, 40, 1

Lacey, C., & Cole, S. 1994, Monthly Notices of the Royal Astronomical Society, 271, 676

Lagos, C. D. P., Cora, S. A., & Padilla, N. D. 2008, Monthly Notices of the Royal Astronomical Society, 388, 587

Lawrence, A. et al. 2007, Monthly Notices of the Royal Astronomical Society, 379, 1599

Lester, D. F. 1995, in Astronomical Society of the Pacific Conference Series, Vol. 73, From Gas to Stars to Dust, ed. M. R. Haas, J. A. Davidson, & E. F. Erickson

Liu, C. T., & Kennicutt, R. C. 1995, The Astrophysical Journal, 450, 547

López Fernández, R. et al. 2016, Monthly Notices of the Royal Astronomical Society, 458, 184

Madau, P., & Dickinson, M. 2014, Annual Review of Astronomy and Astrophysics, 52, 415

Maier, C. et al. 2016, Astronomy & Astrophysics, 590, A108

Mateus, A., Sodré, L., Cid Fernandes, R., Stasińska, G., Schoenell, W., & Gomes, J. M. 2006, Monthly Notices of the Royal Astronomical Society, 370, 721

Mathis, J. S. 1983, The Astrophysical Journal, 267, 119

McIntosh, D. H. et al. 2014, Monthly Notices of the Royal Astronomical Society, 442, 533

Meneses-Goytia, S., Peletier, R. F., Trager, S. C., Falcón-Barroso, J., Koleva, M., & Vazdekis, A. 2015, Astronomy & Astrophysics, 582, A96

Merritt, D., & Quinlan, G. D. 1998, The Astrophysical Journal, 498, 625

Mo, H., van den Bosch, F. C., & White, S. 2010, Galaxy Formation and Evolution

Moore, B., Katz, N., Lake, G., Dressler, A., & Oemler, A. 1996, Nature, 379, 613

Morton, D. 1991, Astrophysical Journal Supplement Series, 77, 119

Muñoz-Mateos, J. C. et al. 2009, Astrophysical Journal, 701, 1965

Nolan, L. A., Raychaudhury, S., & Kabán, A. 2007, Monthly Notices of the Royal Astronomical Society, 375, 381

Oesch, P. A. et al. 2007, The Astrophysical Journal, 671, 1212

Osterbrock, D. E., & Ferland, G. J. 2006, Astrophysics of gaseous nebulae and active galactic nuclei (University Science Books)

Padmanabhan, N. et al. 2007, Monthly Notices of the Royal Astronomical Society, 378, 852

Panter, B., Heavens, A. F., & Jimenez, R. 2004, Monthly Notices of the Royal Astronomical Society, 355, 764

Pattarakijwanich, P., Strauss, M. A., Ho, S., & Ross, N. P. 2016, The Astrophysical Journal, 833, 19

Pawlik, M. M. et al. 2018, Monthly Notices of the Royal Astronomical Society, 477, 1708

Pearce, H. J. 2012, Massive galaxies at high redshift (The University of Edinburgh)

Peebles, P. J. E. 1970, The Astronomical Journal, 75, 13

Peng, Y., Maiolino, R., & Cochrane, R. 2015, Nature, 521, 192

Poggianti, B., Smail, I., Dressler, A., Couch, W., Barger, A., Butcher, H., Ellis, R., & Oemler, A. 1999, The Astrophysical Journal, 518, 576

Poggianti, B. M., Bridges, T. J., Komiyama, Y., Yagi, M., Carter, D., Mobasher, B., Okamura, S., & Kashikawa, N. 2004, The Astrophysical Journal, 601, 197

Poggianti, B. M., & Wu, H. 2000, The Astrophysical Journal, 529, 157

Prugniel, P., & Soubiran, C. 2001, Astronomy & Astrophysics, 369, 1048

Prugniel, P., Soubiran, C., Koleva, M., & Borgne, D. L. 2007, The Astrophysical Journal Supplement Series, 152, 251

Rauch, M. 2000, Lyman Alpha Forest (Bristol: Institute of Physics Publishing)

Renaud, F., Bournaud, F., Kraljic, K., & Duc, P.-A. 2014, Monthly Notices of the Royal Astronomical Society: Letters, 442, L33

Reuland, M. et al. 2007, The Astronomical Journal, 133, 2607

Salpeter, E. E. 1955, The Astrophysical Journal, 121, 161

Sanchez-Blazquez, P. et al. 2006, Monthly Notices of the Royal Astronomical Society, 371, 703

Sandage, A. 1975

Schawinski, K., Thomas, D., Sarzi, M., Maraston, C., Kaviraj, S., Joo, S. J., Yi, S. K., & Silk, J. 2007, Monthly Notices of the Royal Astronomical Society, 382, 1415

Schlegel, D. J., Finkbeiner, D. P., & Davis, M. 1998, The Astrophysical Journal, 500, 525

Schneider, P. 2015, Extragalactic Astronomy and Cosmology (Berlin, Heidelberg: Springer Berlin Heidelberg), 510

Silk, J., & Nusser, A. 2010, Astrophysical Journal, 725, 556

Smith, B. J. 1996, in New Extragalactic Perspectives in the New South Africa, ed. D. L. Block & J. M. Greenberg (Dordrecht: Springer Netherlands), 170–177

Socolovsky, M., Almaini, O., Hatch, N. A., Wild, V., Maltby, D. T., Hartley, W. G., & Simpson, C. 2018, Monthly Notices of the Royal Astronomical Society, 476, 1242

Sparke, L. S., & Gallagher, J. S. 2007, Galaxies in the Universe: An Introduction, 442

Stoughton, C. et al. 2002, The Astronomical Journal, 123, 485

Strateva, I. et al. 2001, The Astronomical Journal, 122, 1861

Swinbank, A. M. et al. 2007, Monthly Notices of the Royal Astronomical Society, 379, 1343

Tacconi, L. J., & Young, J. S. 1986, The Astrophysical Journal, 308, 600

Tinsley, B. M. 1978, The Astrophysical Journal, 222, 14

Tran, K. H., Franx, M., Illingworth, G., Kelson, D. D., & van Dokkum, P. 2003, The Astrophysical Journal, 599, 865

Valdes, F., Gupta, R., Rose, J. a., Singh, H. P., & Bell, D. J. 2004, The Astrophysical Journal Supplement Series, 152, 251

Van den Bergh, S. 2009, The Astrophysical Journal Letters, 694, L120

Vazdekis, A., Koleva, M., Ricciardelli, E., Röck, B., & Falcón-Barroso, J. 2016, Monthly Notices of the Royal Astronomical Society, 463, 3409

Vazdekis, A., Sánchez-Blázquez, P., Falcón-Barroso, J., Cenarro, A. J., Beasley, M. A., Cardiel, N., Gorgas, J., & Peletier, R. F. 2010, Monthly Notices of the Royal Astronomical Society, 404, 1639

Whitaker, K. E., Kriek, M., van Dokkum, P. G., Bezanson, R., Brammer, G., Franx, M., & Labbe, I. 2012, The Astrophysical Journal, 745, 179

Wild, V. et al. 2014, Monthly Notices of the Royal Astronomical Society, 440, 1880

Wild, V., Charlot, S., Brinchmann, J., Heckman, T., Vince, O., Pacifici, C., & Chevallard, J. 2011, Monthly Notices of the Royal Astronomical Society, 417, 1760

Wild, V., Heckman, T., & Charlot, S. 2010, Monthly Notices of the Royal Astronomical Society, 405, 933

Wild, V., & Hewett, P. C. 2005, Monthly Notices of the Royal Astronomical Society, 358, 1083

Wild, V., Kauffmann, G., Heckman, T., Charlot, S., Lemson, G., Brinchmann, J., Reichard, T., & Pasquali, A. 2007, Monthly Notices of the Royal Astronomical Society, 381, 543

Wild, V., Walcher, C. J., Johansson, P. H., Tresse, L., Charlot, S., Pollo, A., Le Fèvre, O., & de Ravel, L. 2009, Monthly Notices of the Royal Astronomical Society, 395, 144

Wong, O. I. et al. 2012, Monthly Notices of the Royal Astronomical Society, 420, 1684

Wood, B. E., Redfield, S., Linsky, J. L., Muller, H., & Zank, G. P. 2005, The Astrophysical Journal Supplement Series, 159, 118

Yan, R. et al. 2008, Monthly Notices of the Royal Astronomical Society, 398, 735

Yang, Y., Zabludoff, A. I., Zaritsky, D., Lauer, T. R., & Mihos, J. C. 2004, The Astrophysical Journal, 607, 258

Yoon, H., Chung, A., Smith, R., & Jaffé, Y. L. 2017, The Astrophysical Journal, 838, 81

Young, J. S., & Knezek, P. M. 1989, The Astrophysical Journal, 347, L55

Zabludoff, A. I., Zaritsky, D., Lin, H., Tucker, D., Hashimoto, Y., Shectman, S. A., Oemler, A., & Kirshner, R. P. 1996, The Astrophysical Journal, 466, 104

Zhuravleva, I. et al. 2014, Natur, 515, 85